

Two-dimensional $\mathcal{N} = (2, 2)$ super Yang-Mills theory on the lattice

Dissertation

zur Erlangung des akademischen Grades
doctor rerum naturalium (Dr. rer. nat.)

vorgelegt dem Rat der Physikalisch-Astronomischen Fakultät
der Friedrich-Schiller-Universität Jena

von M. Sc. Daniel August
geboren am 04. Januar 1989 in Eisenach

Gutachter

1. Prof. Dr. Andreas Wipf (Friedrich-Schiller-Universität Jena)
2. Prof. Dr. Urs Wenger (Universität Bern)
3. Prof. Dr. Simon Catterall (Syracuse University)

Tag der Disputation: 30.04.2019

Abstract

Supersymmetry is one of the possible scenarios for physics beyond the standard model. By introducing a symmetry between bosons and fermions, it might be able to solve several theoretical problems while providing dark matter candidates. As all supersymmetric extensions of the standard model are based on strongly coupled gauge theories, we need non-perturbative methods, to fully investigate them. In this thesis we use lattice calculations, to investigate the two-dimensional $\mathcal{N} = (2, 2)$ super Yang-Mills theory, which we derive by a dimensional reduction of the four-dimensional $\mathcal{N} = 1$ super Yang-Mills theory.

Unfortunately our lattice formulation breaks supersymmetry explicitly. Thus we devote the first part of the thesis to present the lattice theory and analyze it thoroughly. First we have to discretize Majorana fermions, which leads to a real but not necessarily positive fermion determinant. Second, the classical potential of the scalar fields posses flat directions. Both problems could thwart our lattice simulations. Fortunately, as we demonstrate, both of them are absent in our simulations. At last, we show that the lattice theory posses only one relevant operator, the scalar mass, whose value in the continuum limit is known.

The second part of the thesis is devoted to the numerical results. Introducing an additional fine-tuning of the fermion mass, we can reduce the influence of supersymmetry violating terms. Calculating lattice Ward identities, we show the restoration of supersymmetry in the chiral and continuum limit. Finally we calculate the low-lying bound states and extrapolate their masses to the continuum limit. We find two super-multiplets, as predicted from low energy effective theories. The first is the Farrar-Gabadadze-Schwetz super-multiplet which decouples from the theory. The second is the Veneziano-Yankielowicz super-multiplet which becomes massless in the chiral limit. We are further able to estimate the masses of the excited mesons of the latter. They are of the same size as the mass of the gluino-glueball.

Zusammenfassung

Supersymmetry ist ein mögliches Konzept, das Physik jenseits des Standardmodells beschreiben könnte. Durch die Einführung einer Symmetrie zwischen Bosonen und Fermionen werden einige theoretische Probleme gelöst und Kandidaten für die Dunkle Materie eingeführt. Da alle supersymmetrischen Erweiterungen des Standardmodells auf stark gekoppelten Eichtheorien beruhen, benötigen wir nichtperturbative Methoden, um sie vollständig zu untersuchen. In dieser Doktorarbeit nutzen wir Gitterrechnungen um die zweidimensionale $\mathcal{N} = (2, 2)$ supersymmetrische Yang-Mills Theorie zu untersuchen. Wir erhalten dieses Model durch eine dimensionale Reduktion der vierdimensionalen $\mathcal{N} = 1$ supersymmetrischen Yang-Mills Theorie.

Unglücklicherweise bricht unser Gitterformalismus die Supersymmetry explizit. Daher nutzen wir den ersten Teil der Doktorarbeit, um unsere Gittertheorie vorzustellen und sorgfältig zu untersuchen. Zuerst müssen wir Majorana Fermionen diskretisieren. Dies führt zu einer reellen aber nicht notwendigerweise positiven Fermionendeterminante. Weiterhin besitzt das klassische Potential der Skalarfelder flache Richtungen. Beide Probleme könnten unsere Simulation unmöglich machen. Glücklicherweise können wir zeigen, dass beide in unserer Simulation abwesend sind. Zum Schluß zeigen wir, dass die Gittertheorie nur einen relevanten Operator, die skalare Masse, besitzt, deren Wert für den Kontinuumsimes bekannt ist.

Im zweiten Teil der Doktorarbeit präsentieren wir die numerischen Resultate. Durch die Einführung und Feinabstimmung eines zusätzlichen Parameters, die Fermionenmasse, können wir den Einfluss von Operatoren, die Supersymmetry brechen, reduzieren. Durch die Berechnung von Gitterwardidentitäten können wir die Wiederherstellung der Supersymmetry im chiralen und Kontinuumsimes zeigen. Zum Schluß bestimmen wir das Spektrum der leichten Bindungszustände. Wir finden zwei Supermultiplets. Das Erste ist das Farrar-Gabadadze-Schwetz Supermultiplet, welches von der Theorie entkoppelt. Das Zweite ist das Veneziano-Yankielowicz Supermultiplet, welches im chiralen Limes masselos ist. Zusätzlich können wir auch die Massen der angeregten Zustände für das Letztere bestimmen. Sie sind von der gleichen Größenordnung wie die Masse des Gluino-Glueballs.

Contents

1	Introduction	3
2	Theoretical Background	10
2.1	Supersymmetry	10
2.2	Four-dimensional Model	11
2.3	Kaluza-Klein Reduction	14
2.3.1	Representations of Gamma matrices	15
2.3.2	Reduction of the Model	15
2.4	Symmetries	18
2.4.1	Lorentz symmetry	18
2.4.2	Two-dimensional Supersymmetry	21
2.5	Expected Mass Spectrum	22
2.6	Ward Identities	26
3	Lattice Formulation	29
3.1	Euclidean formulation	30
3.2	Supersymmetry on the lattice	31
3.3	Rational Hybrid Monte Carlo algorithm	32
3.4	Discretization of the Action	36
3.4.1	Bosons	37
3.4.2	Fermions	37
3.5	One- and two-point functions	38
3.6	Smearing	40
3.6.1	Low-Pass Filter	40
3.6.2	APE Smearing	42
3.6.3	Stout Smearing	42
3.6.4	Jacobi Smearing	43
3.7	Error estimation	43
4	Lattice Calculations	45
4.1	Fine-tuning of the lattice theory	45

4.2	One-loop calculation	49
4.3	Ward Identities on the Lattice	51
4.4	Glueballs in two-dimensional pure Yang-Mills theory	57
5	Simulation Parameters	62
5.1	β dependency	63
5.2	Volume dependency	66
5.3	Scalar Mass dependency	68
5.4	Fermion Mass dependency	70
5.5	Conclusion	73
6	Results	75
6.1	Flat directions	75
6.2	Sign problem	76
6.3	Continuum limit of the critical fermion mass	78
6.4	Ward Identities	80
6.5	Mass spectrum	83
6.5.1	Mesons	84
6.5.2	Glينو-gluo/scalarball	87
6.5.3	Glueball, Scalarball and Glue-scalarball	89
7	Conclusion	91
	Appendices	94
A	Conventions	94
B	Pure gauge theory on the lattice	95
B.1	Holes	97
B.2	Wilson Loop	99
B.3	Glueballs	101

Chapter 1

Introduction

The two most successful theoretical models describing parts of our universe are the standard model of particle physics and the general theory of relativity. Both were once more validated by the detection of the Higgs boson [1, 2] and gravitational waves [3]. Yet we know both theories can not describe physics at all energy and length scales. The simple explanation is, that both theories fail to include each other. We see this explicitly by the absence of the gravitational interaction in the standard model. A step forward would be to unite both theories into a more general one. Unfortunately we still lack a way to quantize the gravitational force. The difficulty of this task is seen by a comment from Heisenberg and Pauli, who in 1929 thought it to be straight forward [4]. Yet several decades later it is still an unsolved problem. Furthermore the data from astrophysics suggest, that even this unified theory can not describe everything. Looking into these results [5], we find that the particle content of the standard model makes up only 4.9% of the energy density of the universe, while the so called dark matter makes up 26.6%. The remaining 68.5% is the so called dark energy. The name for the last two comes from the fact, that they do not interact with photons, hence they emit no light, like any dark object. While both make up 95% of the universe, we know little about them. Still we have experimental constraints for dark matter. Astronomical observations found that it will most likely not interact via the electromagnetic force, the strong force and the weak force. Thus the most easiest idea was to link it to neutrinos, whose shallow interaction with the rest of the standard model could explain these properties. Unfortunately the combination of the very low mass with its fermionic nature rules out this possibility. Thus we need new particles outside of the standard model.

Over the last decades, there were many proposals for new theories beyond the standard model, introducing several different candidates for the dark matter particles. The most promising of them seems to be supersymmetry (for an introduction see [6, 7]). Derived by a non-trivial extension of the Poincaré algebra, it solves the Hierarchy problem. Another nice feature is the unification of electromagnetism, the strong force and the

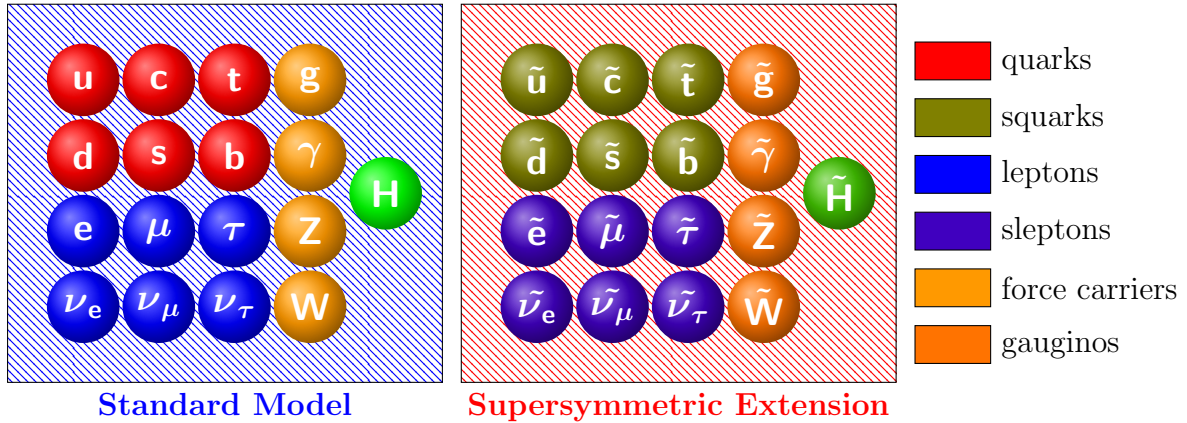


Figure 1.1: Particle content of the Minimal Supersymmetric Standard Model

weak force at high energy scales, as expected by heuristic arguments. Further it delivers a plethora of possible dark matter candidates. The only downside is, that the naive supersymmetric extension of the standard model is not realized in nature. For this let us look at the particle content of the minimal supersymmetric standard model, depicted in Figure 1.1. We see that it introduces a new particle for every particle of the standard model. These must appear because supersymmetry introduces a new symmetry between bosons and fermions. One property of this symmetry is that it conserves the electromagnetic charge and the mass. Thus the supersymmetric partner of the electron, called selectron, should be a boson with negative charge e and a mass of $m_e \approx 9.109 \times 10^{-31} \text{kg}$ [8]. Since these particles are absent in physical experiments, supersymmetry can only be realized in nature if it is broken at low energies¹, e.g. below 10 TeV. Conceptually this is a well understood property of physical systems. For example in magnets: below the Curie temperature isotropy is broken and we observe so called Weiss domains. This is an example of spontaneous symmetry breaking. Another mechanism would be a soft symmetry breaking, where we break it directly in such a way, that we restore it at high energies. Interestingly we can use the latter breaking mechanism to parametrize the former. Anyhow supersymmetric models and theories received a lot of attention over the last decades and are one of the focus point for the LHC [9, 10]. Yet we miss experimental verification of all supersymmetric scenarios considered (see for example the reviews in [8, 11]). Thus we have to take a closer look how to derive these predictions.

Most of the calculations in supersymmetric theories are done with semi-classical and perturbative methods. The reason is that due to the increased amount of symmetry, one finds a high amount of cancellations of quantum corrections, simplifying the calculations. This is further expressed in the non-renormalization theorems [12, 13]. To illustrate this property let us take a look at the Hierarchy problem. In the standard

¹The actual value is not fixed and can be changed inside the model, yet this would have measurable effects. Thus there exist constraints for this value



Figure 1.2: One loop contributions to the Higgs mass squared m_H^2 due to a Dirac fermion λ and a scalar S , reproduced from [6].

model, the Higgs is a boson. Thus its mass squared will get corrections proportional to the scale Λ squared. Here we call Λ the energy after which the standard model is not sufficient to describe physics anymore. This correction is created by the Feynman diagram depicted on the left side of Figure 1.2. Since we do not know Λ yet, it could range from 10 TeV up to the Planck scale² $E_P \approx 1.2209 \times 10^{16}$ TeV. In contrast the experimental result for the mass of the Higgs is known $m_H \approx 125$ GeV [1, 2]. Thus we need a fine-tuning over several magnitudes for the constants in front of the quantum corrections to get the correct Higgs mass. In case of fermions, this problem is not as severe, since the leading correction is proportional to the logarithm of Λ , thus for a large range of energies the prefactors of the corrections will be of the same order. The fine-tuning of the parameters to get the right Higgs mass is called Hierarchy problem. It is purely theoretical in nature because it does not affect the experimental and thus the physical results of the standard model. We can solve this problem with a supersymmetric extension of our theory. By introducing a symmetry between bosons and fermions, we get new corrections for the Higgs mass. We are especially interested in the Feynman diagram depicted on the right hand side of Figure 1.2. Due to supersymmetry, it cancels exactly the contribution from the diagram on the left side [6]. Thus the Hierarchy problem is absent in a supersymmetric model. This kind of cancellation is common in supersymmetric theories to all orders of perturbation theory, leading to the aforementioned non-renormalization theorems. Further it simplifies the calculation leading to many exact results.

This previous discussion hid one very important point, all those argument are only valid in perturbation theory. While it is usually thought to be sufficient to explain results for Quantum electrodynamics (QED) at low energies and Quantum chromodynamics (QCD) at high energies, it can not explain all physical properties. Let us show this for QED. This theory is the quantum field theory describing the electromagnetic interaction. Using perturbation theory, one gets very precise predictions, one of the standard example being the fine structure constant derived from the anomalous magnetic dipole moment of the electron [14]. On the other hand this theory should also be able to describe the hydrogen atom. Looking at the solution for the ground state

²From our current understanding of the universe, this is the highest energy after which the standard model has to fail.

we observe an interesting fact. We can not expand it into a sum of finite elements, which approximately describes the ground state. Thus we will fail to describe it with perturbation theory. Such effects are commonplace in quantum field theory and are called non-perturbative effects. They include the mass generation of mesons and the confinement found in QCD, which are important properties of the theory.

In this work we try to observe such effects, using lattice simulations. This formulation, introduced by Wilson [15], allows to calculate the non-perturbative effects in a theory, as very successfully shown in QCD [16, 17]. Unfortunately the extension to supersymmetric theories is difficult. The reason is supersymmetry itself. Let us assume we could set up a lattice simulation with a conserved supersymmetry. First we have to discretize spacetime. Second we have to introduce the lattice action, which admits a supercharge \mathcal{Q} as demanded. Both steps will introduce conflicting properties of this lattice theory. From the superalgebra we find

$$\{\mathcal{Q}, \mathcal{Q}\} \propto P_\mu, \tag{1.1}$$

where P_μ is the infinitesimal generator of translation. Thus by applying two successive supersymmetry transformations we can shift the fields of our theory to any position in spacetime, without changing the action of the lattice theory. Unfortunately this is impossible, as the lattice action is only invariant under discrete translations. Thus our assumption must be wrong and we can not have a conserved supersymmetric charge. In fact even this statement is wrong for all possible setups. Using a more careful analysis, it was shown, that there exists formulations for theories with more than one supercharge, which can conserve a part of the supersymmetry [18–22]. In those special cases one can combine the supercharges to form a new nilpotent supercharge $\mathcal{Q}^2 = 0$. Still an explicit breaking of supersymmetry via the lattice formulation is not an unsolvable problem. Usually one faces the same problem for chiral symmetry in lattice gauge theories. Using so called fine-tuning of parameters one can restore it in the continuum limit, allowing to study this symmetry with lattice simulations. Unfortunately in the case of the supersymmetry, the amount of parameters to tune is usually very large, making the lattice simulation of those theories infeasible.

One exception is the $\mathcal{N} = 1$ Super Yang Mills (SYM) theory in four dimensions. Tuning the mass of the fermions only, we can recover chiral and supersymmetry in the continuum [23]. Thus it is the focus of several simulations [24–34]. Physically it describes the interaction of gluons with their superpartners, Majorana fermions called gluinos. Both fields transform in the adjoint representation of the gauge group. Thus it allows for a bound state between both, called gluino-glueball. Further the theory is asymptotically free and we expect that the gluinos and gluons will form colorless bound states, like QCD. Additionally it possesses a chiral symmetry $U(1)_A$, which is

anomalously broken to the discrete subgroup \mathbb{Z}_{2N} via instantons. At low temperatures this symmetry is then further broken spontaneously to \mathbb{Z}_2 by the formation of a gluino condensate. Hence one finds N physically equivalent vacua [35].

One interesting aspect of this theory is its mass spectrum. Due to the supersymmetry, the bound states of the theory should form super-multiplets. Using low energy effective theories [36–38], two of them were predicted. The first contains the adjoint f - and η -meson plus the aforementioned gluino-gluonball. The second is formed by a 0^+ gluonball, a 0^- gluonball and again the gluino-gluonball. Of course, the gluino-gluonball ground state can not be part of both multiplets, thus in one of them lies an excited state. Since low energy effective theories depend on free parameters, the exact mass ordering of both multiplets is not known. Yet there exist various arguments in the literature for the possible orderings [36–39]. This is further complicated by the fact, that for every state in one multiplet, there exists a state in the other with the exact same quantum numbers. Therefore, these states can mix which allows for an even more complex multiplet structure.

While the direct determination of the mass spectrum of the $\mathcal{N} = 1$ SYM theory is one focus of ongoing lattice simulations [40, 41], we try to resolve it with a different approach. Instead of simulating the full four-dimensional model, we first apply a dimensional reduction. This leads to the $\mathcal{N} = (2, 2)$ SYM theory in two dimensions. While its dynamics might differ from the four-dimensional model, the super-multiplet structure is preserved. This should allow us to get insight into the four-dimensional model by calculating the mass spectrum of a simpler but related model. The advantage of this approach is, that in two dimensions, we can simulate larger lattices with a greater number of configurations, which allows to reduce the error for the mass considerably. Thus we aim to find a high precision prediction for these masses.

Looking back to our discussion with the supersymmetry on the lattice, we have to first worry about the fine-tuning. It turns out, the two-dimensional $\mathcal{N} = (2, 2)$ SYM theory has also only one relevant fine-tuning operator, the mass of the scalars. Thus the simulation is feasible. Further this theory has an extended supersymmetry, which allows for the aforementioned preserved supersymmetry charge in a lattice simulation.

This allows for another interesting motivation for this lattice study. We can use our work to compare it to the so called \mathcal{Q} -exact formulations. The basis of these is twisting [42], which allows to construct a lattice formulation with one preserved nilpotent supercharge. In fact there exist three different formulations [43–45]. Unfortunately all these models suffer from the same problem [46–48]: In lattice perturbation theory, one expands the link variables as $U_\mu = \mathbb{1} + iaA_\mu + \dots$, which allows for an unique vacuum state. This is possible, because $U_\mu = \mathbb{1}$ is the minimum of the gauge potential. In all of these three models, this is not the case anymore. In fact one finds several different minima, leading to an ambiguous continuum limit. To solve this problem,

the models proposed in [43, 44] introduce the term $\mu^2 \text{tr} (U^\dagger U - \mathbb{1})^2$ to the Lagrangian, which forces the gauge field dynamically into a unique vacuum state. However, this term will break supersymmetry for $\mu \neq 0$, thus one has to take the limit $\mu \rightarrow 0$ to recover supersymmetry. In contrast, by modifying the model proposed in [45], one can solve this problem without breaking supersymmetry [49]. The restoration of the full supersymmetry (not only the one connected to the preserved nilpotent supercharge) for these models was shown in [46, 50–56]. Next the relations between these models were investigated in [57–60]. A more detailed overview of these models can be found in the reviews [18–22].

At last our theory is also interesting from a topological view point. As two-dimensional gauge theories have less dynamical degrees of freedom, the topology of the (Euclidean) spacetime has a larger influence on the physical results. Thus other topological setups were scrutinized in [61–63]. The method used for the investigation was an extension of the \mathcal{Q} -exact methods to arbitrary spacetime, by generalizing the topological twisting [42] to generic Riemann surfaces in two dimensions [61]. The results reveal a connection of the sign problem, which is absent on the torus, to the $U(1)_A$ anomaly. Using a so called compensator, the authors solved the sign problem for Riemann surfaces with genus unequal to one. Further they looked at Ward-Identities and the $U(1)_A$ anomaly. The latter is intimately related to the zero modes of the Dirac operator.

This thesis is structured as follows: in chapter 2 we first derive the two-dimensional theory via the Kaluza-Klein reduction of the four-dimensional mother theory. Since this introduces three different set of indices, we have gathered their conventions in appendix A. After arriving at the $\mathcal{N} = (2, 2)$ SYM theory, we discuss its symmetries. Especially how they appear due to the dimensional reduction and how they are related to different forms of the action. Afterwards we present the expected mass spectrum. For this we summarize the representation theory of supersymmetry in two-dimensional quantum fields theories, which shows, that the super-multiplets of the four-dimensional theory and the two-dimensional consists of the same amount of states. Thus we expect, that the dimensional reduction of the former will lead to the latter. We end this chapter with a discussion of the Ward identities, which we will use to show the restoration of supersymmetry in the continuum limit. In chapter 3 we introduce the lattice formulation. First we have to discuss how to simulate Majorana fermions. Afterwards we give a more detailed introduction to the problems we face for supersymmetric lattice theories. After presenting these theoretical problems for the implementation we describe the relevant parts of our simulation. We start with an introduction into the generation of so called configurations, where we explicitly introduce the RHMC algorithm. Afterwards we introduce the lattice action, by discretizing the continuum action. Next we discuss our observables, namely the one- and two-point functions. We continue with

error suppression techniques, called smearing. Lastly we will discuss the error estimation for our results. In chapter 4 we analyze our lattice setup theoretically. We start with a discussion of the relevant parameters which must be fine-tuned. We follow this up with a reproduction of a one-loop calculation [64], applied to our specific lattice action. Lastly we discuss the two-dimensional pure Yang-Mills theory as a precursor of our lattice results for the glueball.

In chapter 5 we present our first numerical results. Here we show and discuss the dependency of our lattice simulation from the inverse gauge coupling, the lattice volume, the scalar mass and the fermion mass. These allow us to fix our simulation parameter setup, which we use to extrapolate to the correct continuum limit. In chapter 6 we present our physical results. We start with a discussion of the flat directions and the sign problem of the theory, which are absent in our simulations. Next we look at the continuum limit of the critical fermion mass, which confirms our theoretical discussion of the fine-tuning parameters. We continue with presenting the results for the Ward Identities in the continuum limit, which show the restoration of supersymmetry in the continuum limit. Lastly we present our results for the mass spectrum. In chapter 7 we conclude this thesis.

The compilation of this thesis is solely due to the author. However large parts of the work was in collaboration with Björn Wellegehausen and Andreas Wipf. We published different interim results in the proceedings [65, 66]. A publication encompassing all results is to appear in JHEP and is available as a preprint [67]. The code is based on a framework mainly developed by Björn Wellegehausen. The simulations were performed at the HPC-Clusters OMEGA and ARA of the University Jena.

Chapter 2

Theoretical Background

In this chapter we will discuss the basic properties of the $\mathcal{N} = (2, 2)$ Super Yang-Mills theory in two dimensions in the continuum. We start with a short introduction to supersymmetry before we present the four-dimensional $\mathcal{N} = 1$ Super Yang-Mills theory. Next we introduce the Kaluza-Klein reduction which we will apply onto the four-dimensional model to get the two-dimensional $\mathcal{N} = (2, 2)$ Super Yang-Mills theory. For this theory we will discuss the chiral symmetry and supersymmetry for the different representations of the model. In section 2.5, we will discuss the expected mass spectrum, which is constrained by the $\mathcal{N} = (2, 2)$ supersymmetry. We conclude the chapter with the derivation of Ward identities.

2.1 Supersymmetry

Symmetries play an important role in physics, ranging from the global spherical symmetry of black holes to the gauge symmetry of fields in quantum field theory (QFT). Its importance can be seen by the fact that states in particle physics are classified by their transformation under the different symmetries of the standard model of physics. Two of these classifications are based on spin and mass. They come from the two Casimir operators of the Poincaré group, which is the symmetry group of Minkowski spacetime. Its associated Lie algebra is given by

$$\begin{aligned} [P_\mu, P_\nu] &= 0 \\ [M_{\mu\nu}, P_\rho] &= i(\eta_{\mu\rho}P_\nu - i\eta_{\nu\rho}P_\mu) \\ [M_{\mu\nu}, M_{\rho\sigma}] &= i(\eta_{\mu\rho}M_{\nu\sigma} - \eta_{\mu\sigma}M_{\nu\rho} - \eta_{\nu\rho}M_{\mu\sigma} + \eta_{\nu\sigma}M_{\mu\rho}), \end{aligned} \tag{2.1}$$

where P_μ are the generators of translations, $M_{\mu\nu}$ are the generators of the Lorentz transformations and $\eta_{\mu\nu}$ is the Minkowski metric. Internal symmetries are symmetries whose generators commute with the generators P_μ and $M_{\mu\nu}$. In other words, these symmetries do not connect particles of different four-momentum or different spin. Ex-

amples are the well known gauge symmetries of QCD and QED. Using QCD as an example, the complete symmetry group of this theory is locally isomorphic to the direct products of the Poincaré group and the internal symmetry groups of QCD, which are compact Lie groups. The same is true for all other sectors of the standard model and the standard model itself. This raised the question, whether this is a coincidence or a general feature of nature. In 1976 Coleman and Mandula answered this question in favor of the latter [68]. They assumed several physical constraints but they also demanded that any symmetry group is a Lie group. By lifting the latter requirement, Haag, Łopuszański and Sohnius showed that there exists a nontrivial extension of the Poincaré group called supersymmetry [69].

Supersymmetry is a symmetry between fermions and bosons, which is generated by the fermionic generator \mathcal{Q} . The schematic action of this symmetry is

$$\mathcal{Q}|\text{Fermion}\rangle = |\text{Boson}\rangle, \quad \mathcal{Q}|\text{Boson}\rangle = |\text{Fermion}\rangle.$$

Any theory which is invariant under this symmetry is called supersymmetric. As explained earlier, this symmetry is a nontrivial extension of the Poincaré group with the schematic Super Poincaré algebra

$$\begin{aligned} \{\mathcal{Q}_\alpha, \mathcal{Q}_b\} &\sim P_\mu \\ [\mathcal{Q}_\alpha, P_\mu] &= 0 \\ [M_{\mu\nu}, \mathcal{Q}_\alpha] &\sim \mathcal{Q}_\alpha. \end{aligned} \tag{2.2}$$

From this algebra we conclude, that two states, which lie in the same supermultiplet, must have the same mass. Furthermore supersymmetry commutes with gauge symmetries, therefore all states which lie in a super multiplet will have the same electric and color charge.

2.2 Four-dimensional Model

We begin our discussion with the four-dimensional $\mathcal{N} = 1$ Super Yang-Mills theory (SYM) which is the supersymmetric extension of the four-dimensional Yang-Mills theory [70, 71]. The action of this model is given by

$$S = \int dx^4 \left(-\frac{1}{4} F_{MN}^a(x) F_a^{MN}(x) + \frac{i}{2} \bar{\lambda}^a(x) \Gamma^M (D_M \lambda)_a(x) \right). \tag{2.3}$$

The gamma matrices Γ_M form an irreducible representation of the four-dimensional Clifford algebra, while F_{MN} is the field strength tensor

$$F_{MN} = \partial_M A_N - \partial_N A_M - ig [A_M, A_N] \tag{2.4}$$

2. Theoretical Background

of the gauge fields A_M with gauge group $SU(N_c)$ ¹. The Majorana fermions λ transform in the adjoint representation of the gauge group, whose covariant derivative is given by

$$D_M \lambda = \partial_M \lambda - ig [A_M, \lambda]. \quad (2.5)$$

This action is invariant under the supersymmetry transformation

$$\begin{aligned} \mathcal{Q}^\alpha \lambda_\beta &= (\Gamma_{MN})^\alpha{}_\beta F^{MN}, & \bar{\mathcal{Q}}^\alpha \lambda_\beta &= 0, \\ \mathcal{Q}^\alpha \bar{\lambda}_\beta &= 0, & \bar{\mathcal{Q}}^\alpha \bar{\lambda}_\beta &= -(\Gamma_{MN})^\alpha{}_\beta F^{MN}, \\ \mathcal{Q}^\alpha A_M &= \frac{1}{2} \bar{\lambda}^\beta (\Gamma_M)_\beta{}^\alpha, & \bar{\mathcal{Q}}^\alpha A_M &= \frac{1}{2} (\Gamma_M)^\alpha{}_\beta \lambda^\beta, \end{aligned} \quad (2.6)$$

with $[\Gamma_M, \Gamma_N] = 4i\Gamma_{MN}$. Here we use a Weyl-valued supercharge \mathcal{Q} , which also appears in the superspace formalism of the theory. The reason is, that this form of the supersymmetry transformation is more suitable to calculate Ward identities in section 2.6.

Beside supersymmetry, this action is also invariant under chiral symmetry

$$\lambda \rightarrow e^{i\alpha\Gamma_5} \lambda, \quad \Gamma_5 = i\Gamma_0\Gamma_1\Gamma_2\Gamma_3. \quad (2.7)$$

In the quantum theory, instantons break this $U(1)_A$ symmetry down to \mathbb{Z}_{2N} . We find N physically equivalent vacua which are related by the discrete chiral rotations

$$\lambda \rightarrow \exp\left(i\frac{2n\pi}{N}\Gamma_5\right) \lambda, \quad n = 0, 1, 2, \dots, N-1. \quad (2.8)$$

We can make these different vacua visible in the action by introducing the so called theta term [72]

$$\frac{\Theta}{16\pi^2} \tilde{F}_{MN} F^{MN}, \quad \tilde{F}_{MN} = \frac{1}{2} \epsilon_{MNOP} F^{OP}, \quad (2.9)$$

where we used the four-dimensional total antisymmetric Levi-Civita tensor ϵ_{MNOP} to define the dual field strength tensor \tilde{F}_{MN} . Applying the chiral rotations (2.8), we find

$$\Theta \rightarrow \Theta - \frac{2n\pi}{N}. \quad (2.10)$$

If we combine this result with the fact, that the theta term is periodic in Θ with a period of 2π , we retrieve the N physically equivalent vacua. Furthermore the \mathbb{Z}_{2N} can be broken spontaneously to \mathbb{Z}_2 by a formation of a chiral condensate $\langle \bar{\lambda}\lambda \rangle \neq 0$. We find the breaking pattern

$$U(1)_A \xrightarrow{\text{instantons}} \mathbb{Z}_{2N} \xrightarrow{\langle \bar{\lambda}\lambda \rangle} \mathbb{Z}_2. \quad (2.11)$$

In lattice simulations for $\mathcal{N} = 1$ SYM, this spontaneous breaking was investigated [32].

¹In this work we consider $N_c = 2$ only.

The result shows that there exists a critical temperature below which the chiral symmetry is spontaneously broken, while it is restored above this critical temperature.

Since this theory describes the gauge sector of a supersymmetric standard model extension, one is interested in the low energy properties. For this energy region, we expect that the fermions and gauge fields form color neutral bound states. These states include mesons, glueballs and baryons. In contrast to QCD, we can also have color neutral bound states consisting of gauge fields and fermions. To get insight into the dynamics of these particles, Veneziano and Yankielowicz derived a low energy effective theory for $\mathcal{N} = 1$ SYM [36]. The idea of this approach is, that for low energies, a different set of degrees of freedom can be used to describe the theory. Of course this low energy effective theory has to reproduce some quantities of the theory, most important here are the anomalies of the theory. These anomalies also form a supermultiplet [38]. The resulting low energy effective action of $\mathcal{N} = 1$ SYM describes a system with a supermultiplet [36] shown in Table 2.1(a). We will call this multiplet VY-multiplet. It consists of a scalar meson a-f, a pseudoscalar meson a- η and a spin 1/2 bound state between a Majorana fermion and a gauge boson, called gluino-gluonball. The “a” in the meson names stands for adjoint. Since we have no fermion fields in the fundamental representation, we will drop the “a” in those names in the following. Since one would also expect glueballs in a confining non-abelian theory, Farrar, Gabadadze and Schwetz [38] improved this model. They added another super-multiplet which we call FGS-multiplet, depicted in Table 2.1(b). It contains a scalar glueball, a pseudoscalar glueball as well as a spin 1/2 gluino-gluonball. Due to free parameters in the effective action, the mass-hierarchy of these two multiplets varies in the literature [36–39]. Therefore a method which allows an explicit calculation of the masses of the states is desirable.

particle	spin	name	particle	spin	name
$\bar{\lambda}\gamma_5\lambda$	0	a- η	$F^{MN}F_{MN}$	0	0 ⁺⁺ glueball
$\bar{\lambda}\lambda$	0	a-f	$F^{MN}\epsilon_{MNRST}F^{RS}$	0	0 ⁻⁺ glueball
$F_{MN}\Sigma^{MN}\lambda$	$\frac{1}{2}$	gluino-gluonball	$F_{MN}\Gamma^M D^N\lambda$	$\frac{1}{2}$	gluino-gluonball

(a) VY multiplet

(b) FGS multiplet

Table 2.1: Multiplet structure of $\mathcal{N} = 1$ SYM theory as predicted by low energy effective actions [36, 38].

At low energies the $\mathcal{N} = 1$ SYM theory is strongly coupled. Hence we need non-perturbative methods. Here we will use Monte-Carlo simulations, which allow a direct measurement of the masses of bound states. While the main focus of this work are dimensionally reduced models, there exist already simulations for the four-dimensional model. As stated in the introduction, the lattice regularisation will break supersymme-

try (for a more in depth discussion see section 3.2). Fortunately, in the four-dimensional $\mathcal{N} = 1$ SYM, the only relevant operator that breaks supersymmetry is the fermion mass term

$$m_f \bar{\lambda} \lambda. \tag{2.12}$$

To be more precise, it breaks supersymmetry softly. An operator breaks supersymmetry softly if it breaks supersymmetry explicitly but does not generate unwanted quadratic divergences. In [73] this was proven for a large amount of operators. Coming back to the fermion mass term, it was shown that the supersymmetric limit and chiral limit of the lattice theory are reached for the same fermion mass fine-tuning [23]. Therefore the most natural choice would be to use Ginsparg-Wilson fermions in the simulations [24–26]. While these fermions implement chiral symmetry on the lattice, they are computationally very expensive. Another idea is to use Wilson fermions and recover supersymmetry via fine-tuning of m_f . This choice seems to be more efficient. Using the latter simulation strategy, the DESY-Münster collaboration investigated the mass spectrum [34]. They observed the formation of the VY-multiplet, consisting of both fermions and the gluino-gluonball. The 0^{-+} gluonball of the FGS-multiplet seems to be significantly heavier. The mass for the 0^{++} gluonball is within (large) errors the same as the f-meson. Still, due to mass mixing it is not clear, that the operator for the 0^{++} gluonball projects onto the right state. Therefore the formation of the FGS-multiplet was not observed yet.

The problem of mixing is a general problem, plaguing also the low energy effective method. Since for every state in the VY-multiplet there exists a state in the FGS-multiplet with the same quantum numbers, these states can mix. This mechanism of a quantum field theory requires appropriate consideration, if one wants to investigate the mass-hierarchy of the multiplets. Fortunately, as we will see in the results, in the two-dimensional $\mathcal{N} = (2, 2)$ theory, this problem is absent.

2.3 Kaluza-Klein Reduction

In this thesis we will use the Kaluza-Klein (KK) reduction to reduce the four-dimensional $\mathcal{N} = 1$ SYM theory to the $\mathcal{N} = (2, 2)$ SYM theory in two dimensions. The idea stems from Kaluza who showed that one can unify gravity and electromagnetism by reducing a five-dimensional gravity theory to four dimensions [74]. One important ingredient for this is, that the reduced theory does not depend on the fifth coordinate which is called the *cylinder condition*. In [75] Klein argued that this scenario is possible if the length of the fifth dimension is very small, making it undetectable by experiments of the time.

Nowadays the KK reduction has two interesting applications. One is to take the

original idea and apply it in quantum field theory, leading to the introduction of extra dimensions which is a possible scenario for physics beyond the standard model (see [76] and references therein). The other application is to use the KK reduction to find lower-dimensional supersymmetry models with extended supersymmetry from known supersymmetry models in higher dimensions.

2.3.1 Representations of Gamma matrices

The KK reduction of a model is independent of the choice of the gamma matrices but a specific choice makes the calculation much more convenient. For this calculation we chose the Majorana representation in Minkowski space

$$\begin{aligned}
 \Gamma_\mu &= \mathbb{1} \otimes \gamma_\mu, & \Gamma_2 &= i\sigma_1 \otimes \gamma_5, & \Gamma_3 &= i\sigma_3 \otimes \gamma_5, & \Gamma_5 &= \sigma_2 \otimes \gamma_5 \\
 \gamma_0 &= \sigma_2, & \gamma_1 &= i\sigma_3, & \gamma_5 &= \sigma_1 \\
 C_4 &= -\Gamma_0 = \mathbb{1} \otimes C_2, & C_2 &= -\gamma_0,
 \end{aligned} \tag{2.13}$$

where the matrices Γ_M are the four-dimensional gamma matrices and γ_μ are the two-dimensional ones. The Matrices C_4 and C_2 are the charge conjugation matrices in four and two dimensions respectively which are defined by the relation

$$C_4 \Gamma_M C_4^{-1} = -\Gamma_M^T \quad \text{and} \quad C_2 \gamma_\mu C_2^{-1} = -\gamma_\mu^T. \tag{2.14}$$

Using these matrices, we define the four-dimensional Majorana spinors λ and the two-dimensional Majorana spinors χ as those spinors, for which we have

$$\lambda = C_4 \bar{\lambda}^T \quad \text{and} \quad \chi = C_2 \bar{\chi}^T. \tag{2.15}$$

2.3.2 Reduction of the Model

We start the dimensional reduction by decomposing the four-dimensional Majorana spinor in two-dimensional spinors. For this we use the ansatz

$$\lambda = \sum_{r=1}^2 e_r \otimes \chi_r \tag{2.16}$$

where χ_r are spinors and e_r are vectors in \mathbb{R}^2 . Using (2.15) we get two conditions

$$\chi_r = C_2 \bar{\chi}_r^T \quad \text{and} \quad e_r^* = e_r. \tag{2.17}$$

2. Theoretical Background

We chose for the vectors $\{e_1, e_2\}$ the Cartesian basis of \mathbb{R}^2 . This leads to the decomposition of the four-dimensional Majorana spinor into

$$\lambda = \begin{pmatrix} \chi_1 \\ \chi_2 \end{pmatrix}, \quad (2.18)$$

where χ_1 and χ_2 are Majorana fermions as defined in (2.15).

Next we apply the KK reduction from four to two dimensions. Specifically, we implement the dimensional reduction as $\mathbb{R}^4 \rightarrow \mathbb{R}^2 \times \mathbb{T}^2$. More explicitly we choose to compactify the directions two and three, giving us the cylinder condition for any possible field f

$$\partial_M f = \begin{cases} \partial_\mu f & \text{for } M = 0, 1 \\ 0 & \text{for } M = 2, 3. \end{cases} \quad (2.19)$$

The first implication is that the fields A_2 and A_3 do not transform like a gauge field under gauge transformations any more but like a scalar field or a Majorana spinor in the adjoint representation

$$A_2 \rightarrow g^{-1} A_2 g + g^{-1} \partial_2 g \stackrel{(2.19)}{=} g^{-1} A_2 g \quad A_3 \rightarrow g^{-1} A_3 g. \quad (2.20)$$

As these fields transform as scalars under the two-dimensional Lorentz symmetry, they must become scalars in the two-dimensional theory. For this reason we will rename these fields as $A_2 = \phi_1$ and $A_3 = \phi_2$. Further we use (2.19) to dimensionally reduce the action. We start with the field strength tensor

$$F_{MN} F^{MN} = \begin{cases} F_{\mu\nu} F^{\mu\nu} & \text{for } M, N = 0, 1 \\ D_\mu \phi_n D^\mu \phi^n & \text{for } M = 0, 1; N = n + 1 = 2, 3 \\ -g^2 [\phi_m, \phi_n] [\phi^m, \phi^n] & \text{for } M, N = 2, 3, \end{cases} \quad (2.21)$$

where we retrieve the two-dimensional Yang-Mills Lagrangian, the kinetic term for the scalar fields and a potential for the scalar fields. The next term to reduce is the kinetic term for the Majorana fermions

$$\bar{\lambda} \Gamma^M D_M \lambda = \begin{cases} \bar{\lambda} \Gamma^\mu D_\mu \lambda & \text{for } M = 0, 1 \\ -ig \bar{\lambda} \Gamma^{m+1} [\phi_m, \lambda] & \text{for } M = m + 1 = 2, 3, \end{cases} \quad (2.22)$$

where we find the two-dimensional kinetic term of the fermions and a Yukawa interaction between the scalar fields and the fermions. We combine these results to get the

two-dimensional action

$$S = V_{\mathcal{T}} \int d^2x \operatorname{tr} \left\{ -\frac{1}{4} F_{\mu\nu} F^{\mu\nu} + \frac{i}{2} \bar{\lambda} \Gamma_{\mu} D^{\mu} \lambda - \frac{1}{2} D_{\mu} \phi_m D^{\mu} \phi^m + \frac{g}{2} \bar{\lambda} \Gamma_{1+m} [\phi^m, \lambda] + \frac{g^2}{4} [\phi_m, \phi_n] [\phi^m, \phi^n] \right\} \quad (2.23)$$

where $V_{\mathcal{T}} = \int dx_2 dx_3$ is the volume of the compactified space. We absorb this factor by rescaling the coupling $g \rightarrow \sqrt{V_{\mathcal{T}}} g$ which becomes dimensionful in the process. This is in accordance with our expectations for two dimensions. The dimensionful coupling will ensure that the theory is superrenormalizable as we show in section 4.1. Next we rescale the fields as

$$A_{\mu} \rightarrow \frac{1}{g} A_{\mu}, \quad \chi_r \rightarrow \frac{1}{g} \chi_r, \quad \phi_i \rightarrow \frac{1}{g} \phi_i, \quad (2.24)$$

leading to

$$S = \frac{1}{2g^2} \int d^2x \operatorname{tr} \left\{ -\frac{1}{2} F_{\mu\nu} F^{\mu\nu} + i \bar{\lambda} \Gamma^{\mu} D_{\mu} \lambda - D_{\mu} \phi_m D^{\mu} \phi^m + \bar{\lambda} \Gamma^{m+1} [\phi_m, \lambda] + \frac{1}{2} [\phi_m, \phi_n] [\phi^m, \phi^n] \right\}. \quad (2.25)$$

This form of the action is called the reducible action of the $\mathcal{N} = (2, 2)$ SYM theory in two dimensions, since we still have the four-dimensional representation of the gamma matrices instead of the natural two-dimensional representation in two dimensions. Along with these four-dimensional gamma matrices, we still have the four-dimensional Majorana fermions λ . We get the irreducible form by combining (2.13) and (2.18) with the action (2.25)

$$S = \frac{1}{2g^2} \int d^2x \operatorname{tr} \left\{ -\frac{1}{2} F_{\mu\nu} F^{\mu\nu} - D_{\mu} \phi_m D^{\mu} \phi^m + \frac{1}{2} [\phi_m, \phi_n] [\phi^m, \phi^n] + i \bar{\chi}_r \gamma^{\mu} D_{\mu} \chi_r - \bar{\chi}_r (i\sigma_1)^{rs} \gamma_5 [\phi_1, \chi_s] - \bar{\chi}_r (i\sigma_3)^{rs} \gamma_5 [\phi_2, \chi_s] \right\}. \quad (2.26)$$

Another form of this action can be achieved by combining the two Majorana spinors into a Dirac spinor

$$\psi = \frac{1}{\sqrt{2}} (\chi_1 + i\gamma_5 \chi_2), \quad \bar{\psi} = \frac{1}{\sqrt{2}} (\bar{\chi}_1 + i\bar{\chi}_2 \gamma_5), \quad (2.27)$$

and the two real scalar fields into a complex scalar field

$$\varphi = \phi_1 + i\phi_2. \quad (2.28)$$

Inserting these into (2.26) we find yet another form of this action

$$S = \frac{1}{g^2} \int d^2x \operatorname{tr} \left\{ -\frac{1}{4} F_{\mu\nu} F^{\mu\nu} + \frac{1}{2} (D_\mu \varphi)^\dagger (D^\mu \varphi) - \frac{1}{8} [\varphi^\dagger, \varphi]^2 + i \bar{\psi} \gamma^\mu D_\mu \psi - \bar{\psi} P_+ [\varphi, \psi] - \bar{\psi} P_- [\varphi^\dagger, \psi] \right\}, \quad (2.29)$$

where we introduced the chiral projection operators $P_\pm = (1 \pm \gamma_5)/2$. All three forms of the action are relevant for this work. The reducible action (2.25) is the starting point for the lattice formulation. The irreducible action (2.26) will be used to make the symmetries of the model more transparent. Lastly the formulation with the Dirac spinor is the starting point to compare our lattice simulations with results from other groups using \mathcal{Q} -exact lattice actions [43–45]. The basic idea of the latter approach is to retain a nilpotent supersymmetric charge on the lattice, which guarantees the recovery of the full supersymmetry in the continuum limit. The most basic constraint for this method is, that one needs an extended supersymmetry. Thus we can not apply it to the $\mathcal{N} = 1$ SYM model (2.3). Since $\mathcal{N} = (2, 2)$ SYM in two dimensions is the most simple supersymmetric Yang-Mills theory which allows this construction, much effort is used to investigate this model using the \mathcal{Q} -exact method [46–55, 57–60]. For a more detailed overview of this method, we refer the reader to the reviews [18–22].

2.4 Symmetries

The action, having three different forms (2.25), (2.26) and (2.29), has symmetries which we will explore here. Since the field content of these forms looks different, symmetries will look seemingly different. For this reason we will add to the symmetry group the label χ if it is a symmetry of the irreducible form of the action (2.26) and ψ if it is a symmetry of the form of the action with a Dirac spinor (2.29). We will not discuss the symmetries of the reducible model (2.25) since they look almost the same as for the irreducible model (2.26).

2.4.1 Lorentz symmetry

We started with a four-dimensional quantum field theory, which is invariant under the four-dimensional Lorentz symmetry. By applying the KK reduction we break this symmetry explicitly. Namely the fields do not depend on the compactified space (2.19), prohibiting rotations which relate the compactified space to the uncompactified space. We are left with the rotation in the compactified space $\mathrm{SO}(2)_R^\chi$, called R symmetry, and the Lorentz symmetry in the uncompactified space $\mathrm{SO}(1, 1)_L^\chi$. In the Euclidean

theory, the Lorentz symmetry will become an $SO(2)$ also. We find the pattern

$$SO(3, 1) \rightarrow SO(1, 1)_L^X \times SO(2)_R^X, \quad \Lambda_4 \rightarrow \begin{pmatrix} \Lambda_2 & 0 \\ 0 & R \end{pmatrix}, \quad (2.30)$$

where Λ_d ist the d -dimensional Lorentz transformation. To specify the action of these symmetries we have to look at the generators of these rotations. We start with the generator for the two-dimensional Lorentz symmetry

$$\Gamma_{01} = \frac{1}{4i} [\Gamma_0, \Gamma_1] = \frac{1}{4i} [\mathbb{1} \otimes \gamma_0, \mathbb{1} \otimes \gamma_1] = \mathbb{1} \otimes \frac{i}{2} \sigma_1, \quad (2.31)$$

where σ_1 is the generator for the two-dimensional Lorentz transformation. The generator for the rotations in the compactified space \mathbb{R}^2 is the first factor in

$$\Gamma_{23} = \frac{1}{4i} [\Gamma_2, \Gamma_3] = \frac{1}{4i} [\sigma_1 \otimes \gamma_5, \sigma_3 \otimes \gamma_5] = -\frac{1}{2} \sigma_2 \otimes \mathbb{1}. \quad (2.32)$$

The last step is to apply the symmetry transformations on the spinors (2.16). For the Lorentz symmetry we find

$$\exp\left(\frac{i}{2} \omega^{01} \Gamma_{01}\right) \sum_{r=1}^2 e_r \otimes \chi_r = \sum_{r=1}^2 e_r \otimes \exp\left(\frac{i}{2} \omega^{01} \gamma_{01}\right) \chi_r \quad (2.33)$$

showing that we get the expected result for the Lorentz symmetry from the discussion beforehand. Next we look at the R symmetry

$$\begin{aligned} \exp\left(\frac{i}{2} \omega^{23} \Gamma_{23}\right) \sum_{r=1}^2 e_r \otimes \chi_r &= \sum_{r=1}^2 \exp\left(\frac{i}{2} \alpha (\sigma_2)_{rs}\right) e^s \otimes \chi_r \\ &= \sum_{r=1}^2 (R(\alpha))_{rs} e^s \otimes \chi_r = \sum_{r=1}^2 e_r \otimes (R(\alpha))_{sr} \chi^s \end{aligned} \quad (2.34)$$

where we introduced the parameter $\alpha = -2\omega_{23}$ and the rotation matrix $R(\alpha)$ with the rotation angle α . The last equal sign is a result of the basis we have chosen for e_r . We find that the R symmetry relates the two Majorana flavours. In addition the R symmetry will also change the scalar fields non-trivially because it comes from the four-dimensional rotation which connects the gauge fields $A_2 \equiv \phi_1$ and $A_3 \equiv \phi_2$:

$$\tilde{A}_2 = (\Lambda_4)^{2M} A_M \xrightarrow{(2.30)} R(-2\alpha)^{2,n+1} A_{n+1}, \quad \tilde{A}_3 = (\Lambda_4)^{3M} A_M \xrightarrow{(2.30)} R(-2\alpha)^{3,n+1} A_{n+1}. \quad (2.35)$$

2. Theoretical Background

Consequently, the R symmetry will not affect the gauge fields A_0 and A_1 . We end up with the symmetry

$$\chi_r \rightarrow R(\alpha)_r^s \chi_s, \quad \phi_i \rightarrow R(-2\alpha)_i^j \phi_j \quad \text{and} \quad A_\mu \rightarrow A_\mu. \quad (2.36)$$

To calculate the action of this symmetry on the Dirac spinor ψ given in (2.27) we use

$$\sqrt{2}\psi = (1, 1) \begin{pmatrix} 1 & 0 \\ 0 & i\gamma_5 \end{pmatrix} \begin{pmatrix} \chi_1 \\ \chi_2 \end{pmatrix}. \quad (2.37)$$

Applying (2.36) on the Majorana fermions we find

$$\begin{aligned} (1, 1) \begin{pmatrix} 1 & 0 \\ 0 & i\gamma_5 \end{pmatrix} \begin{pmatrix} \chi_1 \\ \chi_2 \end{pmatrix} &\rightarrow (1, 1) \begin{pmatrix} 1 & 0 \\ 0 & i\gamma_5 \end{pmatrix} \begin{pmatrix} \cos(\alpha) & -\sin(\alpha) \\ \sin(\alpha) & \cos(\alpha) \end{pmatrix} \begin{pmatrix} \chi_1 \\ \chi_2 \end{pmatrix} \\ &= (\exp(i\alpha\gamma_5), \exp(i\alpha\gamma_5)) \begin{pmatrix} 1 & 0 \\ 0 & i\gamma_5 \end{pmatrix} \begin{pmatrix} \chi_1 \\ \chi_2 \end{pmatrix} \\ &= \exp(i\alpha\gamma_5) \sqrt{2}\psi. \end{aligned} \quad (2.38)$$

For the complex scalar field φ we have to replace γ_5 in the matrix of (2.38) with the identity, the Majorana fermions with the scalar fields and α with -2α . After this calculation, we find another form of the symmetry

$$\psi \rightarrow \exp(i\alpha\gamma_5) \psi \quad \varphi \rightarrow \exp(-2i\alpha) \varphi \quad \text{and} \quad A_\mu \rightarrow A_\mu. \quad (2.39)$$

We identify this symmetry as the chiral symmetry $U(1)_A^\psi$ for the Dirac spinor. This shows, that the chiral symmetry for the Majorana fermions is not equivalent to the chiral symmetry for the Dirac spinors. Therefore we will now look at the chiral symmetry of the Majorana fermions and its action on the Dirac fermion. We start with the action of the chiral symmetry on the Majorana fermions χ_r . Using the Majorana representation (2.13) we find

$$\exp(i\alpha\Gamma_5) \stackrel{(2.13)}{=} \exp(i\alpha\sigma_2 \otimes \gamma_5) = \cos(\alpha) \mathbb{1} \otimes \mathbb{1} + i \sin(\alpha) \sigma_2 \otimes \gamma_5, \quad (2.40)$$

which we use to represent the action of the chiral symmetry in matrix form for the vector of χ_r spinors

$$\begin{pmatrix} \chi_1 \\ \chi_2 \end{pmatrix} \rightarrow \begin{pmatrix} \cos(\alpha) & \sin(\alpha)\gamma_5 \\ -\sin(\alpha)\gamma_5 & \cos(\alpha) \end{pmatrix} \begin{pmatrix} \chi_1 \\ \chi_2 \end{pmatrix}. \quad (2.41)$$

To calculate the action on the Dirac spinor ψ , we have to use the replacement $\sin(\alpha) \rightarrow -\sin(\alpha) \gamma_5$ in (2.38) which results in

$$\psi \rightarrow \exp(i\alpha) \psi. \quad (2.42)$$

This shows that the chiral symmetry of the reducible model $U(1)_A^\chi$ becomes $U(1)_F^\psi$. Thus we find two different chiral symmetries. As we use Wilson fermions in our lattice formulation, we have to break one of them in our simulations. We have chosen to break the chiral symmetry for the Majorana fermions, as in the four-dimensional mother theory. Therefore we use a lattice formulation which does not break the chiral symmetry of the Dirac fermions. Further we should have no doublers in our simulation. According to the Nielsen-Ninomiya no-go theorem [77–79] this is not possible. Indeed we violate this theorem even for the Dirac fermions. The symmetry $U(1)_F^\psi$ is responsible for the conservation of the fermion number. This number is supposed to be conserved in the proof of the no-go theorem. Since we break this symmetry explicitly, the Nielsen-Ninomiya no-go theorem is not applicable and we can have chiral Dirac fermions on the lattice.

The same analysis for the \mathcal{Q} -exact formalism was done in [80]. They found that their approach also violates the $U(1)_F^\psi$ symmetry while keeping the chiral symmetry unbroken for ψ . In contrast to our formalism, they still have an unbroken supersymmetry.

2.4.2 Two-dimensional Supersymmetry

As already stated in the previous section, we have derived the $\mathcal{N} = (2, 2)$ SYM theory in two dimensions from the $\mathcal{N} = 1$ SYM theory in four dimensions. What we did not explain yet is the transition from $\mathcal{N} = 1$ to $\mathcal{N} = (2, 2)$ in the KK reduction. For this we make the same ansatz for the supersymmetry charge as for the Majorana fermions

$$\mathcal{Q} = \sum_{r=1}^2 e_r \otimes q_r. \quad (2.43)$$

Since the charge is a Majorana spinor we find the same decomposition conditions as for the fermions and again we choose the same basis for e_r . Next we have to introduce the supersymmetry transformation of the scalar fields. Since we did a simple relabeling, we must use the same transformations for the scalar fields as for the gauge fields in (2.6). We end up with

$$\mathcal{Q}^\alpha \phi_i = \frac{1}{2} \bar{\lambda}^\beta (\Gamma_{i+1})_\beta^\alpha \quad \text{and} \quad \bar{\mathcal{Q}}^\alpha \phi_i = \frac{1}{2} (\Gamma_{i+1})^\alpha_\beta \lambda^\beta. \quad (2.44)$$

Applying the decomposition on (2.6) and (2.44), we can project onto two different Majorana supersymmetry charges

$$\begin{aligned}
 q_1 \chi_1 &= \gamma_{\mu\nu} F^{\mu\nu} + i\gamma_\mu \gamma_5 D^\mu \phi_2 & q_2 \chi_1 &= i\gamma_\mu \gamma_5 D^\mu \phi_1 + i[\phi_1, \phi_2] \\
 q_1 \chi_2 &= i\gamma_\mu \gamma_5 D^\mu \phi_1 - i[\phi_1, \phi_2] & q_2 \chi_2 &= \gamma_{\mu\nu} F^{\mu\nu} - i\gamma_\mu \gamma_5 D^\mu \phi_2 \\
 q_1 A_\mu &= \frac{1}{2} \bar{\chi}_1 \gamma_\mu & q_2 A_\mu &= \frac{1}{2} \bar{\chi}_2 \gamma_\mu \\
 q_1 \phi_1 &= \frac{i}{2} \bar{\chi}_2 \gamma_5 & q_2 \phi_1 &= \frac{i}{2} \bar{\chi}_1 \gamma_5 \\
 q_1 \phi_2 &= \frac{i}{2} \bar{\chi}_1 \gamma_5 & q_2 \phi_2 &= -\frac{i}{2} \bar{\chi}_2 \gamma_5.
 \end{aligned} \tag{2.45}$$

The R symmetry introduced in the previous chapter is a symmetry which rotates the two different super charges into each other (see for example [7]). Applying this symmetry, we checked that this is the case, justifying the name R symmetry. A further decomposition of the two charges into two left-handed and two right-handed Majorana-Weyl charges is straight forward, explaining the name $\mathcal{N} = (2, 2)$ SYM theory (for details, see the next section).

2.5 Expected Mass Spectrum

In section 2.2 we already discussed the mass spectrum of the four-dimensional mother-theory. Here we want to do the same for the two-dimensional model. First we start with the irreducible representations of supersymmetry in two dimensions. This will tell us about the structure of the super-multiplet. Applying the dimensional reduction to the states of the four-dimensional multiplet, we find states which should fit into this structure.

The derivation of the super-multiplet follows closely [81], where we only focus on the case of $\mathcal{N} = (2, 2)$. In two dimensions, we can split the particles in two categories, left- and right-moving particles. Therefore it is natural to introduce new coordinates

$$z = x_1 + ix_2, \quad \bar{z} = x_1 - ix_2, \tag{2.46}$$

called light-cone coordinates. The advantage of these coordinates is that under Lorentz transformations with $\omega = \omega^{01}$ we find

$$\delta z = \omega z \quad \delta \bar{z} = -\omega \bar{z}. \tag{2.47}$$

Vectors V_μ in these coordinates take the form

$$V_z = \frac{1}{2} (V_0 + V_1), \quad V_{\bar{z}} = \frac{1}{2} (V_0 - V_1). \tag{2.48}$$

Next we have to concern ourselves with the possible types of spinors found in two-

dimensional Minkowski spacetime. It turns out, that we can have Dirac, Majorana, Weyl and Majorana-Weyl spinors. We can further classify a spinor as left- or right-moving. For a left-moving spinor ψ_+ we have $\partial_{\bar{z}}\psi_+ = 0$ while for a right-moving spinor ψ_- we have $\partial_z\psi_- = 0$.

This richness of different types of spinors is also seen for super charges. Let us start with a complex \mathcal{Q} . We can decompose this spinor into two Weyl spinors $\mathcal{Q}_{W,+}$ and $\mathcal{Q}_{W,-}$. They differ by their eigenvalues for γ_5 . We can further decompose every complex Weyl spinor into two real Majorana-Weyl spinors. These are the real and imaginary part of the Weyl spinor. Analogous we can decompose a Majorana spinor into two Majorana-Weyl spinors. Hence the most fundamental supercharge is of Majorana-Weyl type. This allows to label all supersymmetry algebras as (L, R) , where L and R count the amount of left-handed and right-handed Majorana-Weyl spinors respectively. We will use \mathcal{Q}_+ for left-handed Majorana-Weyl spinors and \mathcal{Q}_- for right-handed Majorana-Weyl spinors.

Introducing $M = M_{01}$, the two-dimensional Poincaré algebra in light-cone coordinates is given as

$$[P_z, M] = -P_z, \quad [P_{\bar{z}}, M] = P_{\bar{z}}. \quad (2.49)$$

The $\mathcal{N} = (2, 2)$ algebra for Majorana-Weyl supercharges without central charges reads

$$\begin{aligned} \{\mathcal{Q}_+^i, \mathcal{Q}_+^j\} &= 2i\delta^{ij}P_z, & [\mathcal{Q}_+^i, M] &= -\frac{1}{2}\mathcal{Q}_+^i, & [\mathcal{Q}_+^i, P_z] &= 0 \\ \{\mathcal{Q}_-^i, \mathcal{Q}_-^j\} &= 2i\delta^{ij}P_{\bar{z}}, & [\mathcal{Q}_-^i, M] &= \frac{1}{2}\mathcal{Q}_-^i, & [\mathcal{Q}_-^i, P_{\bar{z}}] &= 0 \\ \{\mathcal{Q}_+^i, \mathcal{Q}_-^j\} &= 0, & [\mathcal{Q}_+^i, P_{\bar{z}}] &= [\mathcal{Q}_-^i, P_z] = 0. \end{aligned} \quad (2.50)$$

The indices i, j differentiate between the two different left- and right-handed Majorana-Weyl supercharges, while the third row shows that the $(2, 2)$ supersymmetry algebra is just the sum of the $(2, 0)$ and $(0, 2)$ supersymmetry algebras.

In two dimensions particles are either right-moving or left-moving particles. This is a Lorentz invariant statement, which follows from (2.47). Consequently there is no rest frame for a particle if that particle has a non-zero momentum in any frame. This is in stark contrast to the four-dimensional case. Here one uses the rest frame to derive the multiplet structure of massive states. Hence we expect a different picture in two dimensions.

A left-moving particle can be described by fields with the form $\exp(-ik(x_0 + x_1))$ and the right handed particles with the form $\exp(-ik(x_0 - x_1))$. Therefore we find for the left-moving particles $P_z = -ik$ and $P_{\bar{z}} = 0$ and for right-moving particles $P_z = 0$ and $P_{\bar{z}} = -ik$. Since the supercharges commute with the operators P_z and $P_{\bar{z}}$, all states in a super-multiplet are either left- or right-moving. Here we exclude the combination $P_z = 0$ and $P_{\bar{z}} = 0$, because for this momentum configuration no physical states are

propagated. Thus they will decouple from the theory. A similar example are states of the two-dimensional QED. In this theory, the gauge condition and the equation of motion reduce the physical degrees of freedom to zero. Hence it does not admit any dynamics.

We will now consider a left-moving particle in our theory. The $(2, 2)$ algebra takes the form

$$\begin{aligned} \mathcal{Q}_+^i \mathcal{Q}_+^j &= \delta^{ij} k, & [\mathcal{Q}_+^i, M] &= -\frac{1}{2} \mathcal{Q}_+^i \\ \mathcal{Q}_-^i \mathcal{Q}_-^j &= 0, & [\mathcal{Q}_-^i, M] &= \frac{1}{2} \mathcal{Q}_-^i. \end{aligned} \quad (2.51)$$

Now we consider a state $|s\rangle$ with $M|s\rangle = s|s\rangle$. From (2.51) we conclude that the state $\mathcal{Q}_-^i|s\rangle$ will have norm zero. Since any physical state must have a positive norm, this state can not be part of the physical spectrum. Therefore we must have $\mathcal{Q}_-^i|s\rangle \equiv 0$. Consequently, the number of states in the multiplet is reduced and they form an irreducible representation of the $(2, 0)$ algebra. Out of the two Majorana-Weyl supercharges \mathcal{Q}_+^i , we form two complex Weyl supercharges

$$\mathcal{Q}_{W,+} = \frac{1}{2} (\mathcal{Q}_+^1 - i\mathcal{Q}_+^2) \quad \bar{\mathcal{Q}}_{W,+} = \frac{1}{2} (\mathcal{Q}_+^1 + i\mathcal{Q}_+^2), \quad (2.52)$$

which leads to a different algebra for the charges (the commutators with $P_z, P_{\bar{z}}$ and M do not change, because the new Weyl supercharges are just linear combinations of the Majorana-Weyl supercharges)

$$\mathcal{Q}_{W,+}^2 = \bar{\mathcal{Q}}_{W,+}^2 = 0, \quad \{\mathcal{Q}_{W,+}, \bar{\mathcal{Q}}_{W,+}\} = k \quad \mathcal{Q}_{W,+}^* = \bar{\mathcal{Q}}_{W,+}. \quad (2.53)$$

This is an algebra for fermionic creation and annihilation operators. For those we can build the state space by choosing the vacuum state as $\mathcal{Q}_{W,+}|s\rangle = 0$. Thus the super-multiplet is formed by the states

$$|s\rangle, \quad \bar{\mathcal{Q}}_{W,+}|s\rangle \quad (2.54)$$

together with their complex conjugates. For $s = -1/2$ we find a super-multiplet with two real spin 0 fields and a complex Weyl spinor with spin 1/2. The irreducible representation for a right-moving particle can be derived analogously, leading to the same particle content of the super-multiplet. Comparing this result with the four-dimensional $\mathcal{N} = 1$ SYM theory we find the same particle content for the super-multiplets. Therefore the straight forward application of the KK reduction on the four-dimensional particles will result in two independent and complete super-multiplets.

Using the equation of motion (this is possible, because the states in the super-multiplets are on-shell states) we find two different multiplets given in Table 2.2. The dimensional reduction of the gluino-gluon states leads to a complicated structure. In

our simulation we refrained from calculating the whole structure. Instead we looked at the components of these operators. The reason is, that this allows to improve the signal to noise ratio for all components independently. For the dimensionally reduced VY multiplet (upper super-multiplet in Table 2.2), the correlator for the gluino-gluon/scalarball state splits in the correlator for the gluino-gluon $\mathcal{O}_{gg} = F_{\mu\nu}\Gamma^{\mu\nu}\lambda$, the scalar-gluon $\mathcal{O}_{gs} = [\phi_1, \phi_2]\Gamma^{\mu\nu}\lambda$ and a cross correlator $\langle O_{gg}(x)O_{gs}(y) \rangle$. Since all these states are gauge and Lorentz invariant, we expect to observe them on the lattice. We will use their correlation function to derive their masses. This leaves us with a set of three mass spectra. The mass spectrum of the gluino-gluon/scalarball particle will be formed out of these three spectra. Here one has to be careful. Since the full correlation function is the sum of these three different correlation function, one could observe cancellation effects. Therefore the mass spectrum of the gluino-gluon/scalarball particle could be smaller than the raw sum of the these three spectra.

particle	spin	name
$\bar{\lambda}\Gamma_5\lambda$	0	η
$\bar{\lambda}\lambda$	0	f
$F_{\mu\nu}\Gamma^{\mu\nu}\lambda + 2i[\phi_1, \phi_2]\Gamma^{23}\lambda$	$\frac{1}{2}$	gluino-gluon/scalarball

particle	spin	name
$[\phi_1, \phi_2]F_{\mu\nu}$	0	gluon-scalarball
$F_{\mu\nu}F^{\mu\nu} - 2D_\mu\phi_m D^\mu\phi_m - 2[\phi_1, \phi_2]^2$	0	0^{++} -gluonball, scalarball
$F_{\mu\nu}\Gamma^\mu D_\nu\lambda - D_\mu\phi_m (i\Gamma^\mu[\phi^m, \lambda] + \Gamma^{m+1}D^\mu\lambda) - [\phi_m, \phi_n]\Gamma^{m+1}[\phi^n, \lambda]$	$\frac{1}{2}$	gluino-gluon/scalarball

Table 2.2: Two dimensional reduced super-multiplets for the $\mathcal{N} = (2, 2)$ theory. In the main body of the text we will call $F_{\mu\nu}\Gamma^{\mu\nu}\lambda$ the gluino-gluonball and $[\phi_1, \phi_2]\Gamma^{23}\lambda$ the gluino-scalarball.

The masses of these super-multiplets are not known. Still there are theoretical predictions [82, 83] and numerical results based on the discretized light cone quantisation [84, 85] which point to a massless state in the theory. As shown earlier, this will not change the particle content of the super-multiplet in contrast to the four-dimensional theory. On the other hand, the existence of a massless state could obfuscate the existence of spontaneous supersymmetry breaking [86, 87]. The existence of dynamical supersymmetry breaking has been conjectured in [88]. To investigate whether supersymmetry is broken or unbroken, one can employ anti-periodic boundary conditions for the fermions and measure the ground state energy [54]. For the \mathcal{Q} -exact formalism, no spontaneous breaking of supersymmetry was observed [56].

2.6 Ward Identities

Ward identities are useful relations between expectation values based purely on symmetry. Thus they allow to check, whether the theory has a certain symmetry. This is important, as our lattice formulation will break supersymmetry explicitly. Hence the Ward identities are violated in our results. Still, as we aim to restore supersymmetry in the continuum limit (see section 4.1), Ward identities must also be fulfilled in this limit. Thus they provide a check for the restoration of the supersymmetry.

The basic concept of Ward identities is the observation that

$$\langle \mathcal{Q}\mathcal{O} \rangle = 0, \quad (2.55)$$

where \mathcal{O} is an arbitrary operator (a more detailed analysis is done in section 4.3). For example if we choose $\mathcal{O} = A_\mu$ we find

$$0 = \langle \mathcal{Q}A_\mu \rangle = \langle \frac{1}{2} \bar{\lambda}^\beta (\Gamma_\mu)_\beta^\alpha \rangle = \langle \bar{\lambda}^\beta \rangle \frac{1}{2} (\Gamma_\mu)_\beta^\alpha, \quad (2.56)$$

which requires that the expectation value of a single Majorana field must vanish, as expected from Lorentz symmetry. Accordingly we can recover many useful constraints for the expectation values.

Here we want to focus on the bosonic Ward identity which is derived from the operator

$$\mathcal{O}_\alpha(x) = \text{tr}_c \left\{ \bar{\lambda}_\beta(x) (\Gamma^{MN})^\beta_\alpha F_{MN}(x) \right\}. \quad (2.57)$$

After this calculation we will derive three additional Ward identities which we get by restricting the sum over M and N to special cases. Since the operator consists of a Majorana fermion and a field strength tensor, we will get a relation between two expectation values. We start with applying the supersymmetry transformation on the fermionic part of the operator

$$\begin{aligned} & \text{tr}_c \left\{ (\mathcal{Q}^\alpha \bar{\lambda}_\beta(x)) (\Gamma_{MN})^\beta_\alpha F_{MN}(x) \right\} \\ &= \text{tr}_c \left\{ -(\Gamma^{RS})^\alpha_\beta (\Gamma^{MN})^\beta_\alpha F_{RS}(x) F_{MN}(x) \right\} \\ &= \text{tr}_c \left\{ -(\eta^{RM} \eta^{SN} - \eta^{RN} \eta^{SM}) F_{RS}(x) F_{MN}(x) \right\} \\ &= \text{tr}_c \left\{ -2F^{MN}(x) F_{MN}(x) \right\}, \end{aligned} \quad (2.58)$$

where we used that the gamma matrices and their antisymmetrized products form a complete basis in spinor space. Next we apply the supersymmetry transformation on

the bosonic part of the operator

$$\begin{aligned}
 & \text{tr}_c \left\{ \bar{\lambda}_\beta(x) (\Gamma_{MN})^\beta{}_\alpha (\bar{\mathcal{Q}}^\alpha F_{MN}(x)) \right\} \\
 &= \text{tr}_c \left\{ \bar{\lambda}_\beta(x) (\Gamma_{MN})^\beta{}_\alpha (D_M \bar{\mathcal{Q}}^\alpha A_N(x) - D_N \bar{\mathcal{Q}}^\alpha A_M(x)) \right\} \\
 &= \text{tr}_c \left\{ \bar{\lambda}_\beta(x) (\Gamma_{MN})^\beta{}_\alpha D_M (\Gamma_N)^\alpha{}_\gamma \lambda^\gamma(x) \right\} \\
 &= \text{tr}_c \left\{ \bar{\lambda}_\beta(x) \frac{1}{2i} (\Gamma^M \Gamma^N - \eta^{MN})^\beta{}_\alpha (\Gamma_N)^\alpha{}_\gamma D_M \lambda^\gamma(x) \right\} \\
 &= \text{tr}_c \left\{ -\frac{3}{2} i \bar{\lambda}_\alpha(x) (\Gamma^M)^\alpha{}_\gamma D_M \lambda^\gamma(x) \right\}
 \end{aligned} \tag{2.59}$$

where we made use of the Clifford algebra to rewrite Γ_{MN} . Combining these transformations leads to the bosonic Ward identity

$$\langle S_B \rangle = \left\langle \frac{1}{4} F^{MN}(x) F_{MN}(x) \right\rangle = -\frac{3}{8} \left\langle \frac{i}{2} \bar{\lambda}(x) \not{D} \lambda(x) \right\rangle = -\frac{3}{8} \langle S_F \rangle, \tag{2.60}$$

where we suppressed the color and spin trace. This is an on shell result for this theory. In [20] we see the same result for the off shell formulation, where one has to replace the factor $\frac{3}{8}$ with one half. The right hand side of this equation is proportional to the expectation value of the fermionic part of the action. We are able to calculate this term explicitly leading to the final version of this identity

$$\langle S_B \rangle = \frac{3}{2} (N_c^2 - 1) V = \frac{9}{2} V, \tag{2.61}$$

where we have given the explicit result for the gauge group $SU(2)$.

To derive the bosonic Ward identity we used an operator which involved a sum over the spacetime indices M and N . Explicitly written it reads

$$\mathcal{O}_\alpha(x) = \text{tr}_c \left\{ \sum_{M,N=0}^3 \bar{\lambda}_\beta(x) (\Gamma^{MN})^\beta{}_\alpha F_{MN}(x) \right\}. \tag{2.62}$$

By replacing the sum over M and N by partial sums we get projections onto summands of the bosonic Ward identity which are part of their own distinctive Ward identity. This is in accordance with the KK reduction of the action. We have chosen the replacements for $\{N, M\}$ being $\{n, m\}$ for W_1 , $\{\nu, \mu\}$ for W_2 and finally $\{m, \mu\}$ for W_3 . These Ward identities read

$$\begin{aligned}
 W_1 &= \frac{1}{2} \langle [\phi_1, \phi_2]^2 \rangle - \frac{i}{8} \langle \bar{\lambda} \Gamma_2 [\phi_1, \lambda] + \bar{\lambda} \Gamma_3 [\phi_2, \lambda] \rangle = 0, \\
 W_2 &= \frac{1}{4} \langle F_{\mu\nu} F^{\mu\nu} \rangle + \frac{i}{8} \langle \bar{\lambda} \Gamma_2 [\phi_1, \lambda] + \bar{\lambda} \Gamma_3 [\phi_2, \lambda] \rangle = \frac{3}{2}, \\
 W_3 &= \frac{1}{2} \langle D_\mu \phi^m D^\mu \phi_m \rangle = 3.
 \end{aligned} \tag{2.63}$$

2. Theoretical Background

The first Ward identity relates the scalar potential to the Yukawa term, while the second Ward identity does the same for the gauge potential. The sum of both would relate the scalar potential to the potential of the gauge fields. Finally the third Ward identity fixes the expectation value of the kinetic term of the scalars. In total we derived four different Ward identities. Because of the sum rule $W_1 + W_2 + W_3 = W_B$, only three of them are independent of the others.

Chapter 3

Lattice Formulation

In this chapter we will introduce concepts, methods and algorithms of lattice gauge theories. Of course we can not cover all details of this broad topic, thus we refer the interested reader to the textbook introductions like [89–91]. These books will also serve as the basis for most of the discussed topics in this section.

In this work, we want to investigate non-perturbative properties of the $\mathcal{N} = (2, 2)$ SYM theory in two dimensions, hence we make use of lattice calculations. These are based on the path integral formalism introduced by Feynman [92] and suggested in the work of Dirac [93]. The basic idea is to discretize the spacetime, which introduces the lattice spacing a , which we assume is constant in all directions. Defining our quantum field theory on this grid ensures it is well-defined. The reason is that the lattice spacing introduces a natural cut-off for the momentum, preventing the emergence of ultraviolet divergences. Afterwards we look at the limit $a \rightarrow 0$ to get the continuum physics. A detailed introduction into the topic is given for example in [94–96].

While the path integral formalism was originally developed as an analytical tool, we will use it to calculate physical observables on the computer. Starting with the work of Wilson [15], lattice calculations developed into one of the standard methods for non-perturbative calculations, providing predictions and insight into the non-perturbative features of strongly coupled theories. The standard example and most investigated theory is QCD.

Lattice calculations allow for a plethora of different algorithms, fermion types and error reduction techniques. These differ in computation time and physical properties. Thus we have to choose a sensible compromise between both. Another non-negligible part is the time used to implement the different algorithms. To alleviate this influence, we base our code on a C++ framework, which is mainly developed by Björn Wellegehausen.

In this chapter we will first discuss the analytical continuation of the two-dimensional $\mathcal{N} = (2, 2)$ SYM theory from Minkowski spacetime into Euclidean spacetime. Afterwards we discuss the failure of preserving supersymmetry on the lattice, as a result

of general features of the lattice. The main part of this chapter focuses on the lattice formulations we use. Here we start with an introduction of the rational Hybrid Monte Carlo algorithm, which is followed by the discretization of the action. Thereafter we introduce the one- and two-point functions which are the only observables calculated in this work. We conclude the chapter with an introduction of the smearing techniques we used and a presentation of the error estimation for our results.

3.1 Euclidean formulation

Quantum field theories are theories which unify quantum theory and special relativity. Thus they are usually formulated for the Minkowski spacetime. In contrast we have an Euclidean spacetime for lattice simulations. While we are able to formulate quantum field theories for this spacetime, they will differ from those in Minkowski spacetime. This is for example visible in the possible matter content. While four-dimensional Minkowski spacetime admits Majorana fermions, the four-dimensional Euclidean spacetime does not [97]. This seems to imply, that we can not have a four-dimensional quantum field theory defined on the lattice with Majorana fermions.

Fortunately this is not a problem for our simulations because we are interested in results for the quantum field theory with Minkowski spacetime anyway. To get these, we apply the Wick rotation [98]. The main idea is to calculate an analytical continuation of the theory, where we extend the time coordinate into the imaginary plane. Restricting ourselves to purely imaginary time only, we recover an Euclidean metric. Note that the resulting theory itself must not be a genuine quantum field theory, allowing for a larger class of theories. While the idea is simple, the actual continuation of a general quantum field theory is non-trivial. For example, it is not clear that results, calculated in the Euclidean spacetime, will hold in the Minkowski spacetime. In [99, 100], Osterwald and Schrader showed that this analytical continuation is possible for Euclidean correlators in a theory with Dirac fermions, if these correlators obey a set of conditions. An analogue analysis for a theory with Majorana fermions was done in [101–103]. The results showed that we can leave the action unchanged, if we enforce the Majorana condition $\bar{\lambda} = \lambda^T \mathcal{C}$ while breaking the reality condition $\bar{\lambda} = \lambda^\dagger$ in the Euclidean spacetime. Hence the resulting theory is not a genuine quantum field theory, as expected.

Applying the Wick rotation we get an overall negative sign for the action, leading to

$$S = \int d^4x \mathcal{L}, \quad \mathcal{L} = \text{tr} \left(\frac{1}{4} F_{MN} F^{MN} + \frac{1}{2} \bar{\lambda} \Gamma^M D_M \lambda \right) \quad (3.1)$$

where we introduced the four-dimensional Euclidean gamma matrices Γ_M .

Analogous to Minkowski spacetime, we may choose the representation

$$\Gamma_\mu = \mathbb{1} \otimes \gamma_\mu, \quad \Gamma_2 = \sigma_1 \otimes \gamma_5, \quad \Gamma_3 = \sigma_3 \otimes \gamma_5, \quad \Gamma_5 = -\sigma_2 \otimes \gamma_5, \quad (3.2)$$

with the two-dimensional Euclidean gamma matrices γ_μ . The KK reduction is analogous to section 2.3, resulting in

$$\mathcal{L} = \frac{1}{2g^2} \text{tr} \left\{ \frac{1}{2} F_{\mu\nu}^2 + (D_\mu \phi_m)^2 - \frac{1}{2} [\phi_m, \phi_n]^2 + \bar{\lambda} \Gamma^\mu D_\mu \lambda - i \bar{\lambda} \Gamma^{m+1} [\phi_m, \lambda] \right\}. \quad (3.3)$$

Again introducing the Dirac fermion ψ and the complex scalar ϕ we get the form

$$\begin{aligned} \mathcal{L} = \frac{1}{g^2} \text{tr} \left\{ \frac{1}{4} F_{\mu\nu}^2 + \frac{1}{2} (D_\mu \varphi)^\dagger (D^\mu \varphi) + \frac{1}{8} [\varphi^\dagger, \varphi]^2 \right. \\ \left. + \bar{\psi} \gamma^\mu D_\mu \psi + i \bar{\psi} P_+ [\varphi, \psi] + i \bar{\psi} P_- [\varphi^\dagger, \psi] \right\}. \end{aligned} \quad (3.4)$$

In the simulation we discretize the form (3.3) of the action, breaking the chiral symmetry of the reducible model.

3.2 Supersymmetry on the lattice

Supersymmetry is a non-trivial extension of the Poincaré algebra as discussed in section 2.1. Especially the relation

$$\{Q_\alpha, Q_\beta\} \sim P_\mu \quad (3.5)$$

is important for lattice calculations. Assuming we have a lattice formulation which is invariant under supersymmetry transformations, we could create infinitesimal translations on the lattice by applying two successive supersymmetry transformations. These will not leave the lattice theory invariant due to the discretized spacetime. Therefore our assumption must be wrong and supersymmetry must be broken on the lattice.

Another way to show that supersymmetry must be broken on the lattice makes use of the Leibniz rule. In the continuum we have

$$\partial(f \cdot g) = \partial f \cdot g + f \cdot \partial g \quad (3.6)$$

which on the lattice becomes

$$\begin{aligned} \partial(f(x) \cdot g(x)) &= \frac{f(x+a) \cdot g(x+a) - f(x) \cdot g(x)}{a} \\ &= \partial f \cdot g + f \cdot \partial g + \frac{(f(x+a) - f(x)) \cdot (g(x+a) - g(x))}{a}. \end{aligned} \quad (3.7)$$

Here we used the forward lattice derivative

$$\partial f(x) = \frac{f(x+a) - f(x)}{a}. \quad (3.8)$$

In the limit $a \rightarrow 0$ we recover the Leibniz rule but for fixed lattice spacing, we get an extra term. Now we apply a supersymmetry transformation on the lattice action $S = \int \mathcal{L}$ to find

$$S \rightarrow \int \left(\mathcal{L} + \sum \mathcal{O}_i^1 \partial_M \mathcal{O}_i^2 \right) \quad (3.9)$$

where \mathcal{O}_i^1 and \mathcal{O}_i^2 are theory dependent terms consisting of the fields. In the continuum, we can rewrite the sum as the total derivative $\partial_M S_M$, where S_M is the supercurrent. In contrast, on the lattice we are in general not able to do the same as the Leibniz rule is violated. Thus supersymmetry must be broken on the lattice.

A more careful analysis shows that both argument holds in general only for theories with one supersymmetry generator. For theories with more than one supersymmetry generator, there are lattice formulations which keep one of the generators conserved on the lattice [18–22]. Note that we refrained from these lattice formulations and used a more traditional lattice setup without any conserved supercharges.

Fortunately, the absence of supersymmetry in our lattice formulation will not be an insurmountable problem. Lets look for example at the chiral symmetry. The Nielsen-Ninomiya theorem states, that Wilson fermions do not allow for chiral symmetry on the lattice. Yet one can use them to simulate theories which possess this symmetry. This is possible because we are not interested in the lattice theory but its continuum limit, called the target theory. As we will discuss in section 4.1, our lattice formulation allows for a continuum limit, where we restore the full supersymmetry via fine-tuning of parameters. In principle this is possible for all supersymmetric theories, but in practice the large amount of fine-tuning parameters makes this strategy infeasible. Two exceptions are $\mathcal{N} = 1$ SYM in four dimensions and $\mathcal{N} = (2, 2)$ in two dimensions, which have only one relevant parameter.

3.3 Rational Hybrid Monte Carlo algorithm

The simulation of gauge theories on the lattice depends on the fact, that the Euclidean path integral is defined as

$$Z = \int \prod_i \mathcal{D}f_i e^{-S_E[f_i]}, \quad (3.10)$$

where f_i represents any fields given in the model and $S_E[f_i]$ the Euclidean action of the lattice theory. The measure $\mathcal{D}f_i$ is defined as

$$\mathcal{D}f_i = \prod_{x \in \Lambda} df_i(x), \quad (3.11)$$

where Λ is the set of lattice points. The expectation values of the theory are given by

$$\langle \mathcal{O} \rangle = \int \prod_i \mathcal{D}f_i \mathcal{O}(f_i) \frac{e^{-S_E[f_i]}}{Z}. \quad (3.12)$$

Discretizing the spacetime we have to solve a $|\Lambda| \cdot |f|$ dimensional integral, where $|\Lambda|$ is the number of lattice points and $|f|$ is the number of fields involved. For present-day lattice simulations $|\Lambda|$ is of the order $10^6 - 10^8$ showing that a direct numerical integration is not possible. To solve this problem, we realize that we can interpret $\rho[f_i] = \frac{e^{-S_E[f_i]}}{Z}$ as a probability distribution for real $S_E[f_i]$. This allows us to use the methods known from stochastic mechanics. Especially we can use Monte Carlo Methods, rewriting the expectation value as

$$\langle \mathcal{O} \rangle = \lim_{N \rightarrow \infty} \frac{1}{N} \sum_{i=1}^N \mathcal{O}(\mathcal{C}_i) \rho[f_i(\mathcal{C}_i)], \quad (3.13)$$

where we introduced configurations \mathcal{C}_i . A configuration is a set of fields values f_i and is distributed according to $\rho[f_i(\mathcal{C}_i)]$. The task for lattice calculations is to generate these configurations in an efficient algorithm. Note that $\rho[f_i]$ does not have to be real or positive, leading to the famous sign problem [104, 105]. In this case, we can not make use of (3.13). While there are solutions to solve or mitigate this problem, there is no general efficient algorithm to simulate theories with a sign problem. In the following we assume that we have no sign problem.

The general strategy to generate the configurations is called the Markov chain Monte Carlo method which is explained in detail in [89–91]. The basic idea is that we create our configurations successively, thus we can order them as $\mathcal{C}_0, \mathcal{C}_1, \mathcal{C}_2, \dots$. This allows to introduce the so-called Monte Carlo time which is just the index of the configurations. Now we recall that a configuration is just a set of the field values f_i . Therefore we can describe each set by a vector \vec{c} in a high-dimensional vector space \mathcal{V} . Introducing the Monte Carlo time for these vectors, we can replace the configurations \mathcal{C}_t with the variable $\vec{c}(t)$, which describes a trajectory in the space \mathcal{V} . Now let us focus how this trajectory is formed. In our simulations we demand that if we have the given configuration $\vec{c}(t)$ then $\vec{c}(t+1)$ must be chosen randomly. This process is called a stochastic process. To get a Markov chain (of first order), we demand that the random selection of a new configuration depends only on the current configuration. For further

analysis we introduce the two configurations $\vec{a}, \vec{b} \in \mathcal{V}$. We use them to define the transition probability T_{ab} , which is defined as the probability that we get $\vec{c}(t+1) = \vec{b}$, if we start with $\vec{c}(t) = \vec{a}$. This new quantity must meet two constraints

$$0 \leq T_{ab} \leq 1, \quad \sum_b T_{ab} = 1, \quad (3.14)$$

which guarantee this probability is well-defined. To discuss this randomness further we introduce the stochastic vector $\vec{p}(t)$, whose entry $p_a(t)$ is equal to the probability that $\vec{c}(t) = \vec{a}$. Again to have a well defined probability we must demand

$$0 \leq p_a(t) \leq 1 \quad \sum_a p_a(t) = 1. \quad (3.15)$$

Now we can use these vectors to analyse our stochastic process. Using the transition probabilities we find

$$p_b(t+1) = \sum_a p_a(t) T_{ab}. \quad (3.16)$$

This allows us to interpret T_{ab} as a matrix. Further a summation over b shows, that T maps stochastic vectors into stochastic vectors. Lastly we introduce the so-called fixed point \vec{F} , which is defined as

$$\vec{F} = \vec{F}T. \quad (3.17)$$

One can show that if we require the so-called detailed-balance condition

$$\sum_b p_b T_{ba} = \sum_a p_a T_{ab}, \quad (3.18)$$

the vector $\vec{p}(t)$ approaches a unique fixed point, whose entries are just $\rho[f_i]$. Hence the Markov chain with the detailed balance condition will guarantee the right result for an infinite long trajectory through \mathcal{V} . Of course in practice this is not possible. In this case one tries to estimate the so-called thermalisation time after which one approximately has reached the fixed point solution. Discarding this region of the Monte Carlo time, we try to generate enough configurations to get a good estimate of the expectation values. Interestingly the detailed-balance condition allows for a plethora of different T_{ab} , which lead to the different algorithms like Metropolis and the heath bath algorithm. Here we want to focus on the Hybrid Monte Carlo (HMC) algorithm [106], described in detail in [89–91]. The basic idea is to use molecular dynamics to create a new configuration. For this we introduce for every vector¹ x a conjugate momentum p , which we use to define the Hamiltonian

$$H(x, p) = \frac{p^2}{2} + S(x), \quad (3.19)$$

¹For the sake of simplicity we replaced all field variables $f_i(x)$ with a vector x , whose entries are the values $f_i(x)$.

where $S(x)$ is the lattice action. This allows to evolve this system in a fictitious time t_f . On the lattice we achieve this by integrating over

$$\frac{\partial x}{\partial t_f} = \frac{\partial H}{\partial p}, \quad \frac{\partial p}{\partial t_f} = -\frac{\partial H}{\partial x} \quad (3.20)$$

using different numerical algorithms. Since these introduce numerical errors, we have to introduce a second step after the integration, the so-called acceptance step. Calling the initial variables x_i and p_i and the variables after the integration x_f and p_f , we define the probability to accept a new configuration

$$A(x_i, p_i | x_f, p_f) = \min \{1, \exp(H(x_i, p_i) - H(x_f, p_f))\}. \quad (3.21)$$

We see that, if we could integrate without numerical errors, we would always accept the new configuration. Further the initial momenta p_i must be drawn randomly from a Gauss distribution. This is important to fulfill the detailed-balance condition, demanded earlier.

Having discussed the basic HMC algorithm, will now discuss its application to theories with fermions. Let us look for example at a gauge theory with the partition function

$$Z = \int \mathcal{D}\bar{\lambda}\mathcal{D}\lambda\mathcal{D}U \exp \{-S[U] - \bar{\lambda}D[U]\lambda\} \quad (3.22)$$

where λ are Dirac fermions, $D[U]$ is the lattice Dirac operator and U are link variables, which are parallel transporters along the links of the lattice. Using the analytical solution for the Berezin integral [107], we are left with an integral over the link variables

$$Z = \int \mathcal{D}U \det(D[U]) \exp \{-S[U]\}. \quad (3.23)$$

Since the calculation of the determinant of the lattice Dirac operator is computationally costly, we will use pseudofermions [108]. For this technique, we have to introduce the positive operator $\mathcal{M} = DD^\dagger$. Using the Γ_5 -hermiticity of the Dirac operator

$$D^\dagger = \Gamma_5 D \Gamma_5 \quad (3.24)$$

and ignoring a potentially negative sign we find

$$\det(D) = \det(DD^\dagger)^{\frac{1}{2}} = \det(\mathcal{M})^{\frac{1}{2}}. \quad (3.25)$$

Introducing N_{pf} complex valued bosonic fields ϕ , we can rewrite the determinant of the

Dirac operator as an exponential

$$Z = \int \mathcal{D}U \mathcal{D}\phi \exp \left\{ -S[U] - \sum_{i=1}^{N_{\text{pf}}} \phi_i^\dagger \mathcal{M}[U]^{-q} \phi_i \right\}, \quad (3.26)$$

where $q = 1/2N_{\text{pf}}$. In section 6.2, we will explicitly show, that $\det(D)$ is always positive in our simulations, justifying this approach. Still, the exact calculation of the inverse of \mathcal{M} is equally computational challenging as the calculation of the determinant. Hence the different Hybrid Monte Carlo algorithms use different approximations for the inverse of the Dirac operator. The polynomial HMC [109–111] uses a polynomial approximation while the rational HMC uses a rational approximation [112–115] given by

$$r(\mathcal{M}) = \mathcal{M}^{-q} \simeq \alpha_0 + \sum_{r=1}^{N_R} \alpha_r (\mathcal{M} + \beta_r \mathbb{1})^{-1}, \quad (3.27)$$

where N_R allows to set the accuracy of the approximation. The coefficients α_r and β_r can be calculated with the Remez algorithm [116–119] at the start of the simulation. At last one has to calculate the evolution of the pseudo fermions via the molecular dynamics. Here one has to solve

$$y_r = (\mathcal{M} + \beta_r \mathbb{1})^{-1} \phi_j, \quad (3.28)$$

which is still computationally challenging. This can be reduced by using a multishift conjugate gradient solver [120, 121] which solves (3.28) for all β_r simultaneously. Further we make use of the results presented in [122, 123]. There the authors modified the molecular dynamics part of the algorithms further. Introducing different discretizations for the fictitious time in the bosonic and fermionic parts of the action, they reduced the amount of inversions of \mathcal{M} while keeping the same numerical accuracy.

3.4 Discretization of the Action

One of the most important parts of any lattice simulation is the discretization of the action. Here we have different choices for the gauge action, the Dirac Operator and the covariant derivative of the scalars. All of them have different advantages and disadvantages. While we can not show that our choices are optimal, we think that they are sensible. We want to remind the reader, that we will discretize the action of the reducible model given in (3.3).

3.4.1 Bosons

In our simulation we use the tree-level Lüscher-Weisz action [124]

$$\hat{S}_G = \beta \left\{ c_0 \sum_p \text{tr} (\mathbb{1} - \Re U_p) + c_1 \sum_r \text{tr} (\mathbb{1} - \Re U_r) \right\} \quad (3.29)$$

where $c_0 = \frac{5}{3}$ and $c_1 = -\frac{1}{12}$. This action involves a sum over all positive oriented plaquettes $U_p(x)$ and all positive oriented rectangles of size 2×1 called $U_r(x)$. For the scalar sector of the action we expand the scalar fields in Lie-group elements $\phi_i = \phi_i^a T_a$, where we use the conventions

$$[T_a, T_b] = i f_{abc} T^c, \quad \text{tr} (T_a T_b) = \delta_{ab}. \quad (3.30)$$

We get

$$\hat{S}_S = \beta \left\{ \sum_{x,i} \left(\frac{m_s^2}{\beta} + d \right) \phi_i^2(x) - \sum_{x,\mu,i} \phi_i(x + \vec{\mu}) U_\mu^A(x) \phi_i(x) + \frac{1}{4} \sum_{x,i,j} \phi_i^a(x) \phi_j^b(x) \phi_i^c(x) \phi_j^d(x) f_{abe} f_{cde} \right\}, \quad (3.31)$$

where $\vec{\mu}$ is the unit vector in μ direction on the lattice, U^A are the link variables in the adjoint representation

$$(U_\mu^A)^{ab} = \text{tr} (T^a U_\mu^{-1} T^b U_\mu) \quad (3.32)$$

and m_s^2 is the scalar mass term, which we will discuss in detail in sections 4.1 and 4.2. Further we used the forward difference

$$D_\mu^f \phi_i(x) = \phi_i(x + \vec{\mu}) - U_\mu^A(x) \phi_i(x) \quad (3.33)$$

for the kinetic term of the scalar fields.

3.4.2 Fermions

As shown in the previous section, after solving the Berezin integral, we got rid of the fermion fields in the partition function. Yet there are several different lattice fermion types. We can discern them by their Dirac operator. Since we want to simulate a supersymmetric theory, we have to keep the number of fermionic and bosonic degrees of freedom the same. Otherwise we would break the supersymmetry further. Therefore

we have chosen the doubler free Wilson fermions. This leads to the fermion action

$$\hat{S}_F = \frac{\alpha}{2} \bar{\lambda} \left(D_W [U^A] + m_f + \Gamma_a^E \phi_a^i \hat{f}_i \right) \lambda = \frac{\alpha}{2} \bar{\lambda} (D [U^A]) \lambda, \quad (3.34)$$

where $D_W [U^A]$ is the usual Wilson Dirac operator and m_f is the fermion mass. The matrices $\left(\hat{f}_i \right)_{jk} = f_{ijk}$ are formed from the structure constants of the gauge group. They appear due to the Yukawa interactions. We proceed by integrating out the fermions. Since we have Majorana fermions we get the Pfaffian

$$\int D\bar{\lambda} D\lambda e^{-S_F} = \text{Pf} (CD [U^A]), \quad (3.35)$$

where C is the charge conjugation matrix. Using the properties of the Dirac operator, one can show that all eigenvalues come in complex conjugated pairs and are double degenerated [27], meaning that the determinant is positive. Further $\text{Pf}^2 (CD) = \text{Det} (CD)$ and so we have a real but not necessary positive Pfaffian. This is a potential shortcoming for the lattice theory because we could have a sign problem. Simulations in the four-dimensional $N = 1$ SYM theory found that this sign problem is mild in the interesting region of the lattice theory [28, 30]. Since this could change in the dimensionally reduced theory, we have to monitor the sign in our lattice simulation.

3.5 One- and two-point functions

As written in section 3.3 we want to calculate expectation values. In this work these will be one- and two-point functions. Let us start with one-point functions. Given an observable $\mathcal{O}(x)$ defined at a lattice point x , a one-point function is the expectation value

$$\langle \mathcal{O}(x) \rangle. \quad (3.36)$$

Since the lattice action is invariant under discrete translations, this observable can not be dependent on a lattice point. This allows to increase the statistics, by averaging over the whole lattice

$$\langle \mathcal{O}(x) \rangle = \langle \mathcal{O} \rangle = \frac{1}{|\Lambda|} \sum_{x \in \Lambda} \langle \mathcal{O}(x) \rangle. \quad (3.37)$$

Two point functions allow for more variation. They are defined as

$$C(x, y) = \langle \mathcal{O}_1(x) \mathcal{S} \mathcal{O}_2(y) \rangle, \quad (3.38)$$

where \mathcal{S} is an arbitrary constant matrix. The most common setup in our lattice simulations will be $\mathcal{O}_1 = \mathcal{O}_2$ and $\mathcal{S} = \mathbb{1}$. Still our theory allows for gauge invariant fermionic operators \mathcal{O}_i , for which we can choose the gamma matrices for \mathcal{S} . An example for this is the gluino-glueball. In all these cases, we will do a zero momentum projection in the spatial direction. We use it, to calculate correlation functions depending on the time alone

$$\mathcal{O}_i(x_0 = t) = \frac{1}{N_s} \sum_s \mathcal{O}_i(t, x_1 = s), \quad C(t) = \frac{1}{N_t} \sum_\tau \langle \mathcal{O}_1(\tau + t) \mathcal{S} \mathcal{O}_2(\tau) \rangle. \quad (3.39)$$

Again we make use of the translation invariance, by averaging over all possible values of the time τ . Next we have to introduce the connected two point function

$$C_c(t) = \sum_\tau \langle \mathcal{O}_1(\tau + t) \mathcal{S} \mathcal{O}_2(\tau) \rangle - \sum_\tau \langle \mathcal{O}_1(\tau + t) \rangle \mathcal{S} \langle \mathcal{O}_2(\tau) \rangle. \quad (3.40)$$

For simplicity we choose now $\mathcal{O}_1 = \mathcal{O}_2$ and $\mathcal{S} = \mathbb{1}$. In this case we find in the asymptotic behavior [125]

$$\lim_{\beta \rightarrow \infty} C_c(t) = \sum_i C_i e^{-m_i t}, \quad (3.41)$$

where $C_i = |\langle 0 | \mathcal{O}_1 | i \rangle|^2$ is the overlap of the operator \mathcal{O}_1 with state $|i\rangle$ and m_i is the mass of state $|i\rangle$. Thus we can use two-point functions to derive the mass of states on the lattice. Lastly we have to look at the special case of fermions. Since we want to integrate them out, we have to take special care for observables which include them. Once again we use the Berezin integral which translates into the Wick theorem [126] for fermions. In our simulations we have correlation functions containing at most four fermion fields. Introducing an arbitrary gamma Matrix Γ we find

$$\begin{aligned} \langle \bar{\lambda}(x) \Gamma \lambda(x) \rangle_c &= \langle \text{tr}(\Gamma D^{-1}(x, x)) \rangle \\ \langle \bar{\lambda}(x) \Gamma \lambda(x) \bar{\lambda}(y) \Gamma \lambda(y) \rangle_c &= - \langle \text{tr}(\Gamma D^{-1}(x, y) \Gamma D^{-1}(y, x)) \rangle \\ &\quad + \langle \text{tr}(\Gamma D^{-1}(x, x)) \text{tr}(\Gamma D^{-1}(y, y)) \rangle \\ &\quad - \langle \text{tr}(\Gamma D^{-1}(x, x)) \rangle \langle \text{tr}(\Gamma D^{-1}(y, y)) \rangle. \end{aligned} \quad (3.42)$$

In case of the four fermion term, we will call the first term on the right hand side the connected part and the two other terms the disconnected part. This is motivated by a diagrammatic interpretation of these contributions. Furthermore these results show that we have to perform inversions of the Dirac operator again. Albeit we can use very efficient algorithms to calculate the inverse of the Dirac operator, this inversion is still the bottleneck of our computations. In our case we use the following setup. For the inversion of the Dirac operator we use the incremental eigCG algorithm of Stathopoulos and Orginos [127]. For $D^{-1}(x, y)$ and $D^{-1}(x, x)$ we use two different strategies. We

calculate the former with the so called point sources. These are defined at a random lattice point y_{ps} , for which we invert $D_{\alpha\beta_{\text{ps}}}^{ab_{\text{ps}}}(x, y_{\text{ps}})$ for all possible combinations of b_{ps} and β_{ps} , which are the color and spin degrees of freedom of the fermion field at the lattice point y_{ps} . Thus we have reduced the inversion of the whole Dirac operator to the calculation of columns of the inverse Dirac operator. While this approach reduces the computational cost, it is still too costly for $D^{-1}(x, x)$. In this case we try to estimate the inverse of the Dirac operator over the whole lattice by using the so called stochastic estimators, introduced in [128–130]. To be more specific about the simulation setup, we use eight point sources and 1000 stochastic estimators.

3.6 Smearing

3.6.1 Low-Pass Filter

The goal of lattice simulations is to calculate expectation values of stochastic variables. These are determined by their probability distribution. In a lattice calculation, we can only get estimates of these, due to the finite number of configurations. The difference between both is a stochastic variable itself, whose mean is zero. Its variance is usually linearly dependent on the variance of the original stochastic variable and inversely proportional to the square root of the number of configurations, used to calculate the estimate. While we can influence the latter, the former is fixed. Therefore, to get a better estimate of the mean value for a given stochastic variable, we can only increase the amount of configurations created in our simulation. Even this strategy is infeasible in the long run, as the computational cost always increase by a factor of 100 for one digit more precision. Thus there are observables (described by stochastic variables), for which we need a different strategy. In these cases we try to replace the original stochastic variable with a new one, which has the same expectation value but a much smaller variance.

To construct these replacements, let us recall (3.41). Here we saw, that we can extract the mass of any state, as long as our observable has a non-zero overlap with the state in question, meaning the same quantum numbers. Further, we observe that the states with high mass decay quickly. Since we can only identify states whose contribution is visible for several time points t in the correlation function, we can not distinguish them from noise (statistical fluctuations). This realisation leads to a strategy to improve our results. If we construct observables which have less or no overlap with high energy states, we can improve the signal to noise ratio for the low energy states of the theory.

For scalar fields we use a quite common idea, the low pass filter, for example outlined

in [131]. Using the Laplacian we define a new scalar field

$$\tilde{\phi}(x) = \phi(x) + \Delta\phi(x). \quad (3.43)$$

To investigate the spectral properties of $\tilde{\phi}$ we perform a Fourier transform of this equation and rearrange the terms to get

$$\frac{\tilde{\phi}(p)}{1+p^2} = \phi(p). \quad (3.44)$$

We see that in the scalar field $\tilde{\phi}$, contributions from large momenta will be suppressed. Since this corresponds to high energies, we achieve the desired effect. One can redo this process several times to improve the result further. Another idea is to introduce a tunable prefactor for the Laplacian, which allows to control the strength of the suppression of the high modes.

On the lattice we have to use a discretized version

$$\phi_{i+1}(x) = \phi_i(x) + \epsilon \sum_{\mu} (\phi_i(x + \vec{\mu}) + \phi_i(x - \vec{\mu}) - 2\phi_i(x)), \quad (3.45)$$

where we introduced the scalar field ϕ_i which we get after i applications of our algorithm and ϵ is the tunable prefactor of the Laplacian. We see that $\phi_1(x)$ has only contributions from the nearest neighbors, while we get contributions from the next to nearest neighbors for $\phi_2(x)$. The reason is that the sum for $\phi_1(x + \vec{\mu})$ contains $\phi_0(x + 2\vec{\mu})$. Thus, every application of (3.45) will increase the number of contributing original scalar fields ϕ_0 . Algorithms of this kind are called smearing, as we “smear” the scalar field over the neighboring lattice patch. Subsequently an application of formula (3.45) is called a smearing step and ϵ smearing parameter. Lastly we introduce the smearing level S which is the product of the smearing parameter and the amount of smearing steps. For small ϵ , we can use the Taylor expansion, to show that the physical properties of the resulting smeared scalar field only depend on the smearing level and not on the specific combination of smearing steps and smearing parameter. In our simulations, we got mixed results for this technique. While we saw the improvement of the signal to noise ratio on small lattices, on larger lattices it seemed absent. Since the small lattices are plagued by large finite volume lattice artifacts, we would like to find a better smearing algorithm, which also improves the signal-to-noise ratio for the large lattices.

3.6.2 APE Smearing

Having introduced smearing for the scalar fields, we want to use smearing also for the link variables. Unfortunately, they live on the links of the lattice, making the formula (3.45) not applicable. This problem was solved by the APE collaboration [131]. They introduced the smearing step

$$U_\mu^{i+1}(x) = (1 - s) U_\mu^i(x) + \frac{s}{6} \sum_{\nu \neq \mu} C_{\mu\nu}^i(x) \quad (3.46)$$

with

$$C_{\mu\nu}^i = U_\nu^i(x) U_\mu^i(x + \vec{\nu}) U_\nu^{i\dagger}(x + \vec{\mu}) + U_\nu^{i\dagger}(x - \vec{\nu}) U_\mu^i(x - \vec{\nu}) U_\nu^i(x - \vec{\nu} + \vec{\mu}) \quad (3.47)$$

and the real smearing parameter s . As they have shown, this smearing works like a low pass filter for the link variables. Unfortunately this smearing procedure does not always project $SU(N)$ link variables back to $SU(N)$ link variables. In the case of $SU(2)$ we do not encounter this problem, while it would be present for $SU(3)$.

3.6.3 Stout Smearing

Another smearing algorithm for link variables is Stout smearing [132]. The smearing step is defined by

$$\begin{aligned} U_\mu^{i+1}(x) &= e^{iQ_\mu^i(x)} U_\mu^i(x) \\ Q_\mu^i(x) &= \frac{i}{2} \left(\Omega_\mu^{i\dagger}(x) - \Omega_\mu^i(x) - \frac{1}{3} \text{tr} \left[\Omega_\mu^{i\dagger}(x) - \Omega_\mu^i(x) \right] \right) \\ \Omega_\mu^i(x) &= \left(\sum_{\nu \neq \mu} \rho_{\mu\nu} C_{\mu\nu}^i(x) \right) U_\mu^{i\dagger}(x), \end{aligned} \quad (3.48)$$

where the $C_{\mu\nu}^i$ are the same as for the APE smearing, and $\rho_{\mu\nu}$ are weights, the equivalent of the smearing parameter. In this work we have chosen

$$\rho_{\mu\nu} = \begin{cases} s, & \text{for } \mu = \nu = 1 \\ 0, & \text{else.} \end{cases} \quad (3.49)$$

The main advantage of this smearing compared to APE smearing is that it is differentiable, making it applicable in the HMC algorithm. In our simulations we apply the Stout smearing for observables only, ranging from very low to very high smearing levels.

3.6.4 Jacobi Smearing

For fermions the idea of improving the measurement comes from another direction. Till now, we represented fermions as point-like objects on the lattice, in contrast to the continuum, where we expect them to have a spatial distribution. Hence we should be able to improve our overlap with the fermion state in question, by providing a more realistic spatial distribution of the fermions. For this we introduce a smeared fermion

$$\tilde{\lambda}(t, s_0) = \sum_s S(t, s_0, s) \lambda(t, s), \quad (3.50)$$

where S is a smearing function. There are several different possibilities to choose S , some are not even gauge-invariant. Here we have chosen Jacobi smearing [133, 134]. In this case, we have the gauge covariant smearing function

$$S(t, s_0, s) = \iota \left(U_\mu(t, s) \delta_{s_0, s+1} + U_\mu(t, s-1)^\dagger \delta_{s_0, s-1} \right), \quad (3.51)$$

where ι is a smearing parameter again. Analogue to the scalar and gauge field smearing, we can apply this smearing successively to improve the result. We make use of this in our simulations, where we apply five smearing steps with a smearing parameter of 0.2. This setup was the best, to improve the signal to noise ratio of the meson correlation functions.

3.7 Error estimation

At last we have to discuss, how we estimate the errors of our observables. Since we use Monte Carlo methods, we can imagine our simulation as a measurement. The value of an observable on a single configuration can be seen as a sample. Then, the error of the observable would be estimated using the usual standard error. Unfortunately this approach will most likely fail. The reason are the Markov chains. Since we use an old configuration to generate a new configuration, we can not claim, that both are stochastically independent. This is not even possible for the configurations \mathcal{C}_i and \mathcal{C}_j for $|i - j| > 1$. We can measure this dependence with the so called autocorrelation. Fortunately for lattice simulations, it decreases with increasing distance $|i - j|$. In practice, a calculation of the autocorrelation time is too computationally expensive, especially as the autocorrelation time also depends on the simulation parameters. Fortunately, we can use an alternative, the so-called binning techniques. They allow to give good estimates for the observable and the errors of our observables. In our simulations we use the Jackknife resampling method [135–137]. In the following we follow [90]. First we partition the data into N_b equal sized bins of size B . On the i -th bin we calculate the expectation value of the observable called $\langle \tilde{\mathcal{O}}_i \rangle$. Calculating their variance, we

can interpret them as stochastically independent, if it is proportional to $1/B$. These new N_b expectation values form the new data set for the Jackknife resampling. Using these, we calculate a new set of expectation values again

$$\bar{\mathcal{O}} = \frac{1}{N_b} \sum_{i=1}^{N_b} \langle \tilde{\mathcal{O}}_i \rangle, \quad O_n = \frac{1}{N_b - 1} \sum_{i=1, i \neq n}^{N_b} \langle \tilde{\mathcal{O}}_i \rangle. \quad (3.52)$$

The idea of resampling is visible in the second formula. We create new data sets by omitting the n -th member of the set of expectation values. After calculating the mean O_n on every new set, we can estimate the variance for our expectation value $\bar{\mathcal{O}}$

$$\sigma_{\bar{\mathcal{O}}}^2 = \frac{N - 1}{N} \sum_{n=1}^N (O_n - \bar{\mathcal{O}})^2. \quad (3.53)$$

As the final result we quote $\langle \mathcal{O} \rangle = \bar{\mathcal{O}} \pm \sigma_{\bar{\mathcal{O}}}$. A special case in our results are functional fits, which connect different simulation setups, e.g. different β, m_s, m_f, \dots . For these we usually employ data from simulations with a small amount of configurations. To apply the Jackknife method, we would have to increase the number of configurations of these simulations by a factor of twenty, which is computationally expensive. Hence we refrained from resampling in this case and only quote the errors of the functional fits. Note that we still apply the Jackknife resampling for the fits of a single simulation (fixed β, m_s, m_f, \dots), especially for the fits to the correlation functions.

Chapter 4

Lattice Calculations

In the last chapter we presented the lattice formulation of our theory. Here we will analyze it theoretically. First we have to ensure that we extrapolate to the right continuum limit. For this we make use of two approaches. The first is a general analysis of the theory, identifying the relevant fine-tuning parameters. The second is a one-loop calculation, which also allows for a better understanding of the physical implications of our lattice setup. Furthermore the latter allows to calculate the correct fine-tuning value of the scalar mass term in the continuum limit. Another problem is the breaking of supersymmetry by the lattice regularization. As the Ward identities presented in section 2.6 are based on unbroken symmetries, we have to introduce modifications, leading to lattice Ward identities. Lastly we make a detour to the two-dimensional pure gauge theory. This is necessary to interpret our results for the glueball correlation function.

4.1 Fine-tuning of the lattice theory

In the chosen lattice formalism we break supersymmetry and chiral symmetry explicitly. Fortunately we are only interested in the target theory (the continuum limit of the lattice theory), in our case the $\mathcal{N} = (2, 2)$ SYM theory. Thus we do not have to preserve these symmetries on the lattice, if we restore them in the continuum limit. The only open question is how to achieve this. Since we simulate a quantum field theory, we have to consider quantum corrections. We will include them by looking at the effective action of the theory, which can be calculated from the classical action of the theory, by including all quantum effects. An introduction into this topic can be found in [138]. In our analysis, we follow the work of Sugino [80]. In general, the effective action of the lattice theory depends on the lattice volume and lattice spacing. Thus it allows to perform the continuum limit directly, which results in a specific target theory. Comparing it to the desired continuum theory, we can check the continuum limit. Unfortunately we are not able to calculate the effective action for most lattice

theories (otherwise lattice simulations would be unnecessary). Our simulation falls also into this category. Therefore we have to use approximations, like the loop expansion, to analyze the continuum limit of our lattice simulations.

Before we actually analyze our theory, we will introduce the concept of fine-tuning. For this we look at the most common example, lattice QCD with Wilson fermions. In this case one introduces a mass term which explicitly breaks chiral symmetry. While this term will vanish in the continuum limit ($V \rightarrow \infty$, $a \rightarrow 0$), it has severe consequences for the effective action of the lattice theory. Due to the absence of chiral symmetry, we get new possible terms in the effective action, breaking chiral symmetry explicitly.¹ One of these is $m_q \bar{\lambda} \lambda$, which introduces an additional mass term for the fermions. Since we are still discussing a lattice theory, m_q will depend on the lattice spacing and lattice volume. Thus we can distinguish two cases. The first is that this additional mass vanishes in the continuum limit. In this case we will call this operator irrelevant. In all other cases, it is relevant². In a lattice theory, almost all operators are irrelevant and we usually ignore them³ because they will not contribute in the continuum limit. Thus they will not change the target theory in contrast to the relevant operators. Let us keep the example of lattice QCD. In this case $m_q \bar{\lambda} \lambda$ is relevant, resulting in a target theory with broken chiral symmetry. To get a different result we have to perform a so called fine-tuning. The idea behind it is quite simple. By adding $m_f \bar{\lambda} \lambda$ to the action and requiring $m_q + m_f = 0$ for all lattice spacings and lattice volumes, we get rid of the operator proportional to $\bar{\lambda} \lambda$ in the effective action. Thus such a term will be also absent in the target theory. Since in QCD the only relevant operator is the fermion mass term, we restore chiral symmetry in the continuum limit. Unfortunately, while the basic idea is quite simple, the practical implementation is often not. As we usually can not calculate the effective action analytically, we have to search the point $m_q + m_f = 0$ in the whole parameter space of m_f , hence the name fine-tuning.

As stated above, the analytical calculation of the effective action is often not possible. Still one can analyze its structure, identifying the relevant operators. For this we make use of the limit $V \rightarrow \infty$. In this limit, all operators with mass dimension $d > d_0$ will vanish. The reason is that after integrating over spacetime and multiplying with a monomial of the gauge coupling, their contribution will be proportional to L^{d_0-d} , with $L^D = V$, where D is the spacetime dimension. Thus all relevant operators have mass dimension $d \leq d_0$. The value of d_0 depends on our action and D . In our case it is the action of the $\mathcal{N} = (2, 2)$ SYM theory in two dimensions, given in (2.25). The mass

¹Note that the emergence of such terms is also possible if the symmetry of the classical action is not broken. In this case quantum corrections break the symmetry, leading to the so called anomalous symmetries. Here we will ignore this case as it is not relevant for our model.

²In principle one has three kind of operators: irrelevant, marginal and relevant. Since we have to handle the last two in the same manner, we grouped them together in this work.

³Although the irrelevant operators play an important role in the Symanzik improvement program.

dimensions (denoted by $[\cdot]$) of the fields and the gauge coupling are

$$[A_\mu] = 1, \quad [\lambda] = 1.5, \quad [\phi] = 1, \quad [g] = 1. \quad (4.1)$$

These values differ from the usual values one gets by looking at the two-dimensional kinetic terms. The difference comes from a rescaling of the fields using the dimensionful coupling constant. We choose this convention, as it will simplify the discussion of the loop expansion of the effective action. In principle one could also use the mass dimensions, given by the standard kinetic terms of the fields. In this case, we would have to make use of the Feynman rules and diagrams, to conclude our results of the loop expansion. While we did not check this approach thoroughly, it seems to agree with the results presented below.

The determination of d_0 is best explained by an example. Let us look at a term of the form $g_2^c \int dx^2 \mathcal{O}$. It will scale as $L^{2-c-d_{\mathcal{O}}}$, with $d_{\mathcal{O}} = [\mathcal{O}]$, thus $d_0 = 2 - c$. Having established all necessary ingredients, we will now look at the loop expansion of the effective action. First we recall that apart from the fields we can also have derivatives in the terms of the effective action. This allows us to write the effective action in the loop expansion

$$S = \frac{1}{g_2^2} \int d^2x \mathcal{L}_0 + \int d^2x \partial_\mu^{r_1} A_\mu^{s_1} \phi^{t_1} \lambda^{u_1} + g_2^2 \int d^2x \partial_\mu^{r_2} A_\mu^{s_2} \phi^{t_2} \lambda^{u_2} + \dots \quad (4.2)$$

where we wrote all operators without regard of their actual structure but just the amount of fields and derivatives appearing. Following our discussion above, we find the constraints

$$\begin{aligned} r_1 + s_1 + t_1 + 1.5 \cdot u_1 &\leq 2 \\ r_2 + s_2 + t_2 + 1.5 \cdot u_2 &\leq 0. \end{aligned} \quad (4.3)$$

The second line, corresponding to two-loop order, can only be met by the identity operator. Since a constant shift does not affect the physics of the theory, we ignore it. For higher loop orders of the effective action, relevant operators must have a negative mass dimension, which is impossible. Thus we have only to fine-tune terms appearing at the one-loop order. Theories with this property are super-renormalizable. Since the effective action must have the quantum numbers 0^{++} , this must be also true for the extra terms appearing in the loop expansion. This leads to the constraint that u_1 and u_2 are multiple of two, since we need an even amount of fermions to construct a scalar operator. In Table 4.1 we give all relevant operators up to mass dimension two. Additionally we depict that $\bar{\lambda}\lambda$ is a mass dimension three operator, hence it is irrelevant and we restore chiral symmetry in the continuum limit without fine-tuning.

mass dimension	operators
0	$\mathbb{1}$
1	ϕ_i, A_μ
2	$\phi_i\phi_j, A_\mu A_\nu, \phi_i A_\mu, \partial_\mu\phi_i, \partial_\mu A_\nu$
3	$\bar{\lambda}\lambda$

Table 4.1: All relevant operators which can appear in the effective action of the lattice theory up to mass dimension two. Further we give the mass dimension for $\bar{\lambda}\lambda$.

Next we have to find the structure of the relevant operators. First we have $\text{tr}(\phi) = 0$, $\text{tr}(D_\mu\phi) = \partial_\mu\text{tr}(\phi) = 0$ and $\text{tr}(F_{\mu\nu}) = 0$. Further, using gauge invariance, all other terms which feature gauge fields must vanish. Therefore only the term with two scalar fields can be present. We can write down the general form as

$$\text{tr}_c \{ \phi^i \phi^j M_{ij} \} \quad (4.4)$$

where M_{ij} is a tensor which keeps the operator invariant under R symmetry. Since this is a $\text{SO}(2)$ symmetry, δ_{ij} and ϵ_{ij} are the only two independent tensors, from which we can build any invariant tensor. As M_{ij} is a rank two tensor, it must be a linear combination of both. Here we choose the two simplest cases: $M_{ij} = \delta_{ij}$ and $M_{ij} = \epsilon_{ij}$. The first leads to the scalar mass term

$$\text{tr}_c (\phi_i \phi^i), \quad (4.5)$$

while the second leads to a commutator

$$\text{tr}_c ([\phi_1, \phi_2]) = 0 \quad (4.6)$$

which vanishes under the color trace. We are left with only one relevant operator. Hence we must introduce the fine-tuning term

$$m_s^2 \phi_i \phi^i \quad (4.7)$$

into the action for the fine-tuning. We will call m_s^2 the scalar mass. We further introduce a mass term for the fermions

$$m_f \bar{\lambda}\lambda \quad (4.8)$$

into the action, for which we call m_f the fermion mass. While we saw that a $\bar{\lambda}\lambda$ term will vanish in the continuum limit, it will be present for a finite lattice spacing and lattice volume. Therefore we can use the fermion mass m_f to get rid of this term, reaching the chiral limit of the lattice theory. The reason for this additional fine-tuning is, that the

chiral symmetry plays an important role in the four-dimensional mother theory [23]. Thus we think that this importance will also be visible in the dimensional reduced model. Therefore this additional fine-tuning should improve our results for the target theory.

4.2 One-loop calculation

To get a better physical understanding of our simulated theory, we will look at the one-loop calculation of the effective action. Here we follow Suzuki and Taniguchi [64]. In this work the same calculation was done for a similar model, where the KK reduction is applied in the lattice theory instead of the continuum theory. Thus the scalar fields of their model are encapsulated in the link variables U_2 and U_3 . Since these variables are compact by construction, this theory should not suffer from the flat directions in the potential. Therefore both approaches to simulate this model will differ in the dynamics of the scalar sector, which could lead to different effects in the one-loop corrections to the theory. Especially the calculated scalar mass could differ. Note that Suzuki and Taniguchi claim, that a one-loop calculation is sufficient to calculate the scalar mass term in the continuum limit. This is in agreement with our discussion in the previous section.

In [64] Suzuki and Taniguchi did not only do the calculation for the lattice model but also for the continuum model. While they calculated two contributions to the effective action, we will focus here on the following one-loop contribution

$$\frac{1}{L} \left\{ - \sum_{p_f \neq 0} \frac{1}{p_f^2} + \sum_{p_b \neq 0} \frac{1}{p_b^2} \right\} \text{tr}_c \{ \Phi^2 + \Psi^2 \} \quad (4.9)$$

$$\Phi_{ab} = g f_{abc} \phi_1^c \quad \Psi_{ab} = g f_{abc} \phi_2^c,$$

where Φ and Ψ are related to the vacuum expectation values ϕ_1 and ϕ_2 , introduced later. Further we introduced the momenta of the fermionic degrees of freedom p_f and the momenta of the bosonic degrees of freedom p_b . The calculation of this result was done on a finite torus to regularize zero modes. Hence for the result of the full theory, one has to look at the infinite volume limit, introducing infinitely many momenta. Thus we need to regularize them. Choosing the same renormalization scheme for fermionic and bosonic momenta, we see a perfect cancellation at one-loop order. Any other choice would lead to a non-vanishing term, breaking the supersymmetry, which is clear, as we treat fermions and bosons differently. Here we see one of the advantages of supersymmetric theories, the cancellation of most quantum corrections, which leads to non-renormalization theorems [12, 13].

Now we want to calculate the same one-loop result for the lattice theory. First we have to expand the fields

$$A_\mu^a(x) = \sum_p \frac{1}{L} e^{ipx} \tilde{A}_\mu^a(p), \quad \phi_i^a(x) = \phi_i^a + \sum_p \frac{1}{L} e^{ipx} \tilde{\phi}_i^a(p), \quad \lambda_\mu^a(x) = \sum_p \frac{1}{L} e^{ipx} \tilde{\lambda}_i^a(p), \quad (4.10)$$

where the tilde symbols the fluctuations around the vacuum expectation values. Since we are doing calculations in a gauge theory, we have to fix the gauge. This allows that the scalar fields pick up a vacuum expectation value, while Lorentz symmetry prevents it in the case of the vector and spinor fields. We introduce the gauge fixing term

$$S_{\text{gf}} = -a^2 \sum_{x \in \Lambda} \sum_{\mu, \nu=0}^1 \lambda_0 \text{tr} \{ \partial_\mu^b A_\mu(x) \partial_\nu^b A_\nu(x) \} \quad (4.11)$$

into the action, where ∂_μ^b is the backwards difference operator. Further we have to expand the link fields on the lattice

$$U_\mu(x) = e^{aA_\mu}, \quad (4.12)$$

to recover the gauge fields. Lastly we have to mention, that we do the calculation for the standard Wilson action for the gauge fields instead of the Symanzik improved action used in the simulation. The reason is that the calculation will be simpler while leading to the same result. The improved action is reducing the lattice artifacts from discretizing, getting closer to the continuum limit. Hence the effective action of the target theory will be the same as for the lattice theory with the Wilson action. Now we insert the expansion into our lattice action and keep only the terms quadratic in the fluctuation fields. This leads to the result

$$\begin{aligned} S + S_{\text{gf}} = \frac{1}{2} \sum_p \left\{ \tilde{A}_\mu(-p) \left[\delta_{\mu\nu} \hat{p}^2 - (1 - \lambda_0) \frac{1}{a^2} (e^{iap_\mu} - 1) (1 - e^{-iap_\nu}) - \delta_{\mu\nu} \Phi^2 \right] \tilde{A}_\nu(p) \right. \\ + \tilde{\phi}_1(-p) \hat{p}^2 \tilde{\phi}_1(p) + \tilde{\phi}_2(-p) (\hat{p}^2 - \Phi^2) \tilde{\phi}_2(p) \\ + \tilde{A}_\mu(-p) \frac{1}{a} (e^{ip_\mu a} - 1) \Phi \tilde{\phi}_1(p) + \tilde{\phi}_1(-p) \frac{1}{a} (1 - e^{-ip_\mu a}) \Phi \tilde{A}_\mu(p) \\ \left. + 2\tilde{\lambda}(-p) (D_W(p) + m_f - i\Phi + \gamma_5 \Psi) \tilde{\lambda}(p) \right\} + \dots \quad (4.13) \end{aligned}$$

where we neglected Ψ and introduced the lattice momenta

$$\hat{p}_\mu = \frac{2}{a} \sin \left(\frac{1}{2} ap_\mu \right) \quad \check{p}_\mu = \frac{1}{a} \sin(ap_\mu) \quad (4.14)$$

and the Fourier transform of the free Wilson Dirac operator $D_W(p)$

$$D_W(p) = i\Gamma_{\mu}\hat{p}_{\mu} + \frac{1}{2}a\hat{p}^2. \quad (4.15)$$

After the gaussian integration over the fluctuations we end up with

$$\frac{2}{L^2} \sum_{p \neq 0} \left(\frac{1}{\hat{p}^2} - \frac{1 + \frac{1}{2}a^2\hat{p}^2}{\hat{p}^2 + \frac{a^2}{4}(\hat{p}^2)^2} \right) N_c \phi_1 \phi_1 \equiv m_{\text{ol}}^2 N_c \phi_1 \phi_1. \quad (4.16)$$

We see that we retrieved a term similar to (4.9), which does not vanish this time. The reason is that we have introduced Wilson fermions, which lead to different momenta for the fermions and the bosons. Unfortunately, this momentum difference is necessary to get rid of the doublers, which would introduce different amounts of fermionic and bosonic degrees of freedom, breaking supersymmetry as well. Another interesting aspect is that we recover the exact same result as in [64]. Comparing their expansion of $S + S_{\text{gf}}$ with ours, we see that one term is absent. On the other hand they have to introduce an extra term originating from the Jacobian. This is a result of their lattice formulation. Since their scalar fields are encapsulated in two link variables, they have to introduce a shift of the integration variables. Interestingly the associated Jacobian cancels exactly the term, which was absent in our lattice from the start. Hence we get the same result. Introducing the scalar mass term $m_s^2 \phi^2$ into the action will not change the one-loop calculation. Hence for $m_s^2 = -m_{\text{ol}}^2$, at one-loop, our lattice action will have the same effective action as the continuum result.

At last we have to calculate the value of m_s^2 . Assuming the continuum limit $V \rightarrow \infty, a \rightarrow 0$, one can replace the sum in (4.16) with an integral over continuous momenta from $-\pi$ to π , which converges to the final result [64]

$$m_s^2 = 0.65948225(8). \quad (4.17)$$

4.3 Ward Identities on the Lattice

The Ward identities derived in section 2.6 are based on the supersymmetry of the continuum action. Unfortunately the lattice regularization breaks this symmetry (see section 3.2), thus they will not hold anymore. In this chapter, we will derive similar quantities on the lattice, called lattice Ward identities. They serve as a signal for the restoration of supersymmetry. For their derivation, we will proceed as follows. First we introduce a new transformation for the lattice fields, which becomes the supersymmetry transformation in the continuum. Next we discuss the impact of the broken symmetry on the derivation of the Ward identities, leading to a modification stemming from the lattice regularization. Finally by combining both, we can get the aforementioned lattice

Ward identities.

We start with the would-be supersymmetry transformation on the lattice. If the only requirement for them would be, that it will become the supersymmetry transformation in the continuum limit, we could choose from a plethora of possible possibilities. To reduce this set, we impose two additional constraints, leading to our three final requirements:

1. The transformations become the continuum supersymmetry transformations in the continuum limit.
2. The transformations commute with the gauge transformations.
3. The transformation of the covariant derivative is the lattice equivalent of the continuum counterpart.

These are inspired from an analogous discussion in the four-dimensional mother theory [23, 29, 139–141]. All three requirements are met with the transformations

$$\begin{aligned}
 \bar{\mathcal{Q}}^\alpha U_\mu(x) &= U_\mu(x) \frac{a}{2} (\Gamma_\mu)^\alpha{}_\beta \lambda^\beta(x + \vec{\mu}) \\
 \bar{\mathcal{Q}}^\alpha U_\mu^\dagger(x) &= -\frac{a}{2} (\Gamma_\mu)^\alpha{}_\beta \lambda^\beta(x + \vec{\mu}) U_\mu^\dagger(x) \\
 \bar{\mathcal{Q}}^\alpha \lambda_\beta &= 0 \\
 \bar{\mathcal{Q}}^\alpha \bar{\lambda}_\beta &= -(\Gamma^{\mu\nu})^\alpha{}_\beta G_{\mu\nu} \\
 \bar{\mathcal{Q}}^\alpha \phi_i &= \frac{1}{2} \Gamma_{i+1}^\alpha{}_\beta \lambda^\beta,
 \end{aligned} \tag{4.18}$$

where all fields but the link variable U_μ are dimensionful and $G_{\mu\nu}$ is the lattice equivalent of the field strength tensor $F_{\mu\nu}$. In our work, we have chosen to use the clover plaquette $P_{\mu\nu}^C$

$$P_{\mu\nu}^C = \frac{-i}{8} (Q_{\mu\nu}(x) - Q_{\nu\mu}(x)) \tag{4.19}$$

$$Q_{\mu\nu}(x) = P_{\mu\nu}(x) + P_{\nu,-\mu}(x) + P_{-\mu,-\nu}(x) + P_{-\nu,\mu}(x), \tag{4.20}$$

where $P_{\mu\nu}(x)$ is a plaquette with the two corners x and $x + \vec{\mu} + \vec{\nu}$. Expanding this operator in terms of gauge fields shows that $P_{\mu\nu}^C = a^2 G^{\mu\nu}$. Note that while other choices are possible they will make no difference in the continuum limit.

We want to prove that these transformations meet the requirements. We start with the continuum limit of the transformations. In this limit, $G_{\mu\nu}$ becomes $F_{\mu\nu}$, thus the fermions transform correctly. Further, the scalar field already transforms as in the continuum. Thus we are left with the link variables U_μ , which encapsulate the gauge fields A_μ . Using the expansion $U_\mu = e^{aA_\mu} = \mathbb{1} + aA_\mu + O(a^2)$ we get for the left hand

side

$$\overline{\mathcal{Q}}^\alpha U_\mu(x) = \overline{\mathcal{Q}}^\alpha (\mathbb{1} + aA_\mu(x) + O(a^2)) = a\overline{\mathcal{Q}}^\alpha A_\mu(x) + O(a^2) \quad (4.21)$$

and for the right hand side

$$\begin{aligned} U_\mu \frac{a}{2} (\Gamma_\mu)^\alpha{}_\beta \lambda^\beta(x + \vec{\mu}) &= (\mathbb{1} + aA_\mu(x) + O(a^2)) \frac{a}{2} (\Gamma_\mu)^\alpha{}_\beta \lambda^\beta(x + \vec{\mu}) \\ &= \frac{a}{2} (\Gamma_\mu)^\alpha{}_\beta \lambda^\beta(x + \vec{\mu}) + O(a^2) \\ &= \frac{a}{2} (\Gamma_\mu)^\alpha{}_\beta (\lambda^\beta(x) + a\partial_\mu \lambda^\beta(x) + O(a^2)) + O(a^2) \\ &= \frac{a}{2} (\Gamma_\mu)^\alpha{}_\beta \lambda^\beta(x) + O(a^2), \end{aligned} \quad (4.22)$$

where we used the Taylor expansion of the fermion field from the second to the third line. Comparing the leading terms, we see that we recover the continuum transformation for the gauge fields.

The second requirement is a defining property of our lattice supercharge. If $\Omega(x)$ is a gauge transformation, we simply have $\mathcal{Q}\Omega(x) = \Omega(x)\mathcal{Q}$. Unfortunately this is not enough, as we still have to prove, that this property is compatible with the actual gauge transformations of the fields. Fortunately as all of them transform in the adjoint representation, this is straight forward.

For the third requirement we have to calculate the continuum transformation of the covariant derivative

$$\begin{aligned} \overline{\mathcal{Q}}^\alpha D_\mu \lambda(x) &= D_\mu \overline{\mathcal{Q}}^\alpha \lambda(x) - i [\overline{\mathcal{Q}}^\alpha A_\mu(x), \lambda(x)] - i [A_\mu(x), \overline{\mathcal{Q}}^\alpha \lambda(x)] \\ &= -i \left[\frac{1}{2} (\Gamma_\mu)^\alpha{}_\beta \lambda^\beta(x), \lambda(x) \right] \end{aligned} \quad (4.23)$$

We calculate the lattice analogue using (4.18)

$$\begin{aligned} \overline{\mathcal{Q}}^\alpha U_{\mu,adj}^{ab}(x) \lambda_b^\beta(x + \vec{\mu}) &= \overline{\mathcal{Q}}^\alpha \text{Tr} [\sigma^a U_\mu(x) \sigma^b U_\mu^\dagger(x)] \lambda_b^\beta(x + \vec{\mu}) \\ &= \text{tr} \left[\sigma^a U_\mu(x) \frac{a}{2} (\Gamma_\mu)^\alpha{}_\gamma \lambda^\gamma(x + \vec{\mu}) \sigma^b U_\mu^\dagger(x) \right. \\ &\quad \left. + \sigma^a U_\mu(x) \sigma^b \left(-\frac{a}{2} \right) (\Gamma_\mu)^\alpha{}_\gamma \lambda^\gamma(x + \vec{\mu}) U_\mu^\dagger(x) \right] \lambda_b^\beta(x + \vec{\mu}) \\ &= \text{tr} \left[\sigma^a U_\mu(x) \frac{a}{2} (\Gamma_\mu)^\alpha{}_\gamma [\lambda^\gamma(x + \vec{\mu}), \sigma^b] U_\mu^\dagger(x) \right] \lambda_b^\beta(x + \vec{\mu}) \\ &= U_{\mu,adj}^{ad}(x) i f_{dcb} \frac{a}{2} (\Gamma_\mu)^\alpha{}_\gamma \lambda^{\gamma,c}(x + \vec{\mu}) \lambda^{\beta,b}(x + \vec{\mu}) \end{aligned} \quad (4.24)$$

This term is one possible choice to discretize the continuum result, showing that we meet requirement three. A different choice for the lattice supersymmetry transformations would result into additional $O(a^2)$ terms appearing, showing that our transformations are optimized for this operator. The other advantage is that the transformations

of the scalar fields and the fermion fields are straight forward as shown earlier.

Having defined the lattice supersymmetry transformations we have to analyze the influence of the lattice regularization on the Ward identities. For this we recall the continuum form

$$\langle \bar{\mathcal{Q}}\mathcal{O} \rangle = 0. \quad (4.25)$$

To get the equivalent equation for the lattice we have to look at the derivation of this equation. One starts with the expectation value of the operator

$$\langle \mathcal{O} \rangle = \int \prod_i \mathcal{D}f_i \mathcal{O}[f_i] e^{-S[f_i]} \quad (4.26)$$

where f_i are the different fields involved. This expression must be invariant under all supersymmetry transformations of the fields. We chose an infinitesimal supersymmetry transformation which we can linearize as

$$f_i \rightarrow \tilde{f}_i = f_i + \epsilon \bar{\mathcal{Q}}. \quad (4.27)$$

Applying this transformation to the expectation value we find

$$\int \prod_i \mathcal{D}f_i \mathcal{O}[f_i] e^{-S[f_i]} \rightarrow \int \prod_i \mathcal{D}\tilde{f}_i \mathcal{O}[\tilde{f}_i] e^{-S[\tilde{f}_i]} \quad (4.28)$$

$$= \int \prod_i \mathcal{D}f_i \mathcal{O}[f_i] e^{-S[f_i]} + \epsilon \int \prod_i \mathcal{D}f_i [\mathcal{J}\mathcal{O} + (\bar{\mathcal{Q}}S[f_i]) \mathcal{O} + \bar{\mathcal{Q}}\mathcal{O}] e^{-S[f_i]} + O(\epsilon^2) \quad (4.29)$$

where \mathcal{J} is the contribution from the Jacobian, resulting from the transformation of the fields. Since this relation holds for arbitrary small transformations and therefore arbitrary small values of ϵ , the term of the order ϵ must vanish identical if we have a supersymmetric theory. In the continuum the measure and the action are invariant under infinitesimal transformations, hence the contribution from the Jacobian and the action are absent and we recover (4.25). On the lattice we will have a different action, leading to a non-vanishing contribution from the action in the Ward identity. Therefore the lattice Ward identity reads

$$\langle \bar{\mathcal{Q}}\mathcal{O} \rangle + \langle \mathcal{O}\bar{\mathcal{Q}}S \rangle = 0. \quad (4.30)$$

Note that the same line of reasoning can be used to derive Dyson-Schwinger equations.

Lastly we have to combine these new identities with the would-be supersymmetry transformations. In our case we use the same operators for \mathcal{O} as in section 2.6. In general, we will recover the continuum Ward identities, which pick up extra terms,

which we call lattice corrections. Most of those have to vanish in the continuum limit. Again we will call these irrelevant, while we call all others relevant. Here we are interested in the latter, since they will modify our results non-trivially.

We start the calculation of the transformation of the action with the kinetic term of the scalar fields (3.33). Here we will only transform the forward difference operator since we can interchange the transformed operator and the untransformed operator. We get

$$\begin{aligned} \overline{\mathcal{Q}}^\alpha (U_{\mu,adj}(x)\phi_i(x+\vec{\mu}) - \phi_i(x)) \\ = U_{\mu,adj}(x) \left[\frac{a}{2} (\Gamma_\mu)^\alpha{}_\gamma \lambda^\gamma(x+\vec{\mu}), \phi_i(x+\vec{\mu}) \right] + \overrightarrow{D}_\mu \left(\frac{1}{2} (\gamma_{i+1})^\alpha{}_\gamma \lambda^\gamma(x) \right) \end{aligned} \quad (4.31)$$

which is one of the possible lattice formulations of the transformed continuum covariant derivative. The potential term $[\phi_1, \phi_2]^2$ and the Yukawa terms $\bar{\lambda}\Gamma_{1+i}[\phi_i, \lambda]$ transform as the continuum counter parts. The next operator which is also present in the continuum is $F_{\mu\nu}^2$. On the lattice it is associated with the plaquette variable $\text{tr } P_{\mu\nu}$. Applying the transformation we find

$$\begin{aligned} \overline{\mathcal{Q}}^\alpha \text{tr } P_{\mu\nu} = \text{tr} \left\{ \overrightarrow{D}_\mu \frac{a}{2} (\Gamma_\nu)^\alpha{}_\gamma \lambda^\gamma(x+\vec{\nu}) P_{-\nu,\mu}(x+\vec{\nu}) \right. \\ \left. - \overrightarrow{D}_\nu \frac{a}{2} (\Gamma_\mu)^\alpha{}_\gamma \lambda^\gamma(x+\vec{\mu}) P_{\nu,-\mu}(x+\vec{\mu}) \right\}. \end{aligned} \quad (4.32)$$

To get the complete transformation of the Yang-Mills action, we have to evaluate the expression $\text{tr}(\mathbb{1} - \Re U_{\mu\nu})$. Therefore we have to redo the calculation for the adjoint of the plaquette

$$\begin{aligned} \overline{\mathcal{Q}}^\alpha \text{tr } P_{\mu\nu}^\dagger = \text{tr} \left\{ -\overrightarrow{D}_\mu \frac{a}{2} (\Gamma_\nu)^\alpha{}_\gamma \lambda^\gamma(x+\vec{\nu}) P_{\mu,-\nu}(x+\vec{\nu}) \right. \\ \left. + \overrightarrow{D}_\nu \frac{a}{2} (\Gamma_\mu)^\alpha{}_\gamma \lambda^\gamma(x+\vec{\mu}) P_{-\mu,\nu}(x+\vec{\mu}) \right\}. \end{aligned} \quad (4.33)$$

Expanding the plaquette $P_{\mu\nu} \approx \exp(ia^2 F_{\mu\nu} + \mathcal{O}(a^3))$, we recover the right continuum expression for the supersymmetry transformation of the Yang-Mills term. We proceed to calculate the transformation of the kinetic term for the fermions

$$\begin{aligned} \overline{\mathcal{Q}}^\alpha \left(\bar{\lambda}^\beta(x) \left(-\frac{1}{2} \right) \sum_\mu \left\{ (r - (\Gamma_\mu)_{\beta\gamma}) U_{\mu,adj}(x) \lambda_\gamma(x+\vec{\mu}) \right. \right. \\ \left. \left. + (r + (\Gamma_\mu)_{\beta\gamma}) U_{\mu,adj}^\dagger(x-\vec{\mu}) \lambda_\gamma(x-\vec{\mu}) \right\} \right) \\ = (\Gamma_{\mu\nu})^{\alpha\beta} G^{\mu\nu} D_W \lambda_\beta + \mathcal{O}(a). \end{aligned} \quad (4.34)$$

where D_W is the Wilson Dirac operator.

The last terms to calculate are the mass terms

$$\bar{Q}^\alpha \bar{\lambda}^\beta (m_f + dr) \lambda_\beta = -(\Gamma_{MN})^{\alpha\beta} G^{MN} (m_f + dr) \lambda_\beta \quad (4.35)$$

$$\bar{Q}^\alpha m_s^2 \phi^2 = (\Gamma_{i+1})^\alpha{}_\beta \lambda^\beta m_s^2 \phi^i. \quad (4.36)$$

Having derived all lattice transformations we proceed by expanding the link variables $U_\mu(x) = e^{aA_\mu}$ and applying the Taylor expansion $f(x + \vec{\mu}) = f(x) + a\partial_\mu f(x) + \dots$ to all fields. Finally we will only focus on the leading terms while representing all sub-leading terms (contributions of order $O(a)$) with X_S . We get the transformation of the Lagrangian

$$\begin{aligned} \bar{Q}^\alpha \mathcal{L}_{\text{lat}} &= \frac{\beta}{2} \left\{ \partial_\mu s_\mu^\alpha - 2m_f (\Gamma_{MN})^{\alpha\beta} F^{MN} \lambda_\beta \right\} + 2m_s^2 (\Gamma_{m+1})^\alpha{}_\beta \lambda^\beta \phi^m + X_S \\ &= \frac{\beta}{2} \left\{ \partial_\mu s_\mu^\alpha - m_f \chi_f^\alpha \right\} + m_s^2 \chi_s^\alpha + X_S, \end{aligned} \quad (4.37)$$

where all quantities are dimensionful, s_μ is the supercurrent

$$\begin{aligned} s_\mu &= F^{\mu\nu} (D_\nu \Gamma_\mu - D_\mu \Gamma_\nu) \lambda + [\phi_1, \phi_2] ([\Gamma_2 \lambda, \phi_2] + [\phi_1, \Gamma_3 \lambda]) \\ &\quad + D^\mu \phi^i (D_\mu \Gamma_{i+1} \lambda + [\Gamma_\mu \lambda, \phi_i]) + F^{MN} \Gamma_{MN} \not{D} \lambda + F^{MN} \Gamma_{MN} \Gamma_{i+1} [\phi^i, \lambda] \end{aligned} \quad (4.38)$$

and χ_f and χ_s are the contributions coming from the fermion and the scalar mass term respectively

$$\chi_f^\alpha = 2 \text{tr} (\Gamma_{MN}^{\alpha\beta} F^{MN} \lambda_\beta) \quad \text{and} \quad \chi_s^\alpha = 2 \text{tr} (\Gamma_{m+1}^{\alpha\beta} \lambda_\beta \phi^m). \quad (4.39)$$

The contribution of the supercurrent will vanish after the summation over all lattice sites. This result is a tree-level result, since we did not incorporate quantum effects yet. This is visible in the fact, that we would restore supersymmetry for $m_s^2 = 0$ in stark contrast to our previous result. To avoid a thorough calculation of the quantum effects, we use these previous results. At finite lattice size and lattice spacing a fermion mass will be created, which we will incorporate. At one-loop a scalar mass will be created, for which we have to correct for. Its appearance shows, that X_S can contribute beyond tree-level even if this term is original of order $O(a)$. We get the final result

$$\bar{Q}^\alpha \mathcal{L}_{\text{lat}} = \frac{\beta}{2} \partial_\mu s_\mu^\alpha + \Theta + X_S, \quad (4.40)$$

where we introduce the abbreviation

$$\Theta = (m_s^2 - (m_s^c)^2) \chi_s - \frac{\beta}{2} (m_f - m_f^c) \chi_f. \quad (4.41)$$

The term X_S is complicated and could introduce various different quantum cor-

rections into the Ward identities. Fortunately, our Ward identities are based on the action. Here we know the relevant quantum correction already, which is just the scalar mass term. More specific it must appear in the Ward identity W_3 since it contains the kinetic term for the scalar fields. Introducing another abbreviation

$$\Upsilon = \frac{i}{8} (\Gamma_2 [\phi_1, \lambda] + \Gamma_3 [\phi_2, \lambda]), \quad (4.42)$$

we get the final set of lattice Ward identities we will use

$$\begin{aligned} W_B &= \beta V^{-1} \langle S_B \rangle + m_s^2 \langle \text{tr } \phi^2 \rangle + \beta \langle \text{tr } \bar{\lambda} \Gamma^{MN} F_{MN} \Theta \rangle \rightarrow \frac{9}{2}, \\ W_3 &= \frac{\beta}{2} \langle \text{tr } D_\mu \phi^a D^\mu \phi_a \rangle + m_s^2 \langle \text{tr } \phi^2 \rangle + 2\beta \langle \text{tr } \bar{\lambda} \Gamma^{\mu m} D_\mu \phi_m \Theta \rangle \rightarrow 3, \\ W_2 &= \frac{\beta}{4} \langle \text{tr } F_{\mu\nu} F^{\mu\nu} \rangle + \beta \langle \text{tr } \bar{\lambda} \Upsilon \rangle + \beta \langle \text{tr } \bar{\lambda} \Gamma^{\mu\nu} F_{\mu\nu} \Theta \rangle \rightarrow \frac{3}{2}, \\ W_1 &= \frac{\beta}{2} \langle \text{tr } [\phi_1, \phi_2]^2 \rangle - \beta \langle \text{tr } \bar{\lambda} \Upsilon \rangle + \beta \langle \text{tr } \bar{\lambda} \Gamma^{mn} [\phi_m, \phi_n] \Theta \rangle \rightarrow 0. \end{aligned} \quad (4.43)$$

The limit shows, that we ignored irrelevant operators which can also appear at finite lattice size and lattice spacing. Hence our Ward identities will reach the correct values in the continuum limit only.

4.4 Glueballs in two-dimensional pure Yang-Mills theory

In this section we will anticipate the result of the correlation function for the glueball. It shows no correlation for time distances larger than one. To understand this property we will compare it to the glueball correlator of the two-dimensional pure Yang-Mills theory. This theory can be solved analytically. Here we will focus on the analytical results for Wilson loops presented in [142] and the analytical solution to the lattice prescription by Migdal [143]. An introduction to the latter can be found in appendix B.

In the two-dimensional lattice pure Yang Mills theory, the only gauge invariant objects are Wilson Loops

$$W = \frac{1}{N} \text{tr} \left(\mathcal{P} \prod_{i \in \gamma} U(x_i)_{\mu_i} \right) \quad (4.44)$$

where N is the dimension of the representation of the loop, \mathcal{P} is the path ordering operator and γ is a closed planar path on the lattice. The analogous object in the

continuum is

$$W = \frac{1}{N} \text{tr} \left(\mathcal{P} \exp \left[ig \int_0^1 ds \dot{\gamma}^\mu(s) A_\mu(\gamma(s)) \right] \right). \quad (4.45)$$

It was shown in [142], that Wilson loops obey an area law in the continuum

$$\langle W \rangle = \exp \left(-\frac{g^2 C}{2} A \right) \quad (4.46)$$

where C is the Casimir constant

$$C\mathbb{1} = \delta^{ab} T_a T_b \quad (4.47)$$

and A is the area enclosed by the loop. In appendix B, we recovered an analogous result for the Wilson loops in the lattice theory

$$\langle W \rangle = e^{-1.5A}. \quad (4.48)$$

Thus both theories agree as expected. Now we want to focus on the glueball correlation function. Again we start with the continuum case. For this we choose the axial gauge given in [142]

$$A_0(x_1, x_2) = 0 \quad (4.49)$$

$$A_1(0, x_2) = 0 \quad (4.50)$$

which allows for a convenient transformation of the measure

$$\prod_x dA_\mu(x) \delta(A_1(x_1, x_2)) \delta(A_2(0, x+2)) = K \prod_x dF_{01}(x). \quad (4.51)$$

The variable K is a constant which will cancel when we calculate expectations values. Due to this trivial Jacobian, we are able to calculate the glueball correlation function analytically

$$\langle F_{01}^2(x) F_{01}^2(0) \rangle = \frac{K}{Z} \int \prod_{x'} dF_{01}(x') F_{01}^2(x) F_{01}^2(0) e^{-\frac{1}{4} F_{01}^2}. \quad (4.52)$$

Since we have no derivatives of F_{01} in the action, we have no interaction between the different F_{01} living on different positions in spacetime. Therefore these fields decouple and we find

$$\langle F_{01}^2(x) F_{01}^2(0) \rangle = \langle F_{01}^2(x) \rangle \langle F_{01}^2(0) \rangle \quad (4.53)$$

and subsequently

$$\langle F_{01}^2(x)F_{01}^2(0) \rangle_c = \langle F_{01}^2(x)F_{01}^2(0) \rangle - \langle F_{01}^2(x) \rangle \langle F_{01}^2(0) \rangle = 0. \quad (4.54)$$

In section 3.5 we showed that the connected correlation function is proportional to $\sum_n c_n e^{-m_n t}$. Hence we find that m_n must be infinite. As this value is the mass of the state, the glueball must be infinitely heavy. This is supported by the fact that a projection on a specific momentum will always yield the same correlation function despite the energy-momentum relation, which would usually lead to a different mass. The only possible solution which satisfies this property is to have an infinite heavy particle. We interpret this result as a decoupling of the glueball from the theory.

Next we want to derive the same result for the lattice theory. For this we put two non-intersecting plaquettes on the lattice at position x and 0 . Following our result from the appendix B, we find

$$\begin{aligned} \langle U_p(x)U_p(0) \rangle &= \\ &= \frac{\sum_{n=1}^{\infty} \left\{ \frac{(n+1)^2}{n} I_n^{V-2}(\beta) I_{n+1}^2(\beta) + \frac{n(n+2)}{n+1} I_n(\beta) I_{n+1}^{V-2}(\beta) I_{n+2}(\beta) + \frac{n^2}{n+1} I_n^2(\beta) I_{n+1}^{V-2}(\beta) \right\}}{\sum_{n=1}^{\infty} I_n^V(\beta)}, \end{aligned} \quad (4.55)$$

where I_n are the modified Bessel functions of the first kind and V is the lattice volume. Next we to perform the infinite volume limit $V \rightarrow \infty$

$$\langle U_p(x)U_p(0) \rangle \rightarrow \left(2 \frac{I_2(\beta)}{I_1(\beta)} \right) \left(2 \frac{I_2(\beta)}{I_1(\beta)} \right) = \langle U_p(x) \rangle \langle U_p(0) \rangle, \quad (4.56)$$

where we used our result for the Wilson loop (see appendix B)

$$\langle U_p(x) \rangle \rightarrow \left(2 \frac{I_2(\beta)}{I_1(\beta)} \right). \quad (4.57)$$

Since we have $U_p(x) \rightarrow F_{01}(x)$ in the continuum limit ($V \rightarrow \infty, \beta \rightarrow \infty$) we see that we get the same result for the glueball correlator as in the continuum theory. For intersecting or touching plaquettes this statement is not true anymore and we find a non-zero result. The same analogous result can be found for any other possible operators. As long as they do not touch or overlap, the result is always zero (for details see appendix B).

Lastly we want to discuss the shape of the glueball correlation function on the lattice. Here we focus on the projection onto zero momentum

$$C(t) = \sum_{x,y} \langle \mathcal{O}_{\text{gb}}(x,0) \mathcal{O}_{\text{gb}}(y,t) \rangle. \quad (4.58)$$

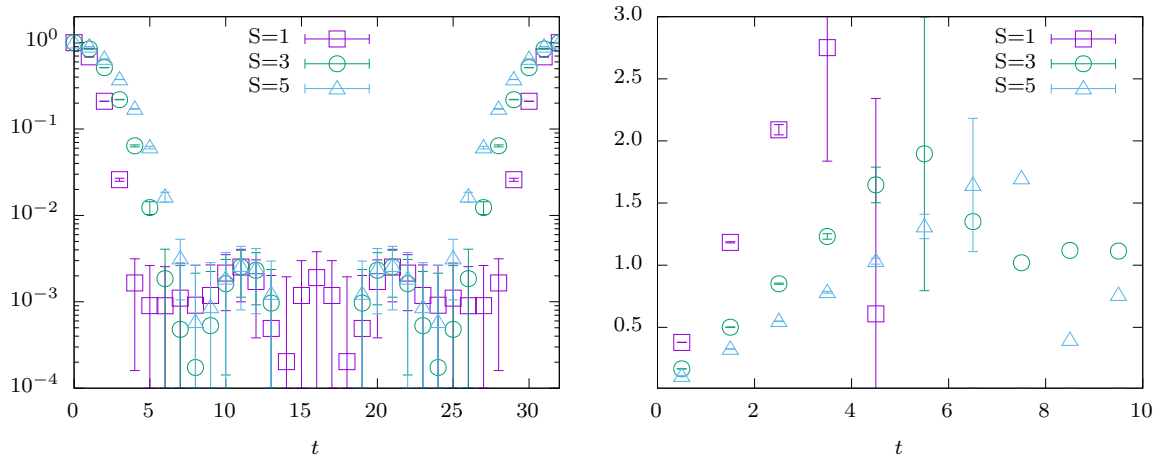


Figure 4.1: Correlation function (left) and effective mass (right) of the Glueball for the two-dimensional Yang-Mills theory and different smearing levels S .

In the previous calculation we used the plaquette for the glueball interpolating operator \mathcal{O}_{gb} but other observables are possible. In case of a plaquette, we can define the support of this operator. In time direction it has a diameter of one in lattice units. Hence two plaquettes will not overlap or touch for $t > 1$. Taking into account the periodicity of the lattice we must also take into account backwards correlation. If our lattice has size L_T in time direction, we expect also non-zero values for $t > L_T - 2$. Therefore we get the correlator

$$C(t) = \begin{cases} A & \text{for } t = 0 \\ B & \text{for } t = 1, L_T - 1 \\ 0 & \text{for } 2 \leq t \leq L_T - 2 \end{cases}, \quad (4.59)$$

with two constants A and B , which we did not determined explicitly. Using an interpolating operator with a larger support in time direction will increase the number of non-zero values. One way to construct these operators is through smearing. As explained in section 3.6, smearing reduces fluctuations by spreading the link variable on the neighboring lattice patch. If we build our plaquette observable out of these smeared links, the size of the support will increase. Hence the diameter in time direction will also increase and we observe more correlation. Since this correlation is absent in the continuum, it must be artificial.

Since an analytical calculation of these effects is tedious while a lattice calculation is computationally cheap, we switch now to the latter to study the effects of smearing. In the left panel of Figure 4.1 we show the correlation functions for different smearing levels, introduced in section 3.6. We observe that the distance in time for which the correlation is non-zero increases for higher smearing levels. Since a higher smearing level corresponds to a higher diameter of the support of the interpolating operator, this effect is as expected. From the correlation function we can extract the so called

effective mass m_{eff}

$$m_{\text{eff}}(t) = \ln \left(\frac{C(t+1)}{C(t)} \right). \quad (4.60)$$

For $t \rightarrow \infty$ this value will correspond to the ground state mass, forming a plateau. If we find another plateau as a function of t , its value signals the mass of an excited state. Therefore the effective mass can be used to extract the masses of states from a correlation function. In our case we know that we should find no plateau as we have no finite mass for this correlator. In the right panel of Figure 4.1 we plot the effective mass of the glueball correlator for the two-dimensional pure Yang-Mills theory. While we observe no plateau, we find a monotonic rising function before it drops to zero. The zero values comes from statistical fluctuations. Since this is a lattice calculation, our correlator will never reach zero. Instead in the region where it should be zero, it is dominated by statistical fluctuations. Thus the value of the correlator is approximately constant and we find an effective mass of value zero. Another property of the effective mass of the glueball correlator is that it decreases with the smearing level for fixed value of t .

With this we want to conclude this section about the pure Yang-Mills theory. Again we want to emphasize that while this chapter seems to be out of place here, it will be crucial later to understand our results of the glueball correlator in the $\mathcal{N} = (2, 2)$ SYM theory.

Chapter 5

Simulation Parameters

In this chapter we will discuss the five simulation parameters N_t, N_s, β, m_s^2 and m_f . The first three form a set which is connected to the physical volume of our simulation. Explicitly the product $N_t N_s$ is the lattice volume while β is linked to the lattice spacing a (see section 5.1). The size of the physical volume will determine the emergence of finite volume lattice artifacts, as we know from simulations of QCD. Along with the finite lattice spacing artifacts, they will spoil our results because they will be absent in the continuum limit. This limit, also called target theory, will be the $\mathcal{N} = (2, 2)$ SYM theory in two dimensions for our simulations. To ensure the correct convergence, we have to be careful. First we must extrapolate to the infinite volume limit and only afterwards extrapolate to zero lattice spacing. Further one has to ensure that we always fine-tune the second set of parameters, namely the scalar mass m_s^2 and the fermion mass m_f . In section 4.1, we showed their emergence for our lattice setup. Here we will discuss their influence on the lattice simulation further. Note that starting in this chapter we will make use of the hopping parameter $\kappa = 1/(2m_f + 4)$, which is proportional to the interaction part of the Wilson Dirac operator. Thus it is the commonly used parameter for lattice calculations. Yet several of our results can be explained better using the fermion mass m_f . Therefore we will use both of them in the following chapters.

This chapter is organized as follows. We start with the discussion of the β dependency of our lattice simulation, especially the relation between the lattice spacing a and the inverse gauge coupling β . Afterwards we discuss the infinite volume limit of our theory in case of the mesons and the Ward identities. The next section is a discussion of the scalar mass. While we know the continuum result from section 4.2, we try to derive this result within our lattice simulation. Then we shift our focus on the discussion of the critical fermion mass. Since we find a spontaneous symmetry breaking in four dimensions, we could observe a non-trivial behavior in the dimensionally reduced theory. Finally we discuss our lattice setup, where we take into account our results to motivate the used values of N_t, N_s, β, m_s^2 and m_f . We will show these in an overview.

5.1 β dependency

The inverse coupling constant β is the parameter which can determine the phase of the lattice theory as well as the lattice spacing. We start with the influence on the phase. For $\beta \rightarrow 0$ we get $g \rightarrow \infty$ in most lattice theories, therefore it is called the strong coupling limit. This limit allows for an expansion, which is accordingly called strong coupling expansion and is analogous to the high temperature expansion in statistical mechanics [91]. Usually one avoids simulations in this phase of the lattice theory, as generally the results can not be extrapolated to the targeted continuum theory. In practice, this is done by choosing values of β which are larger than a theory dependent value. Its size can be estimated by theoretical arguments or by explicit lattice simulations. Unfortunately for our theory this value was not known, as the only comparable simulation was done in the quenched approximation with reweighting [52]. Thus we assumed that it is of the same size as in the four-dimensional mother theory and used $\beta = 2.5, 3, 4$. These values of the inverse gauge coupling are close to the ones used in [34], when we take the different conventions into consideration.

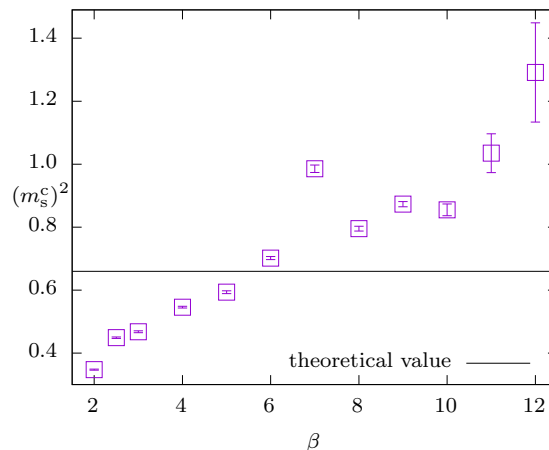


Figure 5.1: Critical scalar mass $(m_s^c)^2$ derived from Ward identity W_1 (5.5), by requiring $W_1(m_s^2 = (m_s^c)^2, m_f) = 0$.

Our simulation reveals, that our assumption is wrong and we have to go to even higher values of the inverse gauge coupling β , to guarantee the continuum limit to our target theory, $\mathcal{N} = (2, 2)$ SYM. For this result, we focus on the Ward identity W_1 (5.5). It allows to define the critical scalar mass $(m_s^c)^2$ as $W_1(m_s^2 = (m_s^c)^2, m_f) = 0$. In section 5.3, we will show that the critical fermion mass is independent on m_s^2 and therefore independent on $(m_s^c)^2$, which allows for two separate fine-tunings of the mass parameters. Further it allows us to discuss only the dependency of W_1 on m_s^2 in the sense that $W_1(m_s^2) = W_1(m_s^2, m_f = m_f^c)$. Simulating in the range $\beta \in [2, 17]$ and the fermion mass close to its critical value, we found a dependence of $(m_s^c)^2$ on the inverse gauge coupling β , which is depicted in Figure 5.1. We find that the critical scalar mass

is a monotonically increasing function, with the exception of $\beta = 7$. Interestingly, the slope of this function seems to decrease for $\beta \in [8, 10]$ while it increases for $\beta > 10$. Thus we find no converging behavior for this value towards the theoretical value of $(m_s^c)^2 = 0.65948225$. In fact our values become significantly larger for $\beta > 10$. As we will show in the following paragraph, the inverse gauge coupling is inversely proportional to the lattice spacing. Thus the observed zero crossing for $W_1(m_s^2)$ in the region $m_s^2 \leq 1$ might be a hint, that we are in the wrong phase of the lattice theory. Thus we discard the region $\beta < 14$ and use the values $\beta = 14, 15.5, 17$. We can also draw a second conclusion, namely we can not use W_1 to determine the critical scalar mass. This statement also holds for all other Ward identities considered in this work, even when we take into account their lattice corrections (in section 5.3 we will show this explicitly). Hence we were forced to use a different approach. Instead of a fine-tuning via a lattice observable, we set the scalar mass term to $m_s^2 = 0.6594823$.

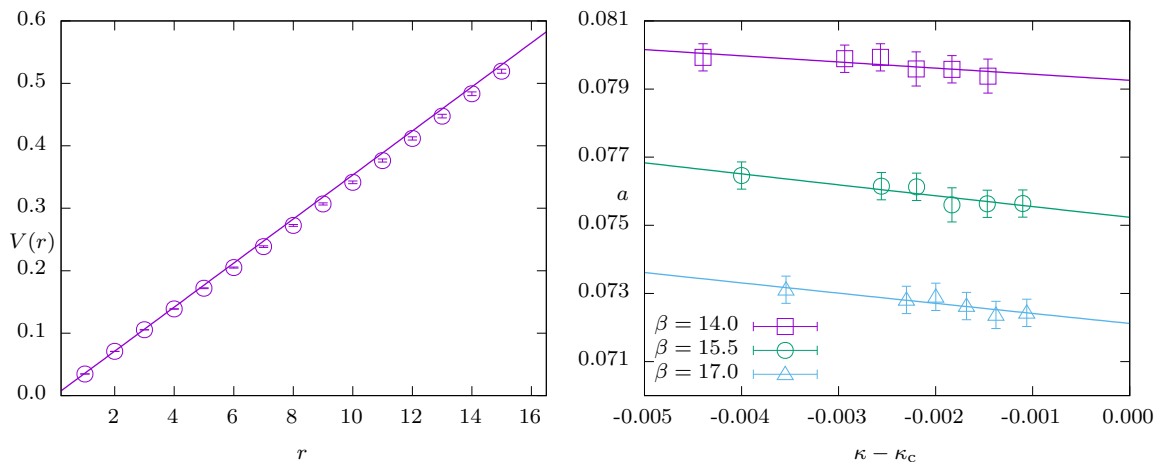


Figure 5.2: Left: Static quark potential and fit to (5.2) for $\beta = 17.0$ and $\kappa = 0.26655$. Right: Lattice spacing a for $\beta = 14.0, 15.5$ and 17.0 as function of m_f on a 64×32 lattice.

Now we will discuss another property of the inverse gauge coupling, its relation to the lattice spacing. This allows to set the physical lattice spacing of our lattice theory, as for example discussed in QCD [90]. In two dimensions this relation becomes more evident because the coupling constant is dimensionful. Thus we end up with the relation

$$\beta = \frac{1}{a^2 g^2}. \quad (5.1)$$

While this equation seems to imply the inverse proportionality $a(\beta) \propto \beta^{-\frac{1}{2}}$, the actual relation could be more involved. This depends on the functional dependency of $g(\beta)$. Hence we have to investigate this relation explicitly. We do this by using a well defined but arbitrary method to measure the lattice spacing. We make use of the static quark-antiquark potential in the fundamental representation of $SU(2)$, introduced for

example in [90]. We show an example on the left hand side of Figure 5.2. Further to compare our results to the usual lattice QCD data, we employ the Sommer scale [144]. In Table 5.1, we give the results for the three different values of the inverse gauge coupling, which we visualize on the right hand side of Figure 5.2. We find that the lattice spacing is dependent on the fermion mass. Thus we use a linear extrapolation to the chiral limit $m_f = m_f^c$. Using this result, we compared it with (5.1), which is depicted in the last column of Table 5.1. Even without errors, we find an excellent agreement between all values, showing that $g(\beta) = \text{const.}$ for all β in consideration. This leads to the conclusion, that we find the limit $a \rightarrow 0$ for $\beta \rightarrow \infty$.

$\beta = 14.0$			$\beta = 15.5$		
$\kappa - \kappa_c$	$a[\text{fm}]$	$\beta a^2[\text{fm}]$	$\kappa - \kappa_c$	$a[\text{fm}]$	$\beta a^2[\text{fm}]$
-0.00440	0.07993(4)	0.08944(9)	-0.00400	0.07646(4)	0.09062(9)
-0.00294	0.07989(4)	0.08935(9)	-0.00256	0.07612(4)	0.08981(9)
-0.00257	0.07993(4)	0.08944(9)	-0.00220	0.07613(4)	0.08983(9)
-0.00220	0.07959(5)	0.08838(11)	-0.00183	0.07560(5)	0.08859(12)
-0.00183	0.07958(4)	0.08833(9)	-0.00167	0.07563(4)	0.08866(9)
-0.00146	0.07938(5)	0.08822(11)	-0.00110	0.07564(4)	0.08868(9)
0	0.07926(322)	0.08795(51)	0	0.07524(310)	0.08774(47)
$\beta = 17.0$					
$\kappa - \kappa_c$	$a[\text{fm}]$	$\beta a^2[\text{fm}]$	$\kappa - \kappa_c$	$a[\text{fm}]$	$\beta a^2[\text{fm}]$
-0.00354	0.07311(4)	0.09087(10)	-0.00168	0.07263(4)	0.08968(10)
-0.00230	0.07281(4)	0.09012(10)	-0.00138	0.07237(4)	0.08904(10)
-0.00200	0.07290(4)	0.09034(10)	-0.00106	0.07243(4)	0.08918(10)
0	0.07212(266)	0.08842(38)			

Table 5.1: Lattice spacing for different combinations of β and κ . In the last rows of each β section we give the extrapolations to the chiral limit.

Lastly we have to draw attention to the static quark-antiquark potential

$$V(r) = A + \sigma r, \quad (5.2)$$

in the fundamental representation of $SU(2)$, shown on the left panel of Figure 5.2. In two dimensions, the Lüscher term is absent, while the Coulomb term is a linear function. Thus we are left with the string tension σ , while a $1/r$ term must be absent. Further it was argued in [145] that the potential is absent in the first place for exactly massless fermions. The reason is that a cloud of massless gluinos can screen both charges. Introducing a small mass for the fermions, this effect will vanish and we observe a confining behavior (linear rising potential). Thus it will be difficult to observe this behavior. Nonetheless we tried to investigate this behaviour by simulating for different

fermion masses $m_f \in [-0.1640, 0.0]$. In all cases we found a linear rising potential, for which the string tension reduces approximately 10% towards the chiral limit. Thus we do not observe the screening behaviour, expected from the theoretical results. The reason could be that we need either exactly massless fermions which is not possible on the lattice or that we have a compact formulation of gauge theories. In the latter case, certain states of the Hilbert space are absent, hence screening is not possible any more. As our main goal of this section was to confirm that we reach the continuum limit for $\beta \rightarrow \infty$, we did not investigate the static quark-antiquark potential any further. Still it is an interesting observation which warrants further analysis.

5.2 Volume dependency

In a lattice simulation, we can only simulate a finite volume. Thus, according to the Fourier transformation, the lattice can only accommodate a minimal momentum $p_{\min} \sim \frac{1}{L_{\max}}$, where L_{\max} is the longest extension in any of the spacetime directions. Considering the energy-momentum relation, this is also the lowest energy, a state can have on the lattice. We will call this threshold the lattice cut-off. Any state with a lower energy will not be represented faithfully leading to large lattice artifacts. The physical interpretation is that the de Broglie wavelength of the particle is too large to fit on the lattice. In our case this cut-off is important because we expect a massless state. This state was predicted by theoretical arguments [82, 83] and measured in numerical calculations based on a discretized light cone quantization [84, 85]. Fortunately, as we show later, the energy of this state is dependent on the fermion mass m_f . Therefore by choosing an appropriate fermion mass, we have only states whose energy is above the lattice cut-off. This guarantees a result with smaller lattice artefacts, which we will extrapolate to the continuum limit.

Not only do massless states pick up lattice artefacts in a finite volume but also all other states. In general this will lead to a volume dependent mass. In [146, 147] Lüscher and Münster calculated these artefacts for general theories. They found the scaling

$$m_L = m - \frac{c}{L} \exp\left(-\frac{L}{L_0}\right), \quad (5.3)$$

where m_L is the mass we measure for the finite volume and m is the mass in the infinite volume limit. The longest extension of the lattice is L , which can be replaced by either L_t or L_s if we fix the ratio of both. For us c represents a fit variable and L_0 is the lattice extension for which we expect suppressed finite volume lattice effects. We can eliminate this parameter by relating it to the infinite volume mass of the lightest particle with $L_0 = \pi/m_\eta$. Calculating the mass of our mesons for different lattice sizes, we were able to use (5.3) as a fit function and determine the infinite volume mass. We

ignored all lattice masses which were much smaller than the lattice cut-off for these fits. In our case the extension in the time direction is the largest, therefore we end up with the requirement $m_L \gtrsim \pi/L_t$. In figure 5.3 we show the results for $\beta = 14$ and four different fermion masses.

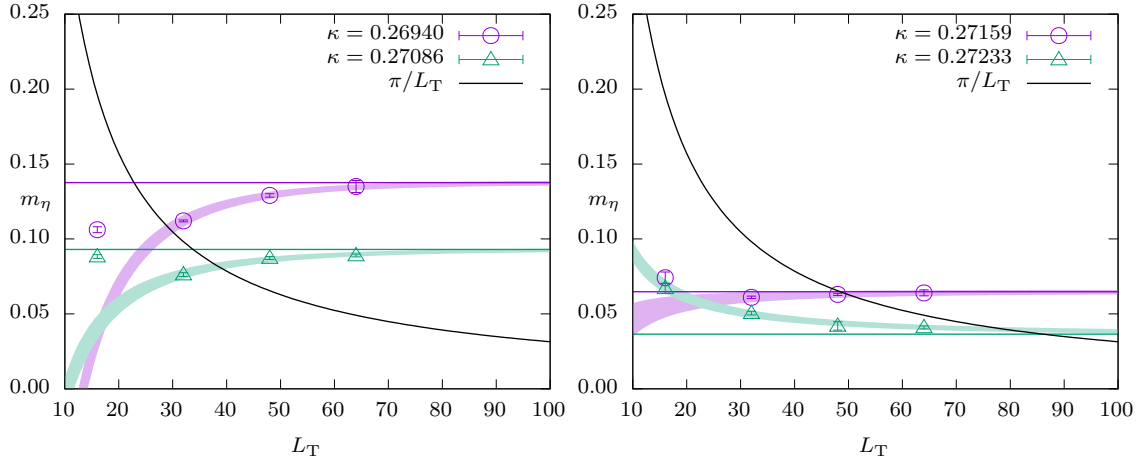


Figure 5.3: Infinite volume extrapolation for the mass of the η -meson at $\beta = 14$ and different values of the hopping parameter κ compared to the smallest lattice momentum π/L_t . The horizontal lines indicate the infinite volume mass m .

Focusing first on the value $\kappa = 0.27159$, we find an infinite volume mass of $m = 0.0648(14)$. In accordance with our previous discussion, this mass is too light for the smallest lattice with $L_t = 16$. This leads to an increased lattice mass which is larger than the infinite volume limit. Closer to the lattice cut-off ($L_T \geq 32$) we see a monotonically increasing lattice mass. The same behavior is seen for $\kappa = 0.26940$ and $\kappa = 0.27086$. For $\kappa = 0.27233$, the lattice mass is monotonically decreasing. In this last case the infinite volume mass of $0.0365(14)$ is much smaller than the lattice cut-off π/L_T for all lattices. Still, the fit function (5.3) works well even in this case, yielding a reliable result for the infinite volume mass. Furthermore we notice, that the lattice masses for our largest lattice with $L_t = 64$ agree very well with the infinite volume results. Therefore we conclude that finite volume effects can be neglected for this meson for $L_t \gtrsim 64$. The same results holds true for all other mesons. Thus we will restrict ourselves to a lattice size of 64×32 for the spectroscopy.

Having estimated the finite volume effects for the meson masses, we want to do the same for the Ward identities. In Figure 5.4 we show the dependence of the Ward identities on the fermion mass for different lattice volumes. While our results for W_2 shows no dependence on the lattice volumes, we see some small deviations for W_1 . We can ignore these as we are only interested in the value for the critical fermion mass, where all three results agree. For the two other Ward identities we see the same behavior. Thus we conclude, that finite volume effects are absent for our Ward identities.

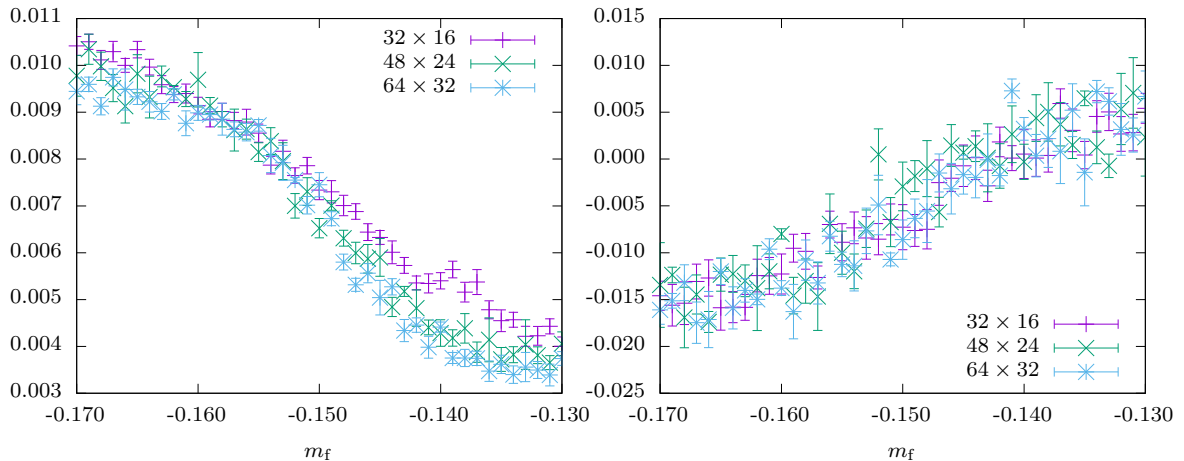


Figure 5.4: The Ward Identities W_1 (left) and W_2 (right) plotted for $\beta = 17$ and three different lattice volumes

5.3 Scalar Mass dependency

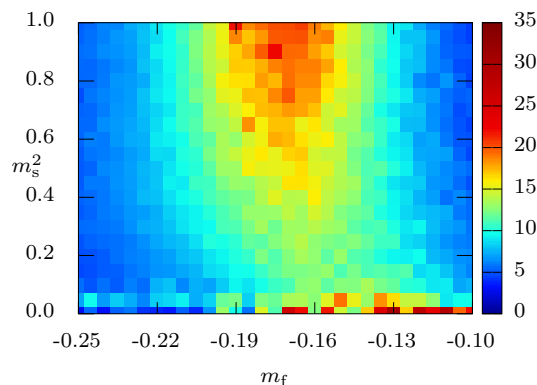


Figure 5.5: Chiral susceptibility plotted over the scalar mass m_s^2 and the fermion mass m_f for $\beta = 14$

In this section we will discuss the dependence of the lattice observables on the scalar mass m_s^2 . Especially we will establish, that the simulation is seemingly independent on m_s^2 for values close to the continuum result for the critical scalar mass. As mentioned already in section 5.1, the critical fermion mass, determined by the peak of the chiral susceptibility, is independent on the value of the scalar mass for $m_s^2 \leq 1$. This is shown in Figure 5.5, where we plot the chiral susceptibility as a function of m_f and m_s^2 for $\beta = 14$. We see that while the height of the peak depends on m_s^2 , the position of peak does not for all $m_s^2 \leq 1$. Thus the critical fermion is independent on the scalar mass in our simulation. While we did not redo the whole parameter scan for larger β and larger scalar masses, we simulated on several different lines through this parameter space. All of those confirmed this property. This leads us to the conclusion that the critical fermion mass is independent on m_s^2 in our simulation. Thus the fine-tuning of

both parameters can be done individually which reduces the computational cost of the simulation tremendously.

Next we want to further investigate the failure to determine the critical scalar mass in our lattice simulations. As derived in section 4.3, we have the lattice Ward identities (4.43) where we ignored lattice contributions which vanish in the continuum limit. Since we have seen, that even for small lattices the Ward identities do not suffer from finite volume effects, the lattice artifacts must stem from the finite lattice spacing. For large enough β , these should be suppressed sufficiently and we should be able to only observe the relevant lattice corrections coming from the term Θ in (4.43). This would allow us to define a critical scalar mass and a critical fermion mass. The latter would be another possible option to determine a critical fermion mass, which is independent on the chiral susceptibility. Unfortunately this method fails in our simulations because either the irrelevant lattice artifacts are still sizeable or the statistical errors are too high. We show this failure explicitly for the Ward identity W_2 .

Here we will focus ourselves on the determination of the critical scalar mass, since we determined the critical fermion mass already. For this we split W_2 of (4.43) into the three parts

$$W_2^b = \beta \left\langle \frac{1}{4} \text{tr} F_{\mu\nu} F^{\mu\nu} + \text{tr} \bar{\lambda} \Upsilon \right\rangle, \quad \mathcal{C}_s = \langle \text{tr} \bar{\lambda} \Gamma^{\mu\nu} F_{\mu\nu} \chi_s \rangle, \quad \mathcal{C}_f = \beta \langle \text{tr} \bar{\lambda} \Gamma^{\mu\nu} F_{\mu\nu} \chi_f \rangle, \quad (5.4)$$

$$W_2 = W_2^b + (m_s^2 - (m_s^c)^2) \mathcal{C}_s + (m_f - m_f^c) \mathcal{C}_f.$$

Now we simulate our theory for a set of values m_s^2 near the one-loop value 0.65948225 and fixed fermion mass m_f . For these simulations we measure W_2^b, \mathcal{C}_s and \mathcal{C}_f . Note that the values $(m_s^c)^2$ and m_f^c are trial masses, which enter only after the simulation, while m_s^2 and m_f are the masses we use to generate the gauge configurations. Since the lattice Ward identities should be satisfied for all m_s^2 and m_f close to their critical value, we should find values for $(m_s^c)^2$ and m_f^c , which satisfies $W_2 \approx 3/2$ for all aforementioned simulations. Of course the result for $(m_s^c)^2$ could deviate from the one-loop result due to lattice artifacts. Still in the continuum limit, both values have to agree.

In Figure 5.6 we show the results for W_2^b and \mathcal{C}_s for different scalar masses. Both do not depend on this value, which is also true for \mathcal{C}_f . These results make it impossible to apply the method described above, because no values of $(m_s^c)^2$ and m_f^c will meet the requirement of $W_2 \approx 3/2$ for all values of m_s^2 . We observed the same behavior for all other Ward identities which we considered in this work.

Still we can use this result for some useful conclusions. First, the magnitude of the corrections coming from the Θ term will be several magnitudes smaller than the value of the Ward identity, close to the critical masses. Therefore we can neglect them in our simulation if we extrapolate to the chiral limit. This leads to our final set of Ward

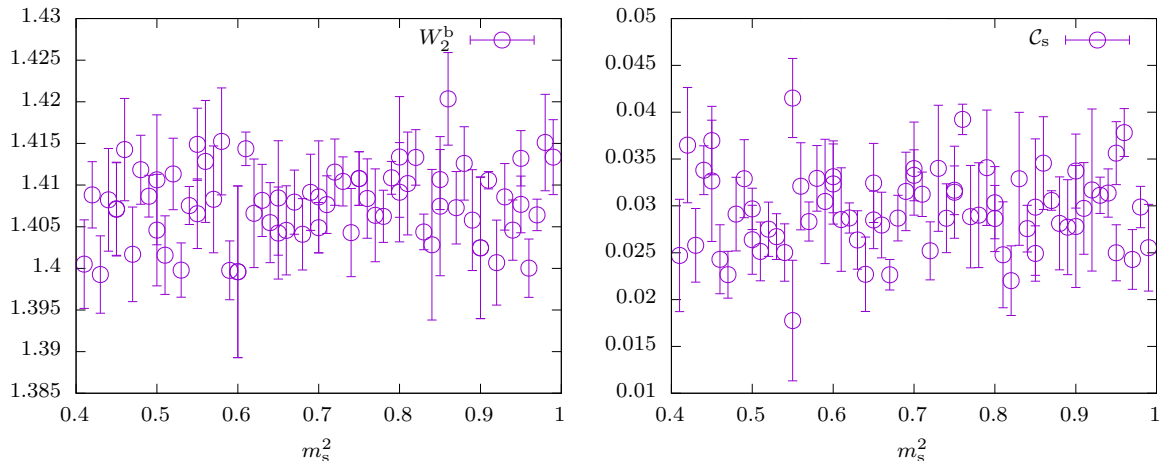


Figure 5.6: Scalar mass dependency of the terms W_2^b (left) and C_s (right) for $\beta = 14$ and close to the critical fermion mass.

identities

$$\begin{aligned}
 W_B &= \beta V^{-1} \langle S_B \rangle + m_s^2 \langle \text{tr } \phi^2 \rangle \rightarrow \frac{9}{2}, & W_3 &= \frac{\beta}{2} \langle \text{tr } D_\mu \phi^a D^\mu \phi_a \rangle + m_s^2 \langle \text{tr } \phi^2 \rangle \rightarrow 3, \\
 W_2 &= \frac{\beta}{4} \langle \text{tr } F_{\mu\nu} F^{\mu\nu} \rangle + \beta \langle \text{tr } \bar{\lambda} \Upsilon \rangle \rightarrow \frac{3}{2}, & W_1 &= \frac{\beta}{2} \langle \text{tr } [\phi_1, \phi_2]^2 \rangle - \beta \langle \text{tr } \bar{\lambda} \Upsilon \rangle \rightarrow 0.
 \end{aligned}
 \tag{5.5}$$

Second, the Ward identity is nearly independent of m_s^2 close to the critical scalar mass. Therefore we use the one-loop result $m_s^2 = 0.6594823$ in our simulations, as this guarantees the right continuum limit. This will reduce the computation cost as we have one mass value less to fine-tune to a critical value. Then again, using the correct critical scalar mass for the given lattice setup could reduce lattice artifacts, bringing us closer to the continuum limit. Unfortunately we found no observable to determine this critical scalar mass.

5.4 Fermion Mass dependency

As stated in section 4.1, the fermion mass is not a relevant operator. Therefore even without fine-tuning the fermion mass m_f , we will reach the correct target theory. Still, in the four-dimensional mother theory, the chiral symmetry and the supersymmetry are connected in such a way, that we can only restore both or none [23]. This lead us to assume, that the fermion mass fine-tuning will improve our lattice results tremendously, leading to results closer to the continuum limit. As shown in the previous section, the critical fermion mass is independent on the scalar mass m_s^2 . Therefore we can ignore the latter it in this section.

By changing the fermion mass term, we influence the chiral symmetry of the system. This could lead to several different properties. We will focus on two of them. The first is spontaneous symmetry breaking, which occurs in the four-dimensional $\mathcal{N} = 1$ SYM

theory but is forbidden in two dimensions [148–150]. Thus it serves as an additional test for the lattice formulation. Second one could encounter a phase transition at the critical fermion mass. In this case one has to determine which of these phases lead to the correct continuum limit. Thus the chiral limit of the theory would become non-trivial.

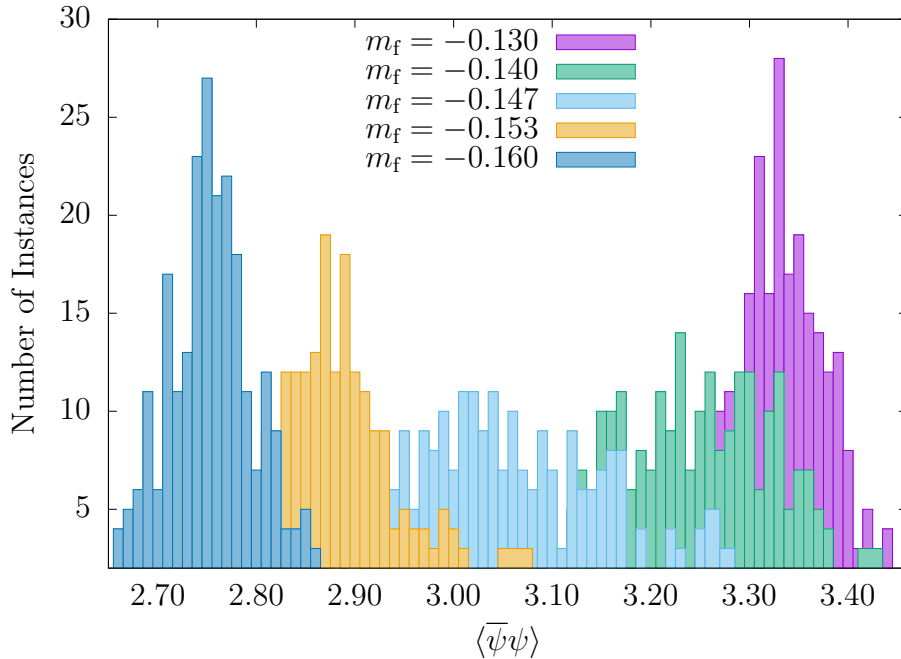


Figure 5.7: Chiral Condensate histogram for four different fermion masses and $\beta = 17$

If chiral symmetry is spontaneously broken, there would be at least two physically equivalent vacuum states, which are related via chiral transformations. They can be discerned by a different value of the chiral condensate. For a finite volume, we can have tunnel events, which lead from one vacuum to the other. Therefore our vacuum state is only meta-stable. In the infinite volume limit, the probability for the tunnel effects vanishes and we recover a stable vacuum state. On the lattice we can observe this behavior only close to the critical fermion mass. The reason is, that if we break chiral symmetry explicitly via the fermion mass, one vacuum is energetically preferred over the other. Close to the critical fermion mass, this energetic difference between the vacua is low increasing the probability of the tunnel effects. If this probability becomes large enough, we can observe the tunnelling effects from one vacuum into the other. Since we do not know their probability, the absence of them in a lattice simulation is no final proof for the absence of spontaneous symmetry breaking. In our work, we try to observe this behavior with the histogram of the chiral condensate. If the tunnelling effect from one vacuum into the other would be observable, we should see a double peak structure. Clearly in Figure 5.7 we do not observe a double peak structure. Even for $m = -0.147$ which is very close to $m_f^c = -0.1488(4)$. Therefore we conclude that

we do not observe any sign of spontaneous symmetry breaking in our simulation, as expected.

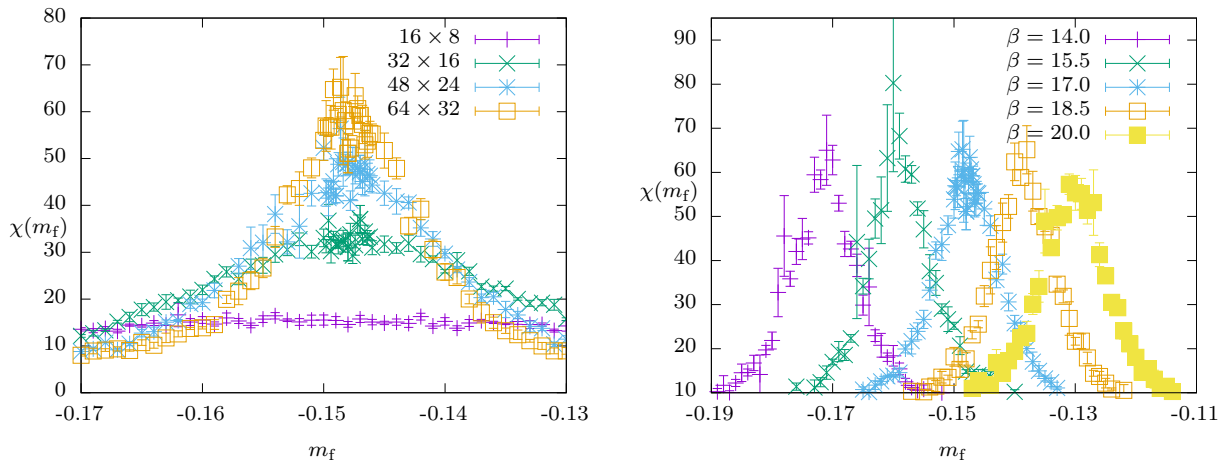


Figure 5.8: Left: χ_{ch} for four different lattice sizes for $\beta = 17$. Right: χ_{ch} for five different β and lattice size 64×32 .

A phase transition can not be observed in a finite volume because it does not allow for nonanalyticities in the partition sum. Still we can do a scaling analysis. Using general arguments we find for the chiral susceptibility $\chi_{\text{ch}} \propto V^e$, where e is a specific exponent depending on the phase transition and V is the physical volume [151, 152]. To relate this equation to the lattice quantities, we use $V = a^2 \tilde{V}$ and $a^2 \propto \beta^{-1}$, where we introduced the lattice volume \tilde{V} . Thus we find $\chi_{\text{ch}} \propto \tilde{V}^e$ and $\chi_{\text{ch}} \propto \beta^{-e}$. To determine e , we measure the chiral susceptibility for different values of the lattice size and inverse gauge coupling β . In the left panel of Figure 5.8 we show the dependency on the lattice size. We find that the peak of the chiral susceptibility is proportional to $\tilde{V}^{\frac{1}{2}}$, which is further emphasized in Table 5.2. In the right panel of Figure 5.8 we show the dependency of the chiral susceptibility on the value of the inverse gauge coupling. We see a decrease of the peak of the chiral susceptibility with increasing β for $\beta \leq 15.5$. Again the data presented in Table 5.2 agree with $e = 1/2$. Note that the errors in the table should be underestimated. The reason is that our data show no clear peak around the critical fermion mass. Instead we find a plateau within the statistical errors. Thus we take the mean value of all possible peak values and give the standard deviation from those. Still as we found agreement between the different lattice volumes and values of the inverse gauge coupling β we think the determination $e \approx 1/2$ should be reliable. Thus our chiral susceptibility grows with the volume and we have a second order phase transition. This is in agreement with the histogram of the chiral condensate, where we see a typical behavior of the first derivative of the partition sum. Therefore in the limit $m_f \rightarrow m_f^c$, the correlation length of fluctuations will increase and long-range interaction become dominant. Hence the actual microscopic interactions are unimportant as long as we meet certain criteria, the most important are symmetries. This means that close

to the critical point m_f^c the error from the discretization of the continuum action will be suppressed and we get closer to the continuum.

β	χ_{ch}	$\chi_{\text{ch}}\beta^{\frac{1}{2}}$	\tilde{V}	χ_{ch}	$\chi_{\text{ch}}\tilde{V}^{-\frac{1}{2}}$
14.0	60(1)	224(4)	16×8	15.2(2)	1.34(2)
15.5	63(2)	248(8)	32×16	32.3(1)	1.43(1)
17.0	58(1)	239(4)	48×24	45.7(7)	1.35(2)
18.5	59(1)	254(4)	64×32	57.5(8)	1.27(2)
20.0	55(1)	246(4)			

Table 5.2: Measurement of chiral susceptibility for different inverse gauge couplings β but fixed lattice volume \tilde{V} (left) and for fixed β and different lattice volumes (right).

5.5 Conclusion

In this chapter, we analyzed the five relevant simulation parameters N_t, N_s, β, m_s^2 and m_f . The result is the final parameter sets, to generate our configuration. These will be used to calculate our lattice results. The first case are the parameter scans we have for example already shown in section 5.3. Since we use them to analyse the Ward identities, the chiral condensate, the chiral susceptibility and the pion mass, only a small amount of configurations was necessary, usually 200 to 1000. The lattice size was 64×32 for all but the cases of $\beta = 40, 60, 80, 100$. Here we used smaller lattices of size 32×16 . The reason is, that we only calculated values which are not dependent on the lattice size for those β values. Furthermore we have to calculate the other mesons, the gluino-gluon/scalarball states, the glueball, the scalarball and the glue-scalarball. All of them seemingly suffer from a bad signal to noise ration. This is the result of large fluctuations, induced by the scalar fields. Hence we need large statistic to resolve the ground state of those states. In Table 5.3 we give the used configurations. They were all simulated on a lattice size of 64×32 . The mass m_f was chosen such that $m_f > m_f^c$. The reason is that we find no sign problem in this region, as we will show in section 6.2.

β	m_f	m_s^2	# C	β	m_f	m_s^2	# C
14.0	-0.1440	0.6594823	10000	15.5	-0.1470	0.6594823	10000
14.0	-0.1550	0.6594823	10000	15.5	-0.1495	0.6594823	10000
14.0	-0.1565	0.6594823	10000	15.5	-0.1520	0.6594823	10000
14.0	-0.1590	0.6594823	10000	17.0	-0.1242	0.6594823	10000
14.0	-0.1615	0.6594823	10000	17.0	-0.1329	0.6594823	10000
14.0	-0.1640	0.6594823	10000	17.0	-0.1350	0.6594823	10000
15.5	-0.1320	0.6594823	10000	17.0	-0.1372	0.6594823	10000
15.5	-0.1420	0.6594823	10000	17.0	-0.1393	0.6594823	10000
15.5	-0.1445	0.6594823	10000	17.0	-0.1415	0.6594823	10000

Table 5.3: Number of Configurations (# C) for the given parameters β , m_f and m_s on a 64×32 lattice.

Chapter 6

Results

After having thoroughly analyzed our lattice setup, we proceed to present our main results of this work. We start with two potential problems of the lattice theory, the so called flat directions and the sign problem. As we will show, both are absent in our lattice formulation. Next we look at the continuum limit of the critical fermion mass. From theoretical argument, we know that it should vanish, hence it represents a further check for our lattice formulation. Afterwards we extrapolate the Ward identities to the continuum limit. They allow us to observe the restoration of supersymmetry. Finally we analyze the mass spectrum of the theory.

6.1 Flat directions

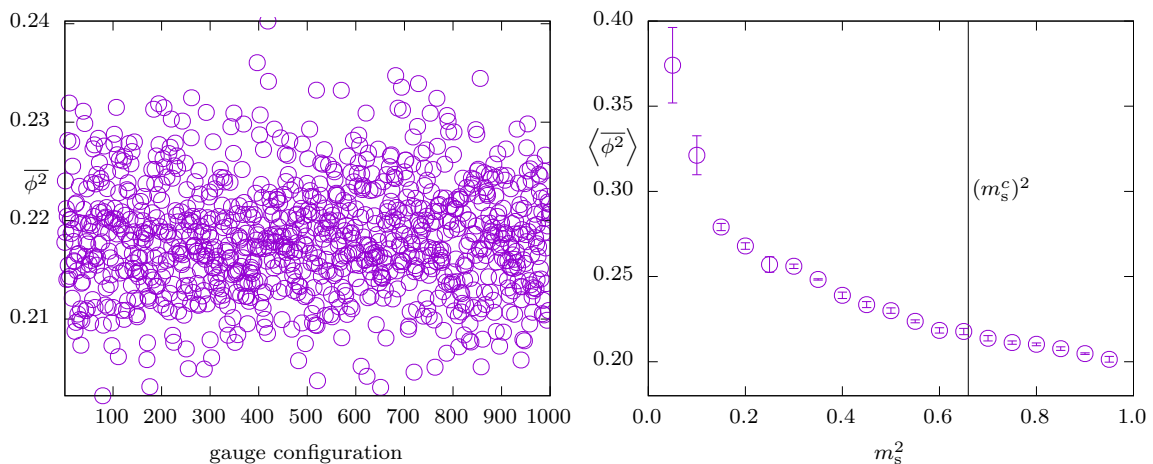


Figure 6.1: Spatial average of squared scalar field as function of Monte-Carlo time for $\beta = 14$, $\kappa = 0.27233$, $m_s^2 = 0.6594826$ (left) and its expectation as function of m_s^2 (right) on a 16×16 lattice.

The potential for the scalar fields

$$V[\phi_1, \phi_2] = [\phi_1, \phi_2]^2 \quad (6.1)$$

has so called flat directions. These flat directions are trajectories in field space which do not change the value of $V[\phi_1, \phi_2]$. One example is the shift

$$\phi_1 \rightarrow \phi_1 + \alpha\phi_2 \quad \phi_2 \rightarrow \phi_2, \quad (6.2)$$

where α is an arbitrary real parameter. Flat directions are a generic feature for SYM-theories with extended supersymmetry. Since they allow scalar fields to grow exponentially, they may destabilize Monte-Carlo simulations. One encounters two different scenarios in lattice calculations. The first is, that quantum effects lift the flat directions dynamically. In this case the problem is not present in the lattice calculation. The second scenario is, that the flat directions are preserved in the lattice theory, which usually spoils the simulation. To solve this problem one can add a mass to the scalar field, lifting the flat directions explicitly. In our lattice formulation, we have to add a scalar mass term anyway (even for $a \rightarrow 0$), to reach the correct continuum limit. Moreover we did not observe the flat directions for a vanishing scalar mass term and small values of the inverse gauge coupling [65]. This is also visible on the right hand side of Figure 6.1, where we observe a finite value of the expectation value of the spatial average $\overline{\phi^2} = 1/V \sum \phi_x^2$ for all m_s^2 considered, including $m_s^2 = 0$. On the left hand side of Figure 6.1 we show the same value as a function of the Monte-Carlo time for $\beta = 14, \kappa = 0.27233$ on a 64×32 lattice. For all set of parameters considered in this work, the value of $\overline{\phi^2}$ never grew to very large values. Hence we conclude, that the flat directions are lifted in our simulation, especially for the m_s^2 close to the continuum value. Therefore the flat directions will not cause problems in our lattice simulations.

6.2 Sign problem

As outlined in section 3.4.2, the sign of the Pfaffian has to be real but could be negative, giving us a possible sign problem in the theory. To measure this sign problem we use the spectral flow method introduced in [28, 30]. The method is based on the idea, that the Pfaffian $\text{Pf}(CD(\kappa))$ is a smooth function of the hopping parameter $\kappa = 1/(2m_f + 4)$. From the definition of the Pfaffian we have the equation

$$\text{Pf}(M)^2 = \det(M) \quad (6.3)$$

where M is a general matrix. In our case M is the Matrix CD , which has double degenerate real eigenvalues λ_i (see section 3.4.2)

$$\det(CD) = \det(D) = \prod_i^{\frac{\Omega(D)}{2}} \lambda_i^2 \quad (6.4)$$

where Ω is the amount of eigenvalues of D . Combining both we get

$$|\text{Pf}(CD)| = \prod_i^{\frac{\Omega(D)}{2}} |\lambda_i|. \quad (6.5)$$

Further we look at the actual computation of the Pfaffian. The result will be a polynomial of κ , showing that the Pfaffian is a smooth function of κ . This is compatible with (6.5) only if any sign change in any eigenvalue as a function of κ induces a sign change in the Pfaffian. For $\kappa = 0$ we have $\det(CD) = \det(C) = 1$ and $\text{Pf}(CD) = \text{Pf}(C) = 1$ showing that the Pfaffian in our theory must be the product

$$\text{Pf}(CD) = \prod_i^{\frac{\Omega(D)}{2}} \lambda_i. \quad (6.6)$$

This also allows us to determine the sign of the Pfaffian. First we introduce the new quantity κ_{spec} which we use to define a new Pfaffian $\tilde{\text{P}}f_{\text{spec}} = \tilde{\text{P}}f_{\text{spec}}(CD[U, \phi, \kappa_{\text{spec}}])$, where U are the link variables and ϕ the scalar fields of the simulation. For a fixed gauge configuration (fixed value of β and κ), characterized by fixed U and ϕ , we can calculate the eigenvalues $\lambda_i(\kappa_{\text{spec}})$ of $CD[U, \phi, \kappa_{\text{spec}}]$ for different values of κ_{spec} . From the previous discussion we know that $\tilde{\text{P}}f_{\text{spec}}(CD[\kappa_{\text{spec}}]) = 1$ for $\kappa_{\text{spec}} = 0$ and $\tilde{\text{P}}f_{\text{spec}}(CD[\kappa_{\text{spec}}]) = \text{Pf}(CD)$ for $\kappa_{\text{spec}} = \kappa$. Therefore by monitoring the flow of the eigenvalues between these two values, we can determine the sign of the Pfaffian, used in the simulation. The sign is only negative, if an odd number of eigenvalues $\lambda_i(\kappa_{\text{spec}})$ change their sign during this flow.

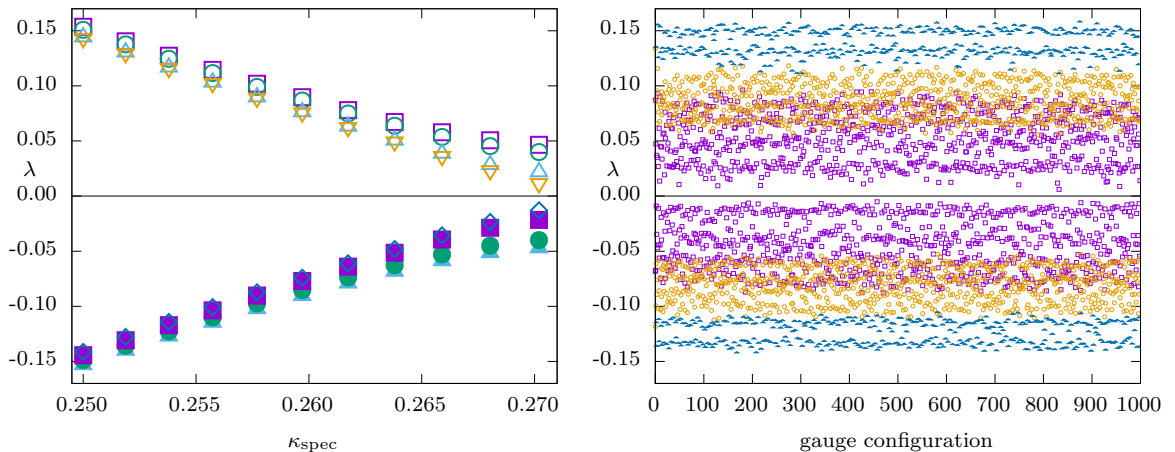


Figure 6.2: Left: Spectral flow of 8 eigenvalues with smallest absolute values for $\beta = 15.5$, $\kappa = 0.27020$ on a 64×32 lattice. Right: Smallest eigenvalues for three different values of the spectral flow parameter κ_{spec} : 0.25379 (blue triangles), 0.26174 (orange circles) and κ (purple squares).

On the left hand side of Figure 6.2, we show the eight eigenvalues with the smallest absolute value for $\beta = 17$ and $\kappa = 0.27020$ as a function of κ_{spec} . We see that the positive eigenvalues decrease monotonously, while the negative eigenvalues increase monotonously. Still neither of them crosses zero, thus the Pfaffian of this gauge configuration must be positive. On the right hand side of Figure 6.2, we show the eigenvalues with the smallest absolute value for three different values of $\kappa_{\text{spec}} = \kappa, 0.25379, 0.26174$ for 1000 gauge configurations. We see that for $\kappa_{\text{spec}} \rightarrow \kappa$ the absolute value of the eigenvalues decreases but they are still large enough to not cross the zero value for all gauge configurations. We checked this by looking explicitly at the spectral flow for all 1000 gauge configurations. This leads to the conclusion, that the Pfaffian is always positive for this parameter set. We repeated this analysis for different volumes, inverse gauge couplings and hopping parameters. For $\kappa < \kappa_c$ we always found a positive sign of the Pfaffian, while for $\kappa > \kappa_c$ we observed approximately one negative sign per thousand configurations. Therefore we conclude, that our simulations do not suffer from a sign problem. In the continuum limit this property should be conserved, because the continuum theory has no inherent sign problem [48].

6.3 Continuum limit of the critical fermion mass

In section 4.1 we explained, that the fermion mass term is not a relevant parameter. Consequently we can decide to not fine-tune the quantity and end up in the right continuum value. This is possible, because all non relevant operators will vanish in the continuum limit. Since we still do a fine-tuning of the fermion mass, we should observe $m_f^c \rightarrow 0$ in the continuum limit. To verify this theoretical result, we introduce a second possibility to determine the critical fermion mass. In section 5.4 we used the peak of the chiral susceptibility to determine the critical fermion mass. While this is a reliable method, it has some small flaws. First, a determination of the position of the peak and its error is quite challenging, as explained in chapter 5.4. The second is, that the peak is in the region of the fermion mass, where we expect massless mesons states in the theory (see section 6.5.1). Still we can measure those mesons masses, which turn out to be non-zero. Thus we have states in this region which can not be represented faithfully in the lattice theory. Hence there must be lattice artifacts which lead to this effect. While these artifacts could have no influence on the chiral susceptibility, we can not exclude it. Therefore we are interested in another independent method.

Fortunately for the four-dimensional theory there is another method, which makes use of the mass of the pion [31, 36, 153]. As in four dimensions, the pion is not a physical particle because we have only one flavor. Still we can define its correlation function in a partially quenched setup. Here we view our lattice theory as if a second fermion flavor is quenched, which means its fermion determinant in the partition function is

set to unity. In this case, the correlation function for the pion will be the connected part of the correlation function of the η -meson

$$C_\pi(x, y) = \langle -\text{tr} (D^{-1}(x, y) \Gamma_5 D^{-1}(y, x) \Gamma_5) \rangle. \quad (6.7)$$

The mass, which we can extract from this correlation function, is related to the renormalized gluino mass by

$$m_q \propto m_\pi^2. \quad (6.8)$$

While all arguments to derive this result were made in the four-dimensional $\mathcal{N} = 1$ SYM theory, we expect it will also hold in two dimensions. Thus we have a second method to determine the critical fermion mass independent from the chiral susceptibility. Note, that this method to derive the critical fermion mass has also flaws. For example it is not clear, for which fermion masses the relation (6.8) holds. We explicitly see this problem in our results, where we find that the pion mass is proportional to the renormalized gluino mass. Thus the relation (6.8) holds only for values very close to the critical fermion mass.

β	14.0	15.5	17.0	40
$m_f^c(\chi_s)$	-0.1738(8)	-0.1595(7)	-0.1488(4)	-0.0757(4)
$m_f^c(\pi)$	-0.1730(11)	-0.1615(6)	-0.1511(7)	-0.0756(7)
β	60	80	100	
$m_f^c(\chi_s)$	-0.0553(3)	-0.0448(3)	-0.0380(5)	
$m_f^c(\pi)$	-0.0542(4)	-0.0433(26)	-0.0365(6)	

Table 6.1: Critical fermion mass m_f^c for different β . To determine the mass we use the chiral susceptibility and the mass of the pion ground state.

The results of both methods are given in Table 6.1. We find comparable values of the critical fermion mass for all values of the inverse gauge coupling β . Since these results do not depend on the lattice size, the continuum limit of the critical fermion mass is reached for $\beta \rightarrow \infty$. This also allowed us to include results for $\beta = 40, 60, 80, 100$ on smaller lattices. Further we find that the fermion mass approaches zero from below in the continuum limit, as expected. In section 5.1 we have shown $\sqrt{\beta} \propto a^{-1}$. With this relation in mind we try to find a continuum extrapolation with the ansatz

$$m_f^c(\beta) = m_\infty + c_1 \beta^{-e_1} + c_2 \beta^{-e_2}. \quad (6.9)$$

The coefficients c_i encode lattice artefacts and m_∞ is the value of the critical fermion mass in the continuum limit. As we did not know the correct dependence of $m_f^c(\beta)$ we tried several integer and half-integer values for e_i and one fit with a free exponent.

m_∞	c_1	c_2	e_1	e_2	χ_w^2	χ^2
0.0051(26)	-0.285(32)	-1.44(8)	<u>1/2</u>	<u>1</u>	1.33	6.33×10^{-7}
-0.0126(8)	-2.64(5)	5.48(69)	<u>1</u>	<u>2</u>	2.31	7.88×10^{-7}
-0.0041(18)	-1.48(6)	<u>0</u>	0.820(18)	-	1.06	5.42×10^{-7}

Table 6.2: Fit values for the fit function given in (6.9), for three different sets of parameters. The mass m_∞ represents the continuum value of the critical fermion mass m_f^c , which should be zero. The underlined parameters are prescribed in the 2-parameter fits.

In Table 6.2 we give the results, which were able to best represent the data over the whole β range. Furthermore we give two different values χ_w^2 and χ^2 for the goodness of the fit. While χ_w^2 takes into account the errors for m_f^c , χ^2 does not. Since the values of χ^2 is well below one, we find that the fit functions describe the data very well. On the other hand χ_w^2 is roughly one. The reason is most probably that we underestimated the error for the critical mass, which we estimated from the fits alone. A better alternative would be to include the statistical error. Unfortunately we would have to increase the number of configurations by a factor of twenty to get reliable jackknife errors. In face of these computing costs we refrained to calculate better errors for a value, which serves mostly as a test of our lattice simulations. Nonetheless, the results for all values of m_∞ are compatible with zero, when taking into account the uncertainties.

6.4 Ward Identities

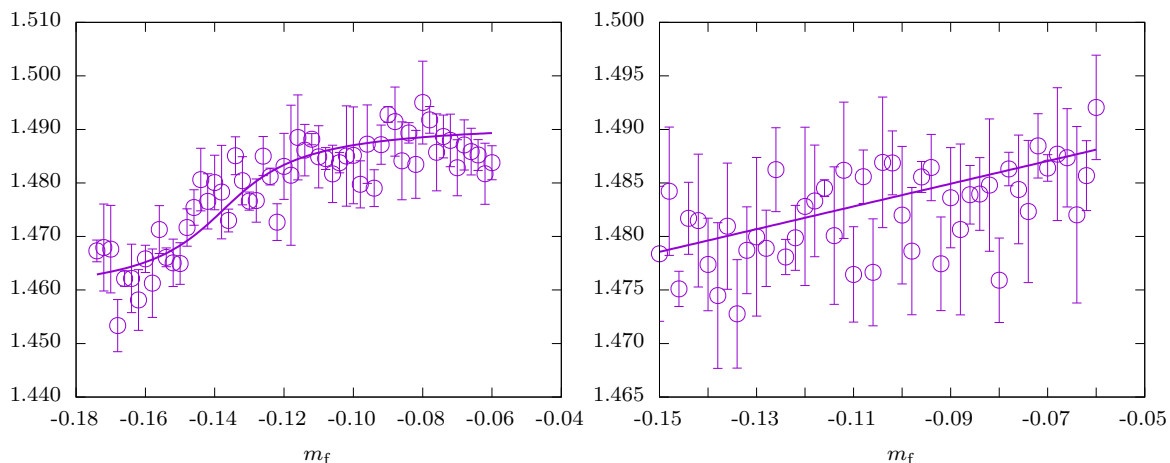


Figure 6.3: The Ward identity W_2 in (5.5) is shown for $\beta = 17$ (left) and $\beta = 40$ (right).

In sections 2.6, 4.3 and 5.3 we have already discussed properties of the Ward identities. Here we want to report on the numerical results for our simulations, especially

the continuum limit. Since the Ward identities do not suffer from finite volume lattice artefacts, we used additional lattices with parameters $\beta = 40, 60, 80, 100$, $L_T = 32$ and $L_S = 16$. As explained in section 5.3, we must extrapolate the Ward identities to the chiral limit. This is only possible if we have a guess for the functional dependence of the Ward identities on the mass m_f . As we have shown in section 5.4, the chiral observables show no sign of a spontaneous symmetry breaking. Therefore, the Ward identities should be smooth functions of m_f . Looking at the actual lattice data we find a smooth step function. Combining these result, we use the following ansatz close the the critical fermion mass m_f^c

$$W(m_f) \sim a \arctan \{ \xi (m_f - m_*) \} + b \quad (6.10)$$

with fit parameters a, b, m_* and ξ . We can interpret the ξ as the lattice correlation length. m_* is a free value which should be equal to the critical fermion mass m_f^c . We found a deviation between both values, which is comparable to the difference between the critical fermion mass determined with the peak of the critical susceptibility and with the pion mass. On the left panel of Figure 6.3 we show the result for the Ward identity W_2 . This Ward identity is dominated by the field strength tensor squared. Still our ansatz proves to be a good approximation for the considered fermion masses. On the right panel of Figure 6.3 we show the same Ward identity for $\beta = 40$. Here we do not observe a step function anymore. Therefore we used a linear extrapolation for $\beta \gtrsim 40$. This is in agreement with our previous ansatz, which becomes linear for $m_f \approx m_*$.

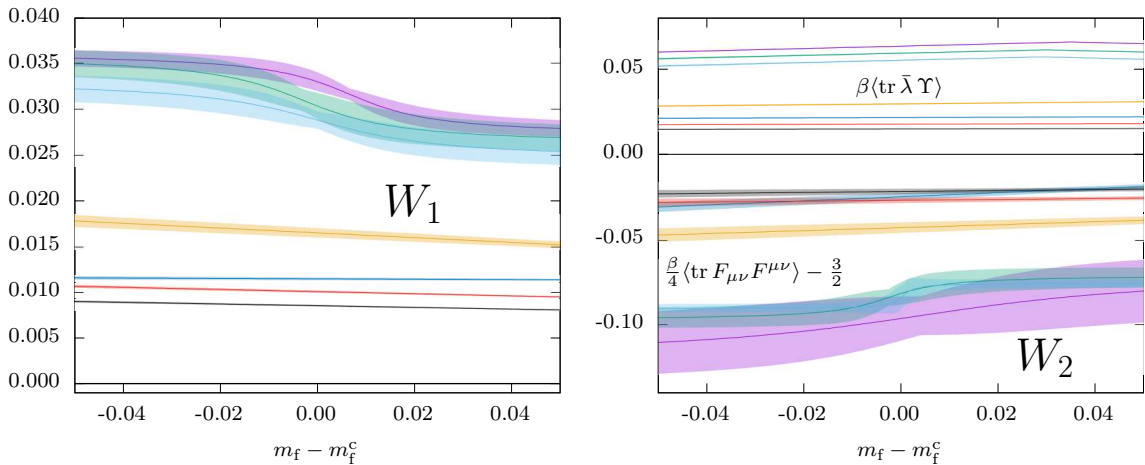


Figure 6.4: Ward identities (5.5) as functions of $m_f - m_f^c$ for various values of β between 14 and 100. The colors represent different β : 14 \color{purple} , 15.5 \color{green} , 17 \color{blue} , 40 \color{orange} , 60 \color{teal} , 80 \color{red} and 100 \color{black} . For W_1 (left panel) we show the fits and standard deviations (confidence band). For W_2 (right panel) we show the two components $\beta \langle \text{tr } \bar{\lambda} \Upsilon \rangle$ (upper half) and $\frac{\beta}{4} \langle \text{tr } F_{\mu\nu} F^{\mu\nu} \rangle$ (lower half).

In Figure 6.4 we show the results for W_1 and the two contributions to W_2 in (5.5) for all considered β . Looking at the value at the critical fermion mass, we see a monotonic convergence to the theoretical value for all Ward identities. Using these points we can perform the extrapolation to the continuum limit ($\beta \rightarrow \infty$). Again we lack the full understanding of the full quantum theory, therefore we do not know the right extrapolation function. Hence we used fit functions of the form

$$W(\beta) = W_\infty + b\beta^{-c}, \quad (6.11)$$

where W_∞ is the value of the Ward identity or its component in the continuum limit. Here we employed the fits, with the prescribed value $c = 1/2$ for Fit 1, $c = 1$ for Fit 2 and no prescribed parameter for Fit 3. We display the fits in Figure 6.5. In contrast to the first two fits, Fit 3 has large error bands. This is due to the additional fit parameter, allowing greater flexibility for the fit parameters. In Table 6.3 we give W_∞ for W_1 , the sum of the extrapolated components of W_2 and W_3 and the sum of these values for W_B . Since we used three different fit functions, we can estimate the systematic error coming from the choice of a particular fit function. This allows us to alleviate our bias in choosing the fit functions by calculating a weighted average, where we took into account the goodness of the fits. Within the statistical errors, all Ward identities clearly point to the restoration of supersymmetry in the continuum limit. Thus we find no sign of spontaneous supersymmetry breaking. This is in accordance with the \mathcal{Q} -exact methods [56].

Ward identity	W_1	W_2	W_3	W_B
$\beta = 14.0$	0.0323(8)	1.4678(79)	3.0222(5)	4.5241(126)
$\beta = 15.5$	0.0304(16)	1.4732(118)	3.0231(8)	4.5298(143)
$\beta = 17.0$	0.0288(10)	1.4688(38)	3.0185(9)	4.5197(128)
$\beta = 40.0$	0.0165(5)	1.4834(6)	3.0007(6)	4.4867(11)
$\beta = 60.0$	0.0123(1)	1.4918(6)	2.9968(8)	4.5053(6)
$\beta = 80.0$	0.0101(1)	1.4901(6)	2.9977(6)	4.4973(9)
$\beta = 100.0$	0.0085(1)	1.4920(5)	2.9972(6)	4.5004(8)
$\beta \rightarrow \infty$ (Fit 1)	-0.0053(3)	1.5105(71)	2.9773(66)	4.4825(140)
$\beta \rightarrow \infty$ (Fit 2)	0.0046(1)	1.4981(46)	2.9909(27)	4.4936(74)
$\beta \rightarrow \infty$ (Fit 3)	-0.0021(14)	1.5507(872)	3.0006(125)	4.5492(1011)
$\beta \rightarrow \infty$ (weighted average)	-0.0024(13)	1.5267(424)	2.9885(70)	4.5128(507)
theor. value	0	$\frac{3}{2}$	3	$\frac{9}{2}$

Table 6.3: Values of Ward identities for different values of β on a 32×16 lattice. The last five rows contain the continuum extrapolations with three different fit functions and a weighted average as well as the theoretical value for unbroken supersymmetry.

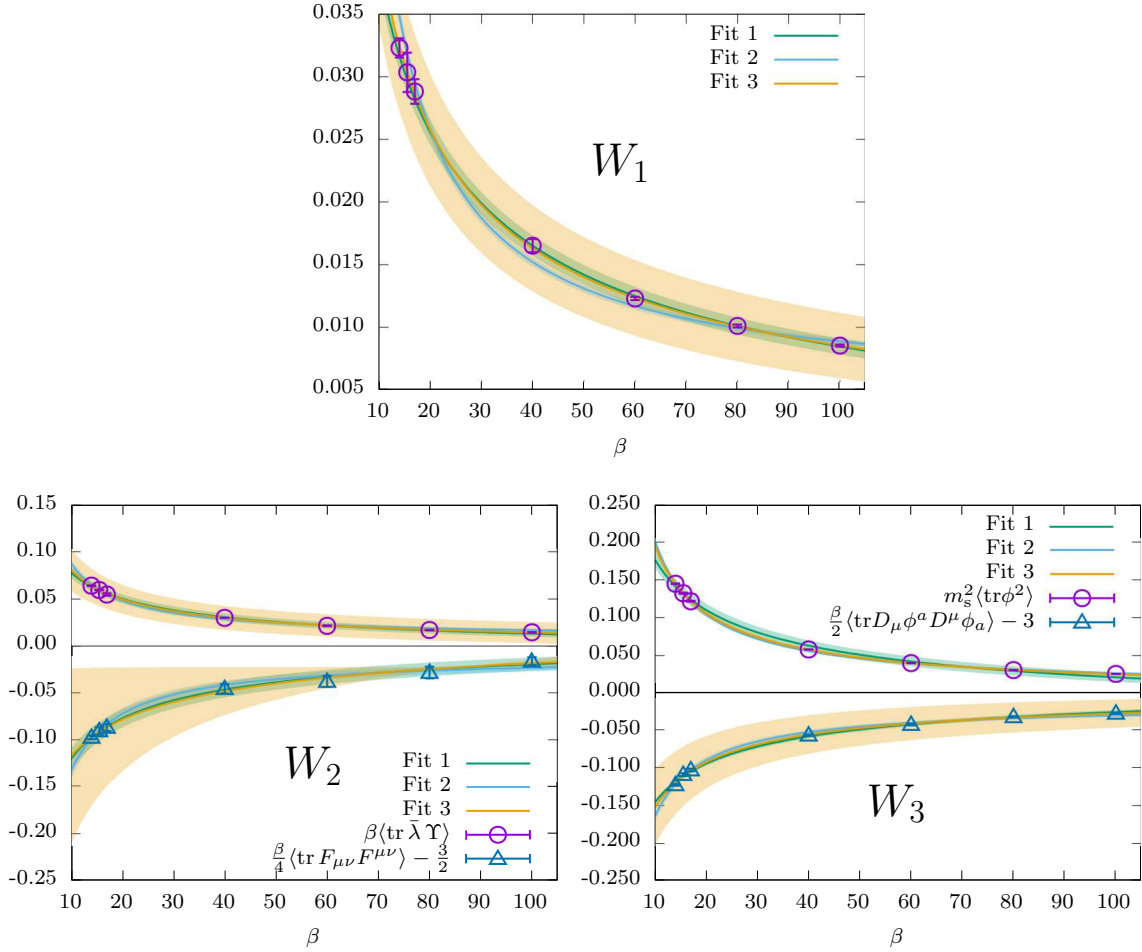


Figure 6.5: Ward identities for different values of β together with three different fits used for the continuum extrapolation.

6.5 Mass spectrum

In order to determine physical results from the lattice, we have to perform the continuum limit. Its first step is the infinite volume limit. We discussed this for the mesons already in section 5.2. Next is the chiral limit. Since we need large statistics to extract the mass of the f -meson, we will calculate the masses for several different values of κ and extrapolate the results to the critical value $\kappa_c(\beta)$. In this limit the gluino mass vanishes and in accordance with 6.8 the pion mass vanishes. Finally we have to extrapolate to vanishing lattice spacing ($\beta \rightarrow \infty$). We use three different values of the inverse gauge coupling β for this purpose. We will split this section further into three subsections, where we grouped the different particles as follows: we start with the mesons, next are the gluino-glueballs and we conclude this subsection with the glueballs, scalarballs and glue-scalarballs.

6.5.1 Mesons

In the dimensional reduced VY-multiplet (see Table 2.2), we find the η - and f -meson. Here we will also include the π -meson into our analysis because we know its continuum value, which will give us a reference point for the masses. We start by depicting the correlation functions for all three mesons for two different values of $\kappa \leq \kappa_c$ in Figure 6.6. For the value $\kappa = 0.26903$, the mass of the ground state of all mesons is slightly above the lattice cut-off. The first observation is, that for both κ the η - and π -meson correlation functions are very similar for intermediate values of t . For even larger t , the slope of the correlation function of the π -meson is steeper than the one for the η -meson. Thus the ground state of the latter must be lighter. This observation holds for all other κ used in this work. As the ground state mass of the pion vanishes in the chiral limit, the same must be true for the η -meson.

Next we turn our attention to the difference between the η - and f -meson correlation functions. While for $\kappa = 0.26655$ the correlation functions differ considerably, closer to the chiral limit ($\kappa = 0.26903$), they become more similar. We observed this trend for all three inverse gauge couplings and will also show it in terms of the masses of the ground and excited states of these mesons. This result leads to the conclusion, that both mesons will form a multiplet in the chiral limit. Thus also the ground state mass of the f -meson must be massless.

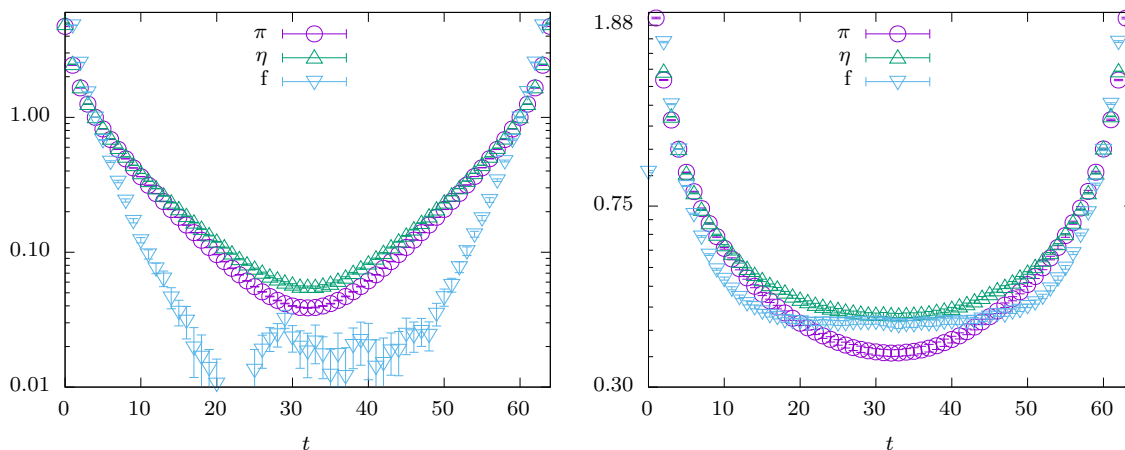


Figure 6.6: The η -, π - and f -meson correlation functions are shown for $\beta = 17$, $\kappa = 0.26655$ (left) and $\kappa = 0.26903$ (right).

To further investigate this non-trivial formation of the multiplet, we scrutinize the two different contributions to the correlation functions. Recalling, that the pion correlation functions is just the connected part of the η -meson correlation function, we have to focus only on the correlation functions of the η - and f -meson, depicted in Figure 6.7. In case of the η -meson correlation function, we find that the connected part is at least one order of magnitude larger than the disconnected part. This explains, why the η - and π -meson correlation functions are similar for intermediate t . Towards

$t = N_T/2$ the disconnected part becomes even smaller, yet we find two different masses for the ground state of both mesons. In the case of the f -meson correlation function, both contributions are roughly of equal size over the whole t range. As it will form a multiplet with the η -meson, we find a non-trivial degeneracy between both correlation functions. The determined masses of the ground state and excited state are depicted in Table 6.4 as well as in Figure 6.8. We observe that the mass of the η -meson ground

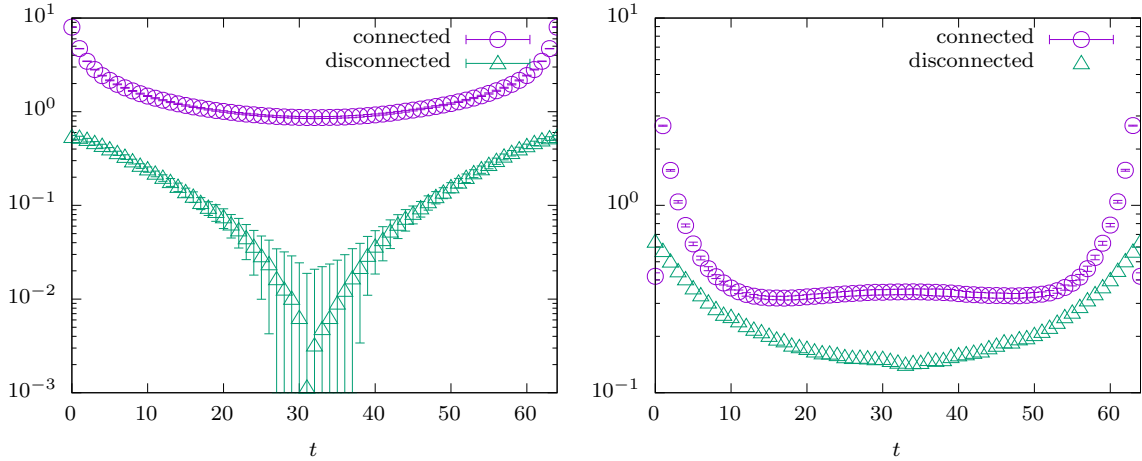


Figure 6.7: Connected and disconnected part of the η -meson (left) and f -meson (right) correlation function for $\beta = 17$ and $\kappa = 0.26903$.

states depends linearly on the fermion mass m_f . Using a linear fit to extrapolate to the chiral limit, we find a zero crossing almost exactly at the value of the critical fermion mass m_f^c . Thus we conclude that $m_\eta \propto m_f - m_f^c$, as also seen from the fits in the left panel of Figure 6.8. For the f -meson we see this proportionality only close to the critical fermion mass, where the ground state mass of both mesons coincide. This agreement improves for large values of β .

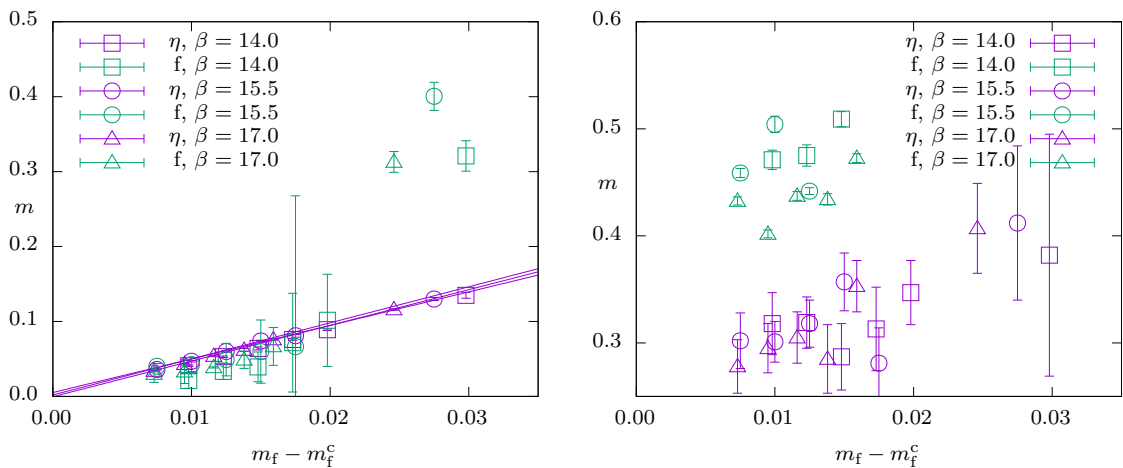


Figure 6.8: Ground (left) and excited (right) state masses of the η - and f -meson as function of the fermion mass for $\beta = 14, 15.5$ and 17 . For the mass of the η -meson ground state, we show linear fits.

In case of the excited states, we find a more involved picture. The reason is that it is more difficult to extract those values. For the η -meson, we use a fit with three masses for the correlation function, which agrees rather well over the whole t -range. As the largest of these three masses is well above one, it is afflicted with large lattice artifacts and thus discarded. Hence we give only the values of the other two, which are the mass of the ground state and the first excited state. For the f -meson this was impossible. Here we used a different strategy. First we scrutinized the effective mass extracted from the correlation function, where we found a plateau for large values of t , corresponding to the mass of the ground state. Using this value as a fixed external input, we proceeded to extract the mass of first excited state from correlation function using the region of small t . Unfortunately this method leads to a large unknown systematic error. Again we see that our results improve for increasing β , which allow to extract more values and more importantly the mass of the first excited state decreases. Thus we could see a convergence of the mass of both excited states in the continuum limit. Unfortunately we can not pursue this idea, as our results do not even allow for an unambiguous extrapolation to the chiral limit.

$\beta = 14.0$						
κ	0.26940	0.27086	0.27122	0.27159	0.27196	0.27233
m_η	0.135(4)	0.089(1)	0.076(1)	0.064(2)	0.053(1)	0.041(1)
m_f	0.359(7)	0.247(4)	0.254(3)	0.074(2)	0.053(1)	0.046(2)
m_{η^*}	0.382(113)	0.347(30)	0.313(39)	0.287(31)	0.319(24)	0.318(29)
m_{f^*}	-	-	-	0.509(7)	0.475(10)	0.471(9)
$\beta = 15.5$						
κ	0.26767	0.26911	0.26947	0.26983	0.27020	0.27056
m_η	0.130(2)	0.081(2)	0.074(1)	0.060(1)	0.047(1)	0.036(1)
m_f	0.362(5)	0.275(4)	0.140(5)	0.059(1)	0.052(1)	0.037(1)
m_{η^*}	0.412(72)	0.281(33)	0.357(27)	0.318(22)	0.301(19)	0.302(26)
m_{f^*}	-	-	0.656(23)	0.442(3)	0.504(8)	0.459(4)
$\beta = 17.0$						
κ	0.26655	0.26779	0.26810	0.26841	0.26872	0.26903
m_η	0.116(1)	0.076(1)	0.062(2)	0.054(1)	0.043(1)	0.034(2)
m_f	0.335(2)	0.094(2)	0.064(3)	0.052(4)	0.030(1)	0.034(1)
m_{η^*}	0.407(42)	0.353(24)	0.285(32)	0.305(24)	0.295(23)	0.278(25)
m_{f^*}	-	0.473(4)	0.434(5)	0.437(4)	0.402(4)	0.433(4)

Table 6.4: Masses of the η - and f -meson ground and excited states.

6.5.2 Gluino-gluon/scalarball

In the dimensional reduced super-multiplet (see Table 2.2), we find the gluino-gluon/scalarball states. As already stated in section 2.5, we will look at first at the individual contributions from the gluino-gluonball and the gluino-scalarball. As interpolating fermionic operator we used

$$\mathcal{O}_{GG} = \Gamma_{\mu\nu} F^{\mu\nu} \lambda \quad (6.12)$$

for the gluino-gluonball and

$$\mathcal{O}_{GS} = \Gamma_{23} [\phi_1, \phi_2] \quad (6.13)$$

for the gluino-scalarball. In our work, we focused on the gluino-gluonball, because the signal to noise ratio for the gluino-scalarball made an extraction of the mass impossible. The operator \mathcal{O}_{GG} transforms as a Majorana fermion. Thus we could use the projectors $P_{\pm} = (1 \pm \Gamma_0)/2$ to get a definite parity for these states. Instead we use a numerical more convenient projection, leading to periodic (S) and antiperiodic (A) correlation functions

$$C_A(t) = \langle \mathcal{O}_{GG}(t) \mathcal{O}_{GG}^{\dagger}(0) \rangle, \quad C_S(t) = \langle \mathcal{O}_{GG}(t) \Gamma_0 \mathcal{O}_{GG}^{\dagger}(0) \rangle. \quad (6.14)$$

Any other contraction of the gluino-gluonball over Γ -matrices can be written as a linear combination of these two correlation functions [154]. This reflects the fact, that we have only two independent physical states, differing by their parity. The determination of this state for large lattice sizes is only possible with noise reduction techniques, namely Jacobi and Stout smearing. Since the effectiveness of the later is tremendously higher, we will focus on this smearing method. As explained in section 3.6, we will only talk about the smearing level S . In the left panel of Figure 6.9 we show the correlation function $C_S(t)$ for different smearing levels. Despite going to very high smearing levels (up to 400), we see a constant improvement of the signal. Another test to check the smearing process was the computation of the expectation value of average of the plaquettes on the lattice, as in [132]. Here we find an ever increasing result, showing no signs of break down due to the high levels of smearing. Therefore we think, that these high levels of smearing will not invalidate our results.

In Table 6.5 we depict the masses of the gluino-gluonball for different smearing levels in the case of $\beta = 17$ and $m_f = -0.1415$. We observe a nice convergence for both masses. Looking at the right panel of Figure 6.9, we see a good agreement of both masses, as expected in a parity symmetric theory. Further, this value depends only very weakly on the inverse gauge coupling β and the bare fermion mass m_f .

Comparing this result with the corresponding results for the mesons, we find that the mass of the gluino-gluonball is comparable to the masses of the excited mesons. Therefore the ground states of the mesons and the ground state of the gluino-gluonball

6. Results

S	0	6	12	18	24	30	36
m_A	0.324(13)	0.531(29)	0.404(16)	0.358(13)	0.333(11)	0.315(10)	0.302(10)
m_S	0.391(12)	0.633(14)	0.517(7)	0.469(5)	0.441(4)	0.421(4)	0.406(4)
S	48	80	240	400	1200	2400	3600
m_A	0.282(9)	0.256(12)	0.234(5)	0.222(1)	0.165(2)	0.163(2)	0.168(2)
m_S	0.384(3)	0.347(11)	0.270(3)	0.252(2)	0.224(5)	0.214(4)	0.214(5)

Table 6.5: Extracted masses for different smearing levels S for the symmetric and antisymmetric gluino-gluon states for $\beta = 17$ and $m_f = -0.1415$.

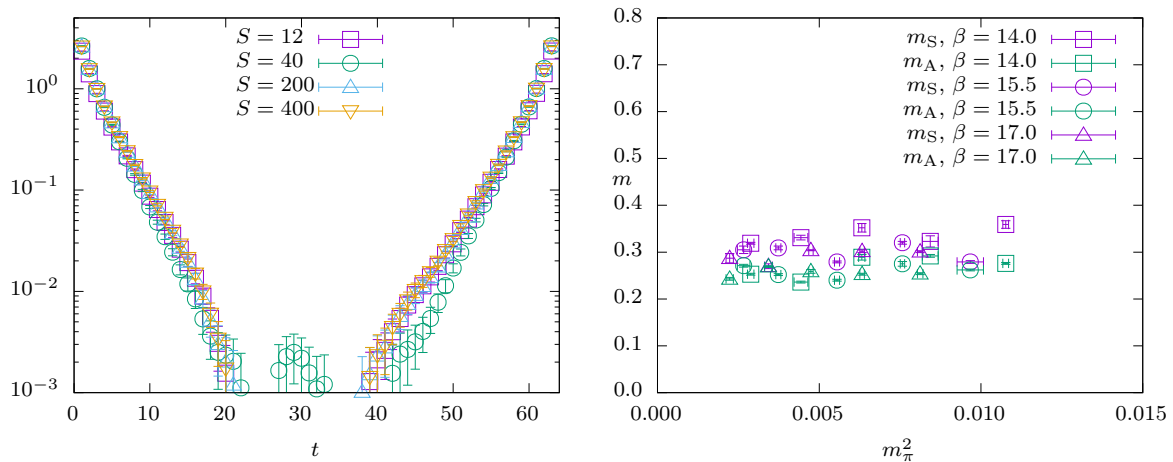


Figure 6.9: Left: Gluino-gluon correlation function $C(t)$ as function of the temporal extent t at $\beta = 17$ and $m_f = -0.1350$ for different smearing levels S . Right: Gluino-gluon mass as a function of the squared pion mass.

does not seem to form a multiplet. We have two possible explanations for this behavior. The first comes from the numerics. Looking at the correlation function for the gluino-gluon, we see a rapid decrease. Hence our signal to noise ratio reduces quickly in the euclidean time t . Since we expect to find the ground state for $t \rightarrow \infty$, the signal of the ground state will be suppressed and we are unable to measure it. On the other hand, smearing should always enhance the signal of the ground state compared to the excited states. Therefore we expect to see only the ground state for high smearing levels. Unfortunately, we see no sign of an excitation with a mass comparable to the mass of the ground states of the mesons in this case. Thus our smearing might not be able to extract the ground state. The second explanation for this problem comes from our statements in section 2.5. Here we saw that the gluino-gluon is not part of the supermultiplet, but a mixture of the gluino-gluon and the gluino-scalarball. Hence the gluino-gluon correlator must not accommodate all masses of this mixed state. It could be that we find a lighter mass for the gluino-scalarball or the cross correlator between the gluino-gluon and the gluino-scalarball. Unfortunately, this remains a conjecture, since we were not able to extract the mass of the gluino-scalarball, even for

high levels of scalar field smearing.

6.5.3 Glueball, Scalarball and Glue-scalarball

In the reduced FGS-multiplet (see Table 2.2), we find a mixed state consisting of glue- and scalarballs and a glue-scalar ball. For the mixed state we looked at the correlation functions of glueballs and scalarballs. In the left panel of Figure 6.10 this is shown for the glueball. The correlation function is zero for all distances t apart from $t = 0, 1, 63$ and 64 . We can compare this result with the glueball correlator of pure Yang-Mills theory on a two-dimensional lattice, derived in section 4.4. In this section, we found that the correlation function of the glueball is only non-zero, when the support of the interpolating operators for the glueballs intersect (both supports have at least one common gauge link). In our work we use the clover plaquette as the interpolating operator. Its support is a square with two link variables per edge. This would suggest that we see also correlation for $t = 2$ and $t = 62$. Looking closer at the clover plaquette, it is a sum of several plaquettes. For a time distant of two, the amount of intersecting plaquettes is reduced, thus this correlation will be suppressed and more difficult to observe in our simulation. Hence the most likely explanation is, that the glueballs only interact via contact interaction.

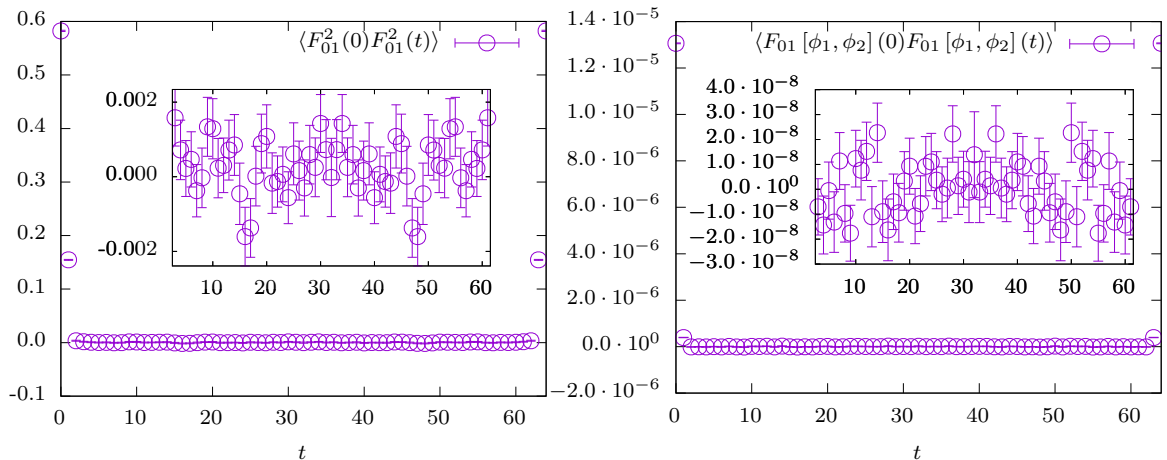


Figure 6.10: The glueball (left) and glue-scalarball(right) correlation function for $\beta = 17$ and $m_f = -0.1350$.

To further compare our result with the pure Yang-Mills case we introduce smearing of the link variables via stout smearing. As argued in section 4.4 smearing increases the support of the interpolating function, inducing more artificial correlation for the glueball correlation function. In Figure 6.11 we compare the results for pure Yang-Mills theory to $\mathcal{N} = (2, 2)$ SYM theory. For both correlation functions we see the same qualitative behavior. With increased smearing levels, we observe more non-zero values of the correlation function, as expected. The smearing effect should also be visible

in the effects mass. Again we see the same qualitative behavior for both theories: the effective mass is an ever increasing function of the distance t , which decreases with higher smearing levels. We conclude, that the glueballs of the two-dimensional $\mathcal{N} = (2, 2)$ SYM behave as the glueballs of the pure two-dimensional Yang-Mills theory. Therefore the glueball correlator will decouple from the theory. The same observation was made for the scalarball and the glue-scalarball. The correlation function of the latter is shown in the right panel of Figure 6.10. It is important for the conclusion about the dimensionally reduced FGS-multiplet. For this multiplet, the only pure state is the glue-scalarball. Since it shows no correlation, we expect from supersymmetry, that the cross correlation function of glue- and scalarball will also show no correlation. Hence the whole multiplet decouples from the theory. In addition to the glue-, scalar- and glue-scalarball, this multiplet contains also an excitation of the gluino-gluon/scalarball. Using our previous analysis, this excitation has to decouple from the lattice theory, hence it should show no correlation. Thus it will not be possible to observe it in our gluino-gluon correlation function and was not seen in our simulation.

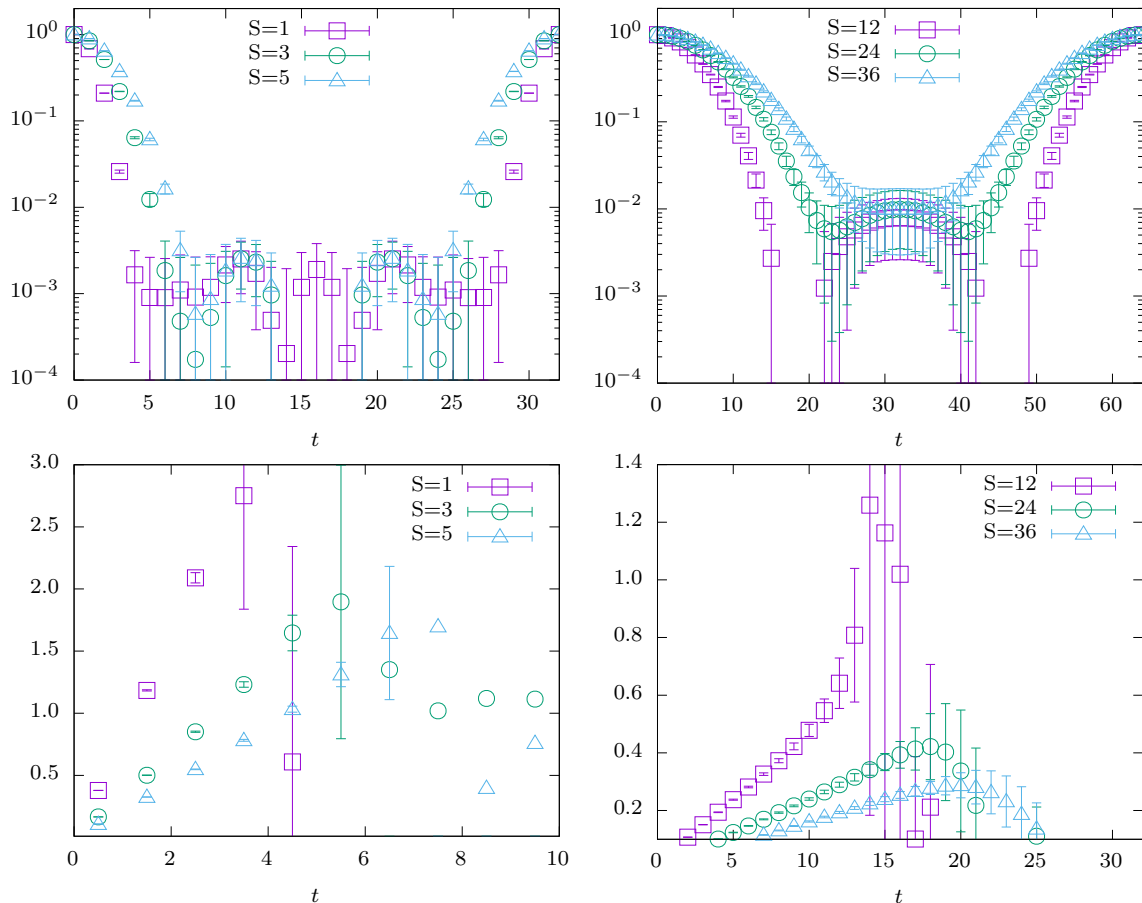


Figure 6.11: Comparison between the Glueball correlation function for the two-dimensional Yang-Mills theory (left) and the two-dimensional Super Yang-Mills theory (right) for different smearing levels S . In the bottom row we plot the effective mass.

Chapter 7

Conclusion

Supersymmetric gauge theories possess interesting non-perturbative features like confinement and chiral symmetry breaking. Thus we need appropriate methods to investigate these models. In this thesis we have chosen numerical lattice calculations, which are used successfully to calculate non-perturbative features of QCD. The investigated model is the two-dimensional $\mathcal{N} = (2, 2)$ SYM theory, which is derived by a dimensional reduction of the four-dimensional $\mathcal{N} = 1$ SYM theory. Therefore we used several results of this mother theory as an inspiration for our simulation.

In the first part of the thesis, we presented our lattice setup and analyzed it theoretically. The first interesting and important point is the choice of the Wilson mass term. As we have seen that we can define two different chiral symmetries, one for the Majorana fermions of the reducible form of the action and one for the Dirac fermions of the irreducible form of the action, we can also introduce two different kinds of Wilson fermions. To keep our simulation close to the four-dimensional mother theory, we have chosen the former. This leads to an asymmetry between the momenta of the fermions and the scalars, introducing a scalar mass term in the effective action of the lattice theory [64]. Thus we need to fine-tune the scalar mass term, which is the only relevant operator for our formulation. Yet we perform an in principle unnecessary additional fine-tuning of the fermion mass term, because this operator is deeply connected to the supersymmetry breaking of the four-dimensional mother theory [23]. In the case of our two-dimensional theory, we saw a considerable improvement of our lattice results.

In the second part of the thesis, we presented results of the numerical simulation of our theory. First we investigated the parameter space, especially the inverse gauge coupling β , the lattice volume and the two mass terms m_s^2 and m_f . We found that for small values of β we seem to be in the wrong lattice phase, which does not allow for an extrapolation to the continuum limit. Thus large values are necessary, which also seem to improve our results of the mass spectrum. Additionally we have shown that $\beta \propto a^{-2}$. Thus we find the continuum limit for $\beta \rightarrow \infty$ as expected in a two-dimensional theory. Another interesting observation is the absence of screening for static charges in

the fundamental representation. Instead we observe a confining behavior, even in the chiral limit. This is in contrast to theoretical predictions [145] for massless fermions.

Simulating for several different lattice sizes revealed, that the Ward identities close to the critical fermion mass do not depend on the lattice volume. For the mesons, we found an explicit dependence on the lattice volume for all values of the fermion mass. Still, the finite volume effects were sufficiently suppressed on the largest lattices. Thus we could ignore this error source for our results. Next we tried to fine-tune the scalar mass of our theory, using the lattice Ward identities. Unfortunately this approach failed and we used the continuum result $m_s^2 = 0.65948255(8)$ instead. Of course this value will differ from the real critical value for a non-vanishing lattice spacing. On the other hand, all our results do not depend on the scalar mass close to its critical value. Thus even if we were able to determine the optimal critical value for the scalar mass, we would still get the same results. Of course this statement must not be true for observables we did not simulate. Lastly we investigated the dependence on the critical fermion mass. For its critical value m_f^c , we find a second order phase transition, which improves our lattice results in the chiral limit, as observed for the meson masses. Further the value of the critical fermion mass vanishes in the continuum limit, as expected for an irrelevant operator.

Apart from the determination of the optimal simulation parameters, our lattice simulation suffers from two severe problems, the flat directions of the classical scalar potential and the sign problem. The former is a generic feature of theories with extended supersymmetry. As they get lifted dynamically even for $m_s^2 = 0$, they pose no problem for our simulation. The same is true for the sign problem for all considered simulation parameters. As the continuum theory has no sign problem [48], it can only appear due to lattice artifacts. Thus in the continuum limit, it should not emerge.

Performing the chiral and the continuum limit, the Ward identities show the restoration of supersymmetry. Thus we observe no spontaneous supersymmetry breaking, which is possible because we have massless states in the theory. The same results was found for the \mathcal{Q} -exact methods [56]. Further we see that the chiral limit is important to retrieve the right continuum limit. This is in contrast to our expectations, as the fermion mass is an irrelevant operator. On the other hand, the chiral and the supersymmetric limit are the same in the four-dimensional mother theory [23]. Thus the breaking of chiral symmetry creates non-negligible lattice artifacts in our lattice theory. Of course, in two dimensions we reach the chiral limit automatically in the continuum limit. Thus these artifacts will vanish in the continuum limit.

The mass spectrum of the theory shows three different sets of particles whose masses are degenerate. The first is formed by the ground states of the η - and f-meson. They are part of the dimensionally reduced Veneziano-Yankielowicz super-multiplet and become massless in the continuum limit. The second set consists of the excited states of

the η - and f-meson and the the gluino-gluonball. Thus both mesons behave according to our theoretical predictions in contrast to the gluino-gluonball, whose ground state mass should be massless also. There are at least two explanations for this unexpected behavior. The first is that we actually see an excited state of the gluino-gluonball. The reason is that we could not resolve the corresponding correlation function for large t -values, where the ground state dominates. Instead we determined the mass for intermediate t -values, for which the correlation function is dominated by the first excited state. On the other hand, our results converged for ever higher smearing levels. As smearing improves the signal of the ground state over the signal of the excited state, our determined mass should belong to the ground state. The second explanation is that we actually need the correlation function of the gluino-gluon/scalarball. Thus we might find the massless ground state, if we analyze the gluino-scalarball correlation function or the cross correlation function of the gluino-gluonball and the gluino-scalarball. Unfortunately we were not able to get a reasonable signal for these correlation functions, even with smearing. Thus we can not check this hypothesis. The last set of states with degenerate mass is formed by the gluonball, the scalarball and the gluon-scalarball. All of these particles are part of the dimensionally reduced Farrar-Gabadadze-Schwetz super-multiplet and decouple from the theory. Comparing with our predictions, we miss a gluino-gluon/scalarball state. As this state must also decouple, its contribution to the gluino-gluonball correlation function will be zero. Thus this state is most likely unobservable on the lattice. Finally we can compare the mass spectrum of the two-dimensional $\mathcal{N} = (2, 2)$ SYM theory to the mass spectrum of the mother theory, the four-dimensional $\mathcal{N} = 1$ SYM theory. In both theories we find super-multiplets formed by the same states. Yet their masses differ drastically. While we find massive super-multiplets in four dimensions, in two dimensions the super-multiplets are either massless or decouple completely from the theory.

Appendix A

Conventions

In this thesis we will work with several different indices for the gauge fields, scalar fields and gamma matrices. To distinguish the different cases we use different indices. For the four-dimensional spacetime indices we use capital letters running from zero to three. In case of the two-dimensional spacetime indices we use Greek indices running from zero to one and for the flavor indices we use lower case letters running from one to two. Summarized we have

$$\begin{aligned}M, N &= 0, 1, 2, 3 \\ \mu, \nu &= 0, 1 \\ m, n &= 1, 2.\end{aligned}\tag{A.1}$$

Further our fields possess color and spin degrees of freedom, expressed by yet a new set of indices. For the former we use again lower case letters, while we use Greek letters for the latter. As we usually contract them using the Einstein summation convention, we will suppress them in most of the thesis. For example we write $\phi^n \phi_n$ instead of $\sum_{n,a} \phi_a^n \phi_n^a$, where a is the color index of the scalar field. In cases where we have an open index or it is important for the calculation, we will write these indices explicitly.

Appendix B

Pure gauge theory on the lattice

In this section, we will review the relevant analytical results for the two-dimensional Yang-Mills theory on the lattice, used in section 4.4. Our calculations are based on the work of Migdal [143]. In the first part of this section we will follow [91], which features a recent introduction into this calculation.

Since pure Yang-Mills theory describes gauge fields only, we have the lattice partition function

$$Z = \int \prod dU e^{-S_g}. \quad (\text{B.1})$$

Here we have chosen the Wilson gauge action

$$S_g = -\beta \sum_x \text{tr}(\mathbb{1} - \Re U_p(x)) \quad (\text{B.2})$$

where $U_p(x)$ is the positive oriented plaquette at the position x . Since we can perform the continuum limit analytically, the Wilson gauge action is sufficient to retrieve the continuum theory. As the action is just a sum over the lattice points x , we can rewrite the integrand as a product

$$e^{-S_g} = \prod_x e^{-\beta \text{tr}(\mathbb{1} - \Re U_p(x))}. \quad (\text{B.3})$$

Further we use results of the group theory to expand the exponential functions in the characters of the gauge group

$$e^{-\beta \text{tr}(\mathbb{1} - \Re U_p(x))} = \sum_R c_R(\beta) \chi_R(U_p(x)) \quad (\text{B.4})$$

where R labels the representation of the gauge group, $c_R(\beta)$ are the expansion coefficients and $\chi_R(U_p)$ the character of U_p , which is a group element. Having replaced the exponential function with characters of the plaquettes, we can make use of group

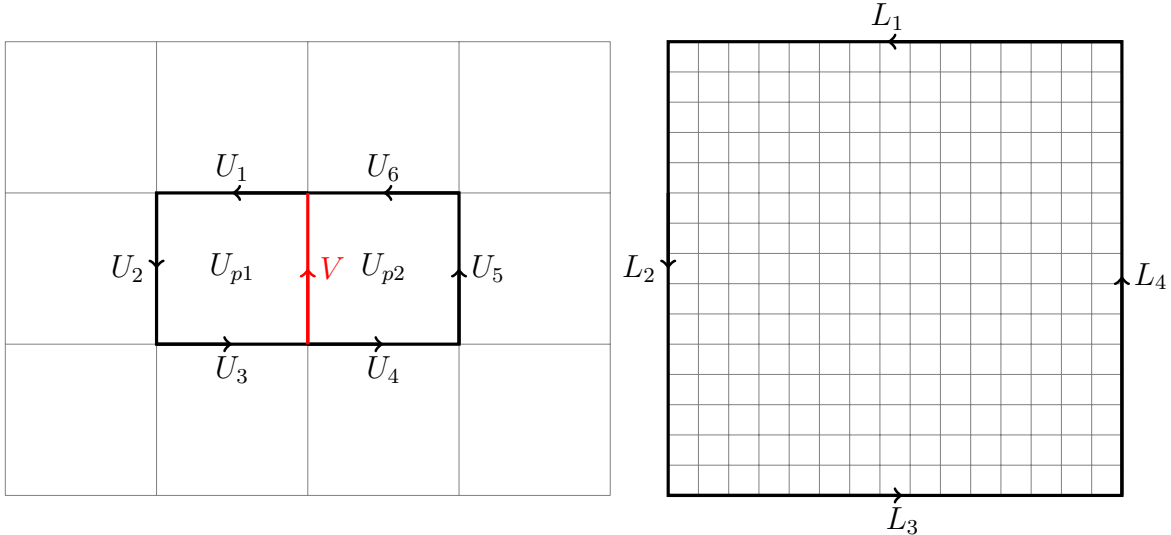


Figure B.1: On the Left: The gluing of two plaquettes. On the right: Resulting loop for the partition sum

theory, to solve the integrals. For this solution we introduce the gluing rule

$$\int d\Omega \chi_R(U\Omega^{-1}) \chi_{R'}(\Omega V) = \frac{\delta_{RR'}}{d_R} \chi_R(UV) \quad (\text{B.5})$$

and the splitting rule

$$\int d\Omega \chi_R(\Omega U \Omega^{-1} V) = \frac{1}{d_R} \chi_R(U) \chi_R(V) \quad (\text{B.6})$$

where Ω, U and V are elements of the gauge group and d_R is the dimension of the representation R , $d_R = \chi_R(\mathbb{1})$. Both rules can be derived with group theory. We proceed to use these mathematical tools to calculate the partition sum. Let us start with a integration over a single link V on the lattice. We show the corresponding sketch in the left panel of figure B.1. As we see, this link is adjacent to two plaquettes U_{p1} and U_{p2} :

$$U_{p1} = \text{tr}(V U_1 U_2 U_3), \quad U_{p2} = \text{tr}(V^{-1} U_4 U_5 U_6). \quad (\text{B.7})$$

Since there are no other plaquettes which contain this link variable, we must solve the integral

$$\int dV \chi_R(V U_1 U_2 U_3) \chi_{R'}(V^{-1} U_4 U_5 U_6). \quad (\text{B.8})$$

After applying a cyclic permutation, we recover the gluing rule (B.5). Therefore we find the result

$$\frac{\delta_{RR'}}{d_R} \chi_R(U_1 U_2 U_3 U_4 U_5 U_6). \quad (\text{B.9})$$

A nice graphical interpretation of this result is, that we glued the plaquettes U_{p1} and U_{p2} together along the link V . Since we did not make use of the position of this link,

we can apply this procedure for every link within the lattice and end up with a loop around the border of our lattice, depicted in the right panel of figure B.1. In this case the partition function reads

$$Z = \sum_R d_R \left(\frac{c_R}{d_R} \right)^V \int dL_1 dL_2 dL_3 dL_4 \chi_R(L_1 L_2 L_3 L_4). \quad (\text{B.10})$$

where V is the number of lattice points of the lattice. Here we will focus on lattices with periodic boundary conditions in time and space direction. Hence we have $L_3 = L_1^{-1}$, $L_4 = L_2^{-1}$ and we lose the integration over L_3 and L_4 . Applying these simplifications we calculate the partition function

$$Z = \sum_R d_R \left(\frac{c_R}{d_R} \right)^V \int dL_1 dL_2 \chi_R(L_1 L_2 L_1^{-1} L_2^{-1}) \quad (\text{B.11})$$

$$= \sum_R \left(\frac{c_R}{d_R} \right)^V \int dL_2 \chi_R(L_2) \chi_R(L_2^{-1}) = \sum_R \left(\frac{c_R}{d_R} \right)^V \quad (\text{B.12})$$

where we used the splitting rule (B.6) from line one to line two and the gluing rule (B.5) together with $d_R = \chi_R(\mathbb{1})$ in the second line. The last step is to calculate the expansion coefficients c_R . This calculation was done for example in [91]. The result reads

$$c_R = \frac{2}{\beta} e^{-\beta} d_R I_n(\beta) \quad (\text{B.13})$$

where $n = 2j + 1$ with j the spin associated with every irreducible representation. $I_n(\beta)$ are the modified Bessel functions of the first kind. The final result for the partition function is

$$Z = e^{-\beta V} \left(\frac{2}{\beta} \right)^V \sum_{n=1}^{\infty} I_n^V(\beta). \quad (\text{B.14})$$

B.1 Holes

Before we can discuss the Wilson Loop, we want to discuss holes of the two-dimensional space. Here we want to discuss a spacetime without holes. Yet they will appear indirectly, if we want to calculate observables. Since we only look at gauge invariant observables, they must be linear combinations of Wilson loops. Here we want to discuss the most easiest case, a single Wilson loop, characterized by the closed planar path γ . Later we will generalize this result to arbitrary holes on the lattice.

If we consider a Wilson loop, we have to calculate

$$\langle W[\gamma] \rangle = \frac{1}{NZ} \int \prod_{U \in \Lambda} dU W[\gamma] e^{-S_g[U]} = \frac{1}{NZ} \int \prod_{U \in \Lambda_L} dU W[\gamma] e^{-S_g[U]} \int \prod_{V \in \Lambda^*} dV e^{-S_g[V]}, \quad (\text{B.15})$$

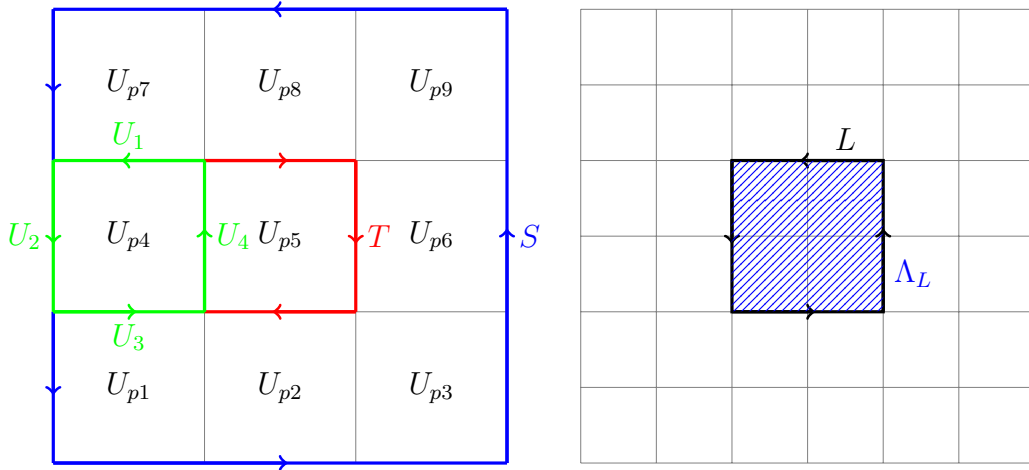


Figure B.2: On the left: Lattice which has a hole at the position of plaquette U_{p5} . On the right: Wilson Loop on the lattice, which is formed by L .

where Λ_L is the set of plaquettes enclosed by γ and Λ^* is the set of all other plaquettes. We will focus on the last integral. This integral is just the partition sum of a two-dimensional space with a hole, whose border is given by γ . Hence we get the analogy to holes in topology. To calculate this integral, we use the sketch on the left hand side of Figure B.2. This is the most easiest of these cases. The set Λ_L is just U_{p5} , while $\Lambda^* = \{U_{p1}, U_{p2}, U_{p3}, U_{p4}, U_{p6}, U_{p7}, U_{p8}, U_{p9}\}$. Now we start to glue the plaquettes $U_{p1}, U_{p2}, U_{p3}, U_{p6}, U_{p9}, U_{p8}$ and U_{p7} together. This leads to the result

$$\sum_{R,R'} d_R c'_R \left(\frac{c_R}{d_R}\right)^7 \int dS dU_1 dU_2 dU_3 \chi_R (SU_1^{-1} T U_3^{-1}) \chi_{R'} (U_1 U_2 U_3 U_4). \quad (\text{B.16})$$

Using the integration over U_1 to apply the gluing rule (B.5) we get

$$\sum_R d_R \left(\frac{c_R}{d_R}\right)^8 \int dS dU_2 dU_3 \chi_R (S U_2 U_3 U_4 T U_3^{-1}). \quad (\text{B.17})$$

Applying the splitting rule (B.6) for the integration over U_3 , we find the final result

$$\sum_R \left(\frac{c_R}{d_R}\right)^8 \int dS dU_2 dU_3 \chi_R (S U_2) \chi_R (U_4 T). \quad (\text{B.18})$$

We end up with two paths, one counter-clockwise around the 3×3 lattice and one going clockwise around the hole, formed by plaquette U_{p5} . Since we did not make use of the periodicity of the lattice, this result will also hold for any 3×3 patch in a larger lattice. Further, this calculation can be generalized to larger lattice patches and an arbitrary form of the hole. Since we used a local calculation only, we can even generalize this result to a setup with more than one hole. If we call N_h the numbers of holes, H_n the counter-clockwise path around the n th hole, $|h|$ the total area covered by holes, A

the counter-clockwise path around the lattice patch we look at and V_A the amount of plaquettes encircled by A , we find

$$\sum_R d_R^{1-N_h} \left(\frac{c_R}{d_R} \right)^{V_A-|h|} \int \prod_{U \in A} dU \chi_R(A) \prod_n^{N_h} \chi_R(H_n^{-1}). \quad (\text{B.19})$$

Another interesting aspect of this result comes from (B.15). Our results allows us to integrate out all plaquettes which are not enclosed by gauge invariant Wilson loops. This is especially true for several non-intersecting Wilson loops (here we regard two Wilson loops to intersect even when they just touch each other). Thus the resulting integral will factorize in the different integrals over the areas enclosed by the Wilson loops. Therefore interaction of two Wilson loops does not depend on the distance between them. The same result was found in [142] for the continuum.

B.2 Wilson Loop

Having solved the second integral in (B.15) we want to focus on the first integral. To not confuse our case with the analysis for holes, we use the sketch in the right panel of figure B.2. We introduce A_L as the number of plaquettes in the set Λ_L . Using the result of the last section and applying it to (B.15) we find

$$\langle W \rangle = \frac{1}{N\bar{Z}} \sum_R \frac{1}{d_R} \left(\frac{c_R}{d_R} \right)^{V-A_L} \int \prod_{U \in \Lambda_L} dU \chi_R(L^{-1}) e^{-S_g[U]} \chi_{R(j=1/2)}(L), \quad (\text{B.20})$$

where we integrated out the link variable lying on the border on the lattice, analogous to the partition function¹. Using the gluing rule (B.5) and the expansion of the exponential function (B.13), we can integrate over all remaining links, which are not part of the Wilson loop, arriving at

$$\langle W \rangle = \frac{1}{N\bar{Z}} \sum_{R,R'} \frac{1}{d_R} \left(\frac{c_R}{d_R} \right)^{V-A_L} d_{R'} \left(\frac{c'_{R'}}{d'_{R'}} \right)^{A_L} \int \prod_{U \in L} dU \chi_R(L^{-1}) \chi_{R(j=1/2)}(L) \chi_{R'}(L) \quad (\text{B.21})$$

¹If a Wilson loop intersects with a border, we will simply shift the lattice. Since the action is invariant under these shifts, the result will not change but the Wilson loop will no longer intersect with the border.

Now we use the Clebsch-Gordon decomposition $\chi_j \chi_{j'} = \chi_{j+j'} + \dots + \chi_{|j-j'|}$ to proceed

$$\begin{aligned} \langle W \rangle &= \frac{1}{N\bar{Z}} \sum_{R,R'} \frac{1}{d_R} \left(\frac{c_R}{d_R} \right)^{V-A_L} d_{R'} \left(\frac{c'_{R'}}{d'_{R'}} \right)^{A_L} \times \\ &\quad \times \int \prod_{U \in L} dU \chi_R(L^{-1}) [\chi_{R'(j'+1/2)}(L) + \chi_{R'(j'-1/2)}(L)] \end{aligned} \quad (\text{B.22})$$

Next we use the gluing rule (B.5) to get $\chi_R(\mathbb{1}) = d_R$ and use the identity (B.13) to get

$$\langle W \rangle = \frac{\sum_{n=1}^{\infty} \left(\frac{n+1}{n} I_n^{V-A_L}(\beta) I_{n+1}^{A_L}(\beta) + \frac{n}{n+1} I_n^{A_L}(\beta) I_{n+1}^{V-A_L}(\beta) \right)}{N \sum_{n=1}^{\infty} (I_n^V)(\beta)} \quad (\text{B.23})$$

Since $I_1(\beta) > I_2(\beta) > \dots$, we can perform the limit $V \rightarrow \infty$ trivially. Combining this with $N = 2$, we find the infinite volume limit

$$\langle W \rangle \rightarrow \left(\frac{I_2(\beta)}{I_1(\beta)} \right)^{A_L}. \quad (\text{B.24})$$

To reach the continuum limit, we have to perform the limit $\beta \rightarrow \infty$ next. For this calculation we look at the asymptotic behaviour of the modified Bessel functions

$$I_n(z) \approx \frac{e^z}{(2\pi z)^{\frac{1}{2}}} \left(1 - \frac{4n^2 - 1}{8z} + O\left(\frac{1}{z^2}\right) \right). \quad (\text{B.25})$$

In this limit, the lattice spacing shrinks to zero. Hence the physical area of the Wilson loop will shrink to zero too. Therefore we have to increase the lattice area of the Wilson loop in this limit, to keep the physical area of the Wilson loop constant. For a two-dimensional theory, the coupling constant is dimensionful. This allows to relate the inverse gauge coupling β to the lattice spacing

$$\beta = \frac{N_c}{a^2 g^2}. \quad (\text{B.26})$$

With this we can give the physical area A_p in terms of β

$$A_p = Aa^2 = \frac{A}{\beta g^2}. \quad (\text{B.27})$$

Since we do not know g we demand simply $\frac{A_L}{\beta} = \text{const}$, where we assume that g is independent on β . In section 5.1 we show this for the two-dimensional $\mathcal{N} = (2, 2)$ SYM

theory. This allows us to calculate the Wilson loop in the continuum limit

$$\langle W \rangle = \lim_{\beta \rightarrow \infty} \left(\frac{1 - \frac{15}{8\beta}}{1 - \frac{3}{8\beta}} \right)^{\beta A_p} = \lim_{\beta \rightarrow \infty} \left(1 - \frac{1.5}{\beta - 0.375} \right)^{\beta A_p} = e^{-1.5 A_p}. \quad (\text{B.28})$$

This is the same results as the continuum result given in (4.46) for $g = 1$. This results shows us that the formulation of Migdal [143] leads to the correct continuum results, as expected. Second we have shown all relevant analytical tools, which we will use to calculate more complicated objects like glueballs.

B.3 Glueballs

The last step is to calculate the glueball correlation function

$$\langle F_{01}^2(x) F_{01}^2(0) \rangle = \frac{C}{Z} \int \prod_{x'} dF_{01}(x') F_{01}^2(x) F_{01}^2(0) e^{-\frac{1}{4} F_{01}^2}. \quad (\text{B.29})$$

For the lattice equivalent, we put two non-intersecting plaquettes on the lattice at position x and 0 . Following our result from before, we find

$$\begin{aligned} \langle U_p(x) U_p(0) \rangle &= \frac{1}{Z} \sum_{R, R', R''} \frac{1}{d_R} \left(\frac{c_R}{d_R} \right)^{V-2} c_{R'} c_{R''} \times \\ &\quad \times \int dU_p(x) \chi_R(U_p^{-1}(x)) \chi'_R(U_p(x)) \chi_{j=1/2}(U_p(x)) \times \\ &\quad \times \int dU_p(0) \chi_R(U_p^{-1}(0)) \chi'_R(U_p(0)) \chi_{j=1/2}(U_p(0)) \\ &= \frac{\sum_{n=1}^{\infty} \left\{ \frac{(n+1)^2}{n} I_n^{V-2}(\beta) I_{n+1}^2(\beta) + \frac{n(n+2)}{n+1} I_n(\beta) I_{n+1}^{V-2}(\beta) I_{n+2}(\beta) + \frac{n^2}{n+1} I_n^2(\beta) I_{n+1}^{V-2}(\beta) \right\}}{\sum_{n=1}^{\infty} I_n^V(\beta)} \end{aligned} \quad (\text{B.30})$$

Again we perform the infinite volume limit $V \rightarrow \infty$

$$\langle U_p(x) U_p(0) \rangle \rightarrow \left(2 \frac{I_2(\beta)}{I_1(\beta)} \right) \left(2 \frac{I_2(\beta)}{I_1(\beta)} \right) = \langle U_p(x) \rangle \langle U_p(0) \rangle \quad (\text{B.31})$$

where we used our previous result for the Wilson loop. Since we have $U_p(x) \rightarrow F_{01}$ in the continuum limit ($V \rightarrow \infty, \beta \rightarrow \infty$) we see that the glueball correlator vanishes.

Bibliography

- [1] S. Chatrchyan et al. “Observation of a new boson at a mass of 125 GeV with the CMS experiment at the LHC”. In: *Phys. Lett.* B716 (2012), pp. 30–61. arXiv: 1207.7235 [hep-ex].
- [2] G. Aad et al. “Observation of a new particle in the search for the Standard Model Higgs boson with the ATLAS detector at the LHC”. In: *Phys. Lett.* B716 (2012), pp. 1–29. arXiv: 1207.7214 [hep-ex].
- [3] B. P. Abbott et al. “Observation of Gravitational Waves from a Binary Black Hole Merger”. In: *Phys. Rev. Lett.* 116.6 (2016), p. 061102. arXiv: 1602.03837 [gr-qc].
- [4] W. Heisenberg and W. Pauli. “Zur Quantendynamik der Wellenfelder”. In: *Zeitschrift für Physik* 56.1 (1929), pp. 1–61.
- [5] P. A. R. Ade et al. “Planck 2015 results. XIII. Cosmological parameters”. In: *Astron. Astrophys.* 594 (2016), A13. arXiv: 1502.01589 [astro-ph.CO].
- [6] S. P. Martin. “A Supersymmetry primer”. In: (1997). [Adv. Ser. Direct. High Energy Phys.18,1(1998)], pp. 1–98. arXiv: hep-ph/9709356 [hep-ph].
- [7] S. Weinberg. *The quantum theory of fields. Vol. 3: Supersymmetry*. Cambridge University Press, 2013.
- [8] C. Patrignani et al. “Review of Particle Physics”. In: *Chin. Phys.* C40.10 (2016), p. 100001.
- [9] M. Aaboud et al. “Search for supersymmetry in events with four or more leptons in $\sqrt{s} = 13$ TeV pp collisions with ATLAS”. In: (2018). arXiv: 1804.03602 [hep-ex].
- [10] M. Aaboud et al. “Search for supersymmetry in final states with charm jets and missing transverse momentum in 13 TeV pp collisions with the ATLAS detector”. In: (2018). arXiv: 1805.01649 [hep-ex].
- [11] P. Bechtle, T. Plehn, and C. Sander. “Supersymmetry”. In: *The Large Hadron Collider: Harvest of Run 1*. Ed. by T. Schörner-Sadenius. 2015, pp. 421–462. arXiv: 1506.03091 [hep-ex].

-
- [12] M. Grisaru, W. Siegel, and M. Rocek. “Improved methods for supergraphs”. In: *Nuclear Physics B* 159.3 (1979), pp. 429–450.
- [13] A. Salam and J. Strathdee. “Superfields and Fermi-Bose symmetry”. In: *Phys. Rev. D* 11 (6 1975), pp. 1521–1535.
- [14] G. Gabrielse, D. Hanneke, T. Kinoshita, M. Nio, and B. Odom. “New Determination of the Fine Structure Constant from the Electron g Value and QED”. In: *Phys. Rev. Lett.* 97 (3 2006), p. 030802.
- [15] K. G. Wilson. “Confinement of Quarks”. In: *Phys. Rev. D* 10 (1974). [45(1974)], pp. 2445–2459.
- [16] H.-W. Lin. “Review of Baryon Spectroscopy in Lattice QCD”. In: *Chin. J. Phys.* 49 (2011), p. 827. arXiv: 1106.1608 [hep-lat].
- [17] C. Ratti. “Lattice QCD and heavy ion collisions: a review of recent progress”. In: (2018). arXiv: 1804.07810 [hep-lat].
- [18] D. B. Kaplan. “Recent developments in lattice supersymmetry”. In: *Nucl. Phys. Proc. Suppl.* 129 (2004). [109(2003)], pp. 109–120. arXiv: hep-lat/0309099 [hep-lat].
- [19] J. Giedt. “Deconstruction and other approaches to supersymmetric lattice field theories”. In: *Int. J. Mod. Phys. A* 21 (2006), pp. 3039–3094. arXiv: hep-lat/0602007 [hep-lat].
- [20] S. Catterall, D. B. Kaplan, and M. Unsal. “Exact lattice supersymmetry”. In: *Phys. Rept.* 484 (2009), pp. 71–130. arXiv: 0903.4881 [hep-lat].
- [21] A. Joseph. “Supersymmetric Yang-Mills theories with exact supersymmetry on the lattice”. In: *Int. J. Mod. Phys. A* 26 (2011), pp. 5057–5132. arXiv: 1110.5983 [hep-lat].
- [22] G. Bergner and S. Catterall. “Supersymmetry on the lattice”. In: *Int. J. Mod. Phys. A* 31.22 (2016), p. 1643005. arXiv: 1603.04478 [hep-lat].
- [23] G. Curci and G. Veneziano. “Supersymmetry and the Lattice: A Reconciliation?” In: *Nucl. Phys. B* 292 (1987), pp. 555–572.
- [24] J. Giedt, R. Brower, S. Catterall, G. T. Fleming, and P. Vranas. “Lattice super-Yang-Mills using domain wall fermions in the chiral limit”. In: *Phys. Rev. D* 79 (2009), p. 025015. arXiv: 0810.5746 [hep-lat].
- [25] M. G. Endres. “Dynamical simulation of $N=1$ supersymmetric Yang-Mills theory with domain wall fermions”. In: *Phys. Rev. D* 79 (2009), p. 094503. arXiv: 0902.4267 [hep-lat].

- [26] S. W. Kim, H. Fukaya, S. Hashimoto, H. Matsufuru, J. Nishimura, and T. Onogi. “Lattice study of 4d $N=1$ super Yang-Mills theory with dynamical overlap gluino”. In: *PoS LATTICE2011* (2011), p. 069. arXiv: 1111.2180 [hep-lat].
- [27] I. Montvay. “SUSY on the lattice”. In: *Nucl. Phys. Proc. Suppl.* 63 (1998), pp. 108–113. arXiv: hep-lat/9709080 [hep-lat].
- [28] I. Campos, R. Kirchner, I. Montvay, J. Westphalen, A. Feo, S. Luckmann, G. Munster, and K. Spanderen. “Monte Carlo simulation of $SU(2)$ Yang-Mills theory with light gluinos”. In: *Eur. Phys. J. C* 11 (1999), pp. 507–527. arXiv: hep-lat/9903014 [hep-lat].
- [29] F. Farchioni, C. Gebert, R. Kirchner, I. Montvay, A. Feo, G. Munster, T. Galla, and A. Vladikas. “The Supersymmetric Ward identities on the lattice”. In: *Eur. Phys. J. C* 23 (2002), pp. 719–734. arXiv: hep-lat/0111008 [hep-lat].
- [30] I. Montvay. “Supersymmetric Yang-Mills theory on the lattice”. In: *Int. J. Mod. Phys. A* 17 (2002), pp. 2377–2412. arXiv: hep-lat/0112007 [hep-lat].
- [31] G. Münster and H. Stüwe. “The mass of the adjoint pion in $\mathcal{N} = 1$ supersymmetric Yang-Mills theory”. In: *JHEP* 05 (2014), p. 034. arXiv: 1402.6616 [hep-th].
- [32] G. Bergner, P. Giudice, G. Münster, S. Piemonte, and D. Sandbrink. “Phase structure of the $\mathcal{N} = 1$ supersymmetric Yang-Mills theory at finite temperature”. In: *JHEP* 11 (2014), p. 049. arXiv: 1405.3180 [hep-lat].
- [33] G. Bergner and S. Piemonte. “Compactified $\mathcal{N} = 1$ supersymmetric Yang-Mills theory on the lattice: continuity and the disappearance of the deconfinement transition”. In: *JHEP* 12 (2014), p. 133. arXiv: 1410.3668 [hep-lat].
- [34] G. Bergner, P. Giudice, G. Münster, I. Montvay, and S. Piemonte. “The light bound states of supersymmetric $SU(2)$ Yang-Mills theory”. In: *JHEP* 03 (2016), p. 080. arXiv: 1512.07014 [hep-lat].
- [35] D. Amati, K. Konishi, Y. Meurice, G. C. Rossi, and G. Veneziano. “Nonperturbative Aspects in Supersymmetric Gauge Theories”. In: *Phys. Rept.* 162 (1988), pp. 169–248.
- [36] G. Veneziano and S. Yankielowicz. “An Effective Lagrangian for the Pure $N=1$ Supersymmetric Yang-Mills Theory”. In: *Phys. Lett.* 113B (1982), p. 231.
- [37] G. R. Farrar, G. Gabadadze, and M. Schwetz. “The spectrum of softly broken $N=1$ supersymmetric Yang-Mills theory”. In: *Phys. Rev. D* 60 (1999), p. 035002. arXiv: hep-th/9806204 [hep-th].

-
- [38] G. R. Farrar, G. Gabadadze, and M. Schwetz. “On the effective action of $N=1$ supersymmetric Yang-Mills theory”. In: *Phys. Rev. D* 58 (1998), p. 015009. arXiv: hep-th/9711166 [hep-th].
- [39] A. Feo, P. Merlatti, and F. Sannino. “Information on the super Yang-Mills spectrum”. In: *Phys. Rev. D* 70 (2004), p. 096004. arXiv: hep-th/0408214 [hep-th].
- [40] S. Ali, G. Bergner, H. Gerber, P. Giudice, G. Münster, I. Montvay, S. Piemonte, and P. Scior. “The light bound states of $\mathcal{N} = 1$ supersymmetric $SU(3)$ Yang-Mills theory on the lattice”. In: (2018). arXiv: 1801.08062 [hep-lat].
- [41] M. Steinhauser, A. Sternbeck, B. Wellegehausen, and A. Wipf. “Spectroscopy of four-dimensional $\mathcal{N} = 1$ supersymmetric $SU(3)$ Yang-Mills theory”. In: *35th International Symposium on Lattice Field Theory (Lattice 2017) Granada, Spain, June 18-24, 2017*. 2017. arXiv: 1711.05086 [hep-lat].
- [42] E. Witten. “Topological Quantum Field Theory”. In: *Commun. Math. Phys.* 117 (1988), p. 353.
- [43] A. G. Cohen, D. B. Kaplan, E. Katz, and M. Unsal. “Supersymmetry on a Euclidean space-time lattice. 2. Target theories with eight supercharges”. In: *JHEP* 12 (2003), p. 031. arXiv: hep-lat/0307012 [hep-lat].
- [44] S. Catterall. “A Geometrical approach to $N=2$ super Yang-Mills theory on the two dimensional lattice”. In: *JHEP* 11 (2004), p. 006. arXiv: hep-lat/0410052 [hep-lat].
- [45] F. Sugino. “A Lattice formulation of superYang-Mills theories with exact supersymmetry”. In: *JHEP* 01 (2004), p. 015. arXiv: hep-lat/0311021 [hep-lat].
- [46] I. Kanamori and H. Suzuki. “Restoration of supersymmetry on the lattice: Two-dimensional $N = (2,2)$ supersymmetric Yang-Mills theory”. In: *Nucl. Phys. B* 811 (2009), pp. 420–437. arXiv: 0809.2856 [hep-lat].
- [47] M. Hanada and I. Kanamori. “Lattice study of two-dimensional $N=(2,2)$ super Yang-Mills at large- N ”. In: *Phys. Rev. D* 80 (2009), p. 065014. arXiv: 0907.4966 [hep-lat].
- [48] M. Hanada and I. Kanamori. “Absence of sign problem in two-dimensional $N = (2,2)$ super Yang-Mills on lattice”. In: *JHEP* 01 (2011), p. 058. arXiv: 1010.2948 [hep-lat].
- [49] S. Matsuura and F. Sugino. “Lattice formulation for $2d = (2, 2), (4, 4)$ super Yang-Mills theories without admissibility conditions”. In: *JHEP* 04 (2014), p. 088. arXiv: 1402.0952 [hep-lat].

- [50] S. Catterall. “Simulations of $N=2$ super Yang-Mills theory in two dimensions”. In: *JHEP* 03 (2006), p. 032. arXiv: hep-lat/0602004 [hep-lat].
- [51] S. Catterall. “First results from simulations of supersymmetric lattices”. In: *JHEP* 01 (2009), p. 040. arXiv: 0811.1203 [hep-lat].
- [52] H. Suzuki. “Two-dimensional $N = (2,2)$ super Yang-Mills theory on computer”. In: *JHEP* 09 (2007), p. 052. arXiv: 0706.1392 [hep-lat].
- [53] I. Kanamori and H. Suzuki. “Some physics of the two-dimensional $N = (2,2)$ supersymmetric Yang-Mills theory: Lattice Monte Carlo study”. In: *Phys. Lett.* B672 (2009), pp. 307–311. arXiv: 0811.2851 [hep-lat].
- [54] I. Kanamori, F. Sugino, and H. Suzuki. “Observing dynamical supersymmetry breaking with euclidean lattice simulations”. In: *Prog. Theor. Phys.* 119 (2008), pp. 797–827. arXiv: 0711.2132 [hep-lat].
- [55] D. Kadoh and H. Suzuki. “SUSY WT identity in a lattice formulation of 2D $N = (2,2)$ SYM”. In: *Phys. Lett.* B682 (2010), pp. 466–471. arXiv: 0908.2274 [hep-lat].
- [56] S. Catterall, R. G. Jha, and A. Joseph. “Nonperturbative study of dynamical SUSY breaking in $\mathcal{N} = (2,2)$ Yang-Mills”. In: (2017). arXiv: 1801.00012 [hep-lat].
- [57] T. Takimi. “Relationship between various supersymmetric lattice models”. In: *JHEP* 07 (2007), p. 010. arXiv: 0705.3831 [hep-lat].
- [58] P. H. Damgaard and S. Matsuura. “Lattice Supersymmetry: Equivalence between the Link Approach and Orbifolding”. In: *JHEP* 09 (2007), p. 097. arXiv: 0708.4129 [hep-lat].
- [59] P. H. Damgaard and S. Matsuura. “Relations among Supersymmetric Lattice Gauge Theories via Orbifolding”. In: *JHEP* 08 (2007), p. 087. arXiv: 0706.3007 [hep-lat].
- [60] M. Unsal. “Twisted supersymmetric gauge theories and orbifold lattices”. In: *JHEP* 10 (2006), p. 089. arXiv: hep-th/0603046 [hep-th].
- [61] S. Matsuura, T. Misumi, and K. Ohta. “Topologically twisted $N = (2, 2)$ supersymmetric Yang–Mills theory on an arbitrary discretized Riemann surface”. In: *PTEP* 2014.12 (2014), 123B01. arXiv: 1408.6998 [hep-lat].
- [62] S. Kamata, S. Matsuura, T. Misumi, and K. Ohta. “Anomaly and sign problem in $\mathcal{N} = (2, 2)$ SYM on polyhedra: Numerical analysis”. In: *PTEP* 2016.12 (2016), 123B01. arXiv: 1607.01260 [hep-th].

-
- [63] S. Kamata, S. Matsuura, T. Misumi, and K. Ohta. “Numerical Analysis of Discretized $\mathcal{N} = (2, 2)$ SYM on Polyhedra”. In: *PoS LATTICE2016* (2016), p. 210. arXiv: 1612.01968 [hep-lat].
- [64] H. Suzuki and Y. Taniguchi. “Two-dimensional $N = (2, 2)$ super Yang-Mills theory on the lattice via dimensional reduction”. In: *JHEP* 10 (2005), p. 082. arXiv: hep-lat/0507019 [hep-lat].
- [65] D. August, B. Wellegehausen, and A. Wipf. “Spectroscopy of two dimensional $N=2$ Super Yang Mills theory”. In: *PoS LATTICE2016* (2016), p. 234. arXiv: 1611.00551 [hep-lat].
- [66] D. August, B. Wellegehausen, and A. Wipf. “Two-dimensional $\mathcal{N} = 2$ Super-Yang-Mills Theory”. In: *EPJ Web Conf.* 175 (2018), p. 08021. arXiv: 1711.01109 [hep-lat].
- [67] D. August, B. H. Wellegehausen, and A. Wipf. “Mass spectrum of 2-dimensional $\mathcal{N} = (2, 2)$ super Yang-Mills theory on the lattice”. In: (2018). arXiv: 1802.07797 [hep-lat].
- [68] S. R. Coleman and J. Mandula. “All Possible Symmetries of the S Matrix”. In: *Phys. Rev.* 159 (1967), pp. 1251–1256.
- [69] R. Haag, J. T. Lopuszanski, and M. Sohnius. “All Possible Generators of Supersymmetries of the s Matrix”. In: *Nucl. Phys.* B88 (1975), p. 257.
- [70] A. Salam and J. A. Strathdee. “Supersymmetry and Nonabelian Gauges”. In: *Phys. Lett.* 51B (1974), pp. 353–355.
- [71] S. Ferrara and B. Zumino. “Supergauge Invariant Yang-Mills Theories”. In: *Nucl. Phys.* B79 (1974), p. 413.
- [72] I. Montvay. “SYM on the lattice”. In: *Theory of elementary particles. Proceedings, 31st International Symposium Ahrenshoop, Buckow, Germany, September 2-6, 1997*. 1997, pp. 361–372. arXiv: hep-lat/9801023 [hep-lat].
- [73] L. Girardello and M. Grisaru. “Soft breaking of supersymmetry”. In: *Nuclear Physics B* 194.1 (1982), pp. 65–76.
- [74] T. Kaluza. “On the Problem of Unity in Physics”. In: *Sitzungsber. Preuss. Akad. Wiss. Berlin (Math. Phys.)* 1921 (1921), pp. 966–972.
- [75] O. Klein. “The Atomicity of Electricity as a Quantum Theory Law”. In: *Nature* 118 (1926), p. 516.
- [76] C. Csáki and P. Tanedo. “Beyond the Standard Model”. In: *Proceedings, 2013 European School of High-Energy Physics (ESHEP 2013): Paradfurdo, Hungary, June 5-18, 2013*. 2015, pp. 169–268. arXiv: 1602.04228 [hep-ph].

- [77] H. B. Nielsen and M. Ninomiya. “Absence of Neutrinos on a Lattice. 1. Proof by Homotopy Theory”. In: *Nucl. Phys.* B185 (1981). [,533(1980)], p. 20.
- [78] H. B. Nielsen and M. Ninomiya. “Absence of Neutrinos on a Lattice. 2. Intuitive Topological Proof”. In: *Nucl. Phys.* B193 (1981), pp. 173–194.
- [79] H. B. Nielsen and M. Ninomiya. “No Go Theorem for Regularizing Chiral Fermions”. In: *Phys. Lett.* 105B (1981), pp. 219–223.
- [80] F. Sugino. “A Lattice formulation of super Yang-Mills theories with exact supersymmetry”. In: *Nucl. Phys. Proc. Suppl.* 140 (2005). [,763(2004)], pp. 763–765. arXiv: [hep-lat/0409036](#) [[hep-lat](#)].
- [81] P. C. West. *Introduction to supersymmetry and supergravity*. 1990.
- [82] E. Witten. “Bound states of strings and p-branes”. In: *Nucl. Phys.* B460 (1996), pp. 335–350. arXiv: [hep-th/9510135](#) [[hep-th](#)].
- [83] H. Fukaya, I. Kanamori, H. Suzuki, M. Hayakawa, and T. Takimi. “Note on massless bosonic states in two-dimensional field theories”. In: *Prog. Theor. Phys.* 116 (2007), pp. 1117–1129. arXiv: [hep-th/0609049](#) [[hep-th](#)].
- [84] F. Antonuccio, H. C. Pauli, S. Pinsky, and S. Tsujimaru. “DLCQ bound states of $N=(2,2)$ superYang-Mills at finite and large N ”. In: *Phys. Rev.* D58 (1998), p. 125006. arXiv: [hep-th/9808120](#) [[hep-th](#)].
- [85] M. Harada, J. R. Hiller, S. Pinsky, and N. Salwen. “Improved results for $N=(2,2)$ super Yang-Mills theory using supersymmetric discrete light-cone quantization”. In: *Phys. Rev.* D70 (2004), p. 045015. arXiv: [hep-th/0404123](#) [[hep-th](#)].
- [86] B. de Wit, M. Luscher, and H. Nicolai. “The Supermembrane Is Unstable”. In: *Nucl. Phys.* B320 (1989), pp. 135–159.
- [87] S. Sethi and M. Stern. “D-brane bound states redux”. In: *Commun. Math. Phys.* 194 (1998), pp. 675–705. arXiv: [hep-th/9705046](#) [[hep-th](#)].
- [88] K. Hori and D. Tong. “Aspects of Non-Abelian Gauge Dynamics in Two-Dimensional $N=(2,2)$ Theories”. In: *JHEP* 05 (2007), p. 079. arXiv: [hep-th/0609032](#) [[hep-th](#)].
- [89] H. J. Rothe. “Lattice gauge theories: An Introduction”. In: *World Sci. Lect. Notes Phys.* 43 (1992). [World Sci. Lect. Notes Phys.82,1(2012)], pp. 1–381.
- [90] C. Gattringer and C. B. Lang. “Quantum chromodynamics on the lattice”. In: *Lect. Notes Phys.* 788 (2010), pp. 1–343.
- [91] A. Wipf. “Statistical approach to quantum field theory”. In: *Lect. Notes Phys.* 864 (2013), pp.1–390.

-
- [92] R. P. Feynman. “Space-time approach to nonrelativistic quantum mechanics”. In: *Rev. Mod. Phys.* 20 (1948), pp. 367–387.
- [93] P. A. M. Dirac. “The Lagrangian in quantum mechanics”. In: *Phys. Z. Sowjetunion* 3 (1933), pp. 64–72.
- [94] R. Feynman and A. Hibbs. *Quantum mechanics and path integrals*. International series in pure and applied physics. New York: McGraw-Hill, 1965.
- [95] L. s. Schulman. *TECHNIQUES AND APPLICATIONS OF PATH INTEGRATION*. 1981.
- [96] R. J. Rivers. *PATH INTEGRAL METHODS IN QUANTUM FIELD THEORY*. Cambridge University Press, 1988.
- [97] T. Kugo and P. K. Townsend. “Supersymmetry and the Division Algebras”. In: *Nucl. Phys.* B221 (1983), pp. 357–380.
- [98] G. C. Wick. “Properties of Bethe-Salpeter Wave Functions”. In: *Phys. Rev.* 96 (1954), pp. 1124–1134.
- [99] K. Osterwalder and R. Schrader. “AXIOMS FOR EUCLIDEAN GREEN’S FUNCTIONS”. In: *Commun. Math. Phys.* 31 (1973), pp. 83–112.
- [100] K. Osterwalder and R. Schrader. “Axioms for Euclidean Green’s Functions. 2.” In: *Commun. Math. Phys.* 42 (1975), p. 281.
- [101] I. Montvay. “Majorana fermions on the lattice”. In: 2001. arXiv: hep-lat/0108011 [hep-lat].
- [102] H. Nicolai. “A Possible constructive approach to (SUPER ϕ^{*3}) in four-dimensions. 1. Euclidean formulation of the model”. In: *Nucl. Phys.* B140 (1978), pp. 294–300.
- [103] P. van Nieuwenhuizen and A. Waldron. “On Euclidean spinors and Wick rotations”. In: *Phys. Lett.* B389 (1996), pp. 29–36. arXiv: hep-th/9608174 [hep-th].
- [104] P. de Forcrand. “Simulating QCD at finite density”. In: *PoS LAT2009* (2009), p. 010. arXiv: 1005.0539 [hep-lat].
- [105] C. Gattringer and K. Langfeld. “Approaches to the sign problem in lattice field theory”. In: *Int. J. Mod. Phys.* A31.22 (2016), p. 1643007. arXiv: 1603.09517 [hep-lat].
- [106] S. Duane, A. D. Kennedy, B. J. Pendleton, and D. Roweth. “Hybrid Monte Carlo”. In: *Phys. Lett.* B195 (1987), pp. 216–222.
- [107] F. A. Berezin. “The method of second quantization”. In: *Pure Appl. Phys.* 24 (1966), pp. 1–228.

- [108] F. Fucito, E. Marinari, G. Parisi, and C. Rebbi. “A Proposal for Monte Carlo Simulations of Fermionic Systems”. In: *Nucl. Phys.* B180 (1981). [,586(1980)], p. 369.
- [109] P. de Forcrand and T. Takaishi. “Fast fermion Monte Carlo”. In: *Nucl. Phys. Proc. Suppl.* 53 (1997), pp. 968–970. arXiv: [hep-lat/9608093](#) [[hep-lat](#)].
- [110] T. Takaishi and P. de Forcrand. “Odd flavor hybrid Monte Carlo algorithm for lattice QCD”. In: *Int. J. Mod. Phys.* C13 (2002), pp. 343–366. arXiv: [hep-lat/0108012](#) [[hep-lat](#)].
- [111] R. Frezzotti and K. Jansen. “A Polynomial hybrid Monte Carlo algorithm”. In: *Phys. Lett.* B402 (1997), pp. 328–334. arXiv: [hep-lat/9702016](#) [[hep-lat](#)].
- [112] A. D. Kennedy, I. Horvath, and S. Sint. “A New exact method for dynamical fermion computations with nonlocal actions”. In: *Nucl. Phys. Proc. Suppl.* 73 (1999), pp. 834–836. arXiv: [hep-lat/9809092](#) [[hep-lat](#)].
- [113] M. A. Clark and A. D. Kennedy. “The RHMC algorithm for two flavors of dynamical staggered fermions”. In: *Nucl. Phys. Proc. Suppl.* 129 (2004). [,850(2003)], pp. 850–852. arXiv: [hep-lat/0309084](#) [[hep-lat](#)].
- [114] M. A. Clark, P. de Forcrand, and A. D. Kennedy. “Algorithm shootout: R versus RHMC”. In: *PoS LAT2005* (2006), p. 115. arXiv: [hep-lat/0510004](#) [[hep-lat](#)].
- [115] M. A. Clark. “The Rational Hybrid Monte Carlo Algorithm”. In: *PoS LAT2006* (2006), p. 004. arXiv: [hep-lat/0610048](#) [[hep-lat](#)].
- [116] E. Y. Remez. “Sur la détermination des polynomes d’approximation de degré donnée”. In: *Comm. Soc. Math. Kharkov* 10 (1934).
- [117] E. Y. Remez. “Sur le calcul effectif des polynomes d’approximation de Tchebychef”. In: *Compt. Rend. Acad. Sci.* 199 (1934), pp. 337–340.
- [118] E. Y. Remez. “Sur un procédé convergent d’approximations successives pour déterminer les polynomes d’approximation”. In: *Compt. Rend. Acad. Sci.* 198 (1934), pp. 2063–2065.
- [119] W. Fraser. “A Survey of Methods of Computing Minimax and Near-Minimax Polynomial Approximations for Functions of a Single Independent Variable”. In: *J. ACM* 12.3 (July 1965), pp. 295–314.
- [120] A. Frommer, B. Nockel, S. Gusken, T. Lippert, and K. Schilling. “Many masses on one stroke: Economic computation of quark propagators”. In: *Int. J. Mod. Phys.* C6 (1995), pp. 627–638. arXiv: [hep-lat/9504020](#) [[hep-lat](#)].
- [121] B. Jegerlehner. “Krylov space solvers for shifted linear systems”. In: (1996). arXiv: [hep-lat/9612014](#) [[hep-lat](#)].

-
- [122] J. C. Sexton and D. H. Weingarten. “Hamiltonian evolution for the hybrid Monte Carlo algorithm”. In: *Nucl. Phys.* B380 (1992), pp. 665–677.
- [123] C. Urbach, K. Jansen, A. Shindler, and U. Wenger. “HMC algorithm with multiple time scale integration and mass preconditioning”. In: *Comput. Phys. Commun.* 174 (2006), pp. 87–98. arXiv: hep-lat/0506011 [hep-lat].
- [124] M. Luscher and P. Weisz. “On-Shell Improved Lattice Gauge Theories”. In: *Commun. Math. Phys.* 97 (1985). [Erratum: *Commun. Math. Phys.* 98,433(1985)], p. 59.
- [125] M. Lüscher and P. Weisz. “Definition and general properties of the transfer matrix in continuum limit improved lattice gauge theories”. In: *Nuclear Physics B* 240.3 (1984), pp. 349–361.
- [126] G. C. Wick. “The Evaluation of the Collision Matrix”. In: *Phys. Rev.* 80 (1950). [592(1950)], pp. 268–272.
- [127] A. Stathopoulos and K. Orginos. “Computing and deflating eigenvalues while solving multiple right hand side linear systems in quantum chromodynamics”. In: *SIAM J. Sci. Comput.* 32 (2010), pp. 439–462. arXiv: 0707.0131 [hep-lat].
- [128] K. Bitar, A. Kennedy, R. Horsley, S. Meyer, and P. Rossi. “The QCD finite temperature transition and hybrid Monte Carlo”. In: *Nuclear Physics B* 313.2 (1989), pp. 348–376.
- [129] H. R. Fiebig and R. M. Woloshyn. “Monopoles and chiral-symmetry breaking in three-dimensional lattice QED”. In: *Phys. Rev. D* 42 (10 1990), pp. 3520–3523.
- [130] S.-J. Dong and K.-F. Liu. “Stochastic estimation with Z2 noise”. In: *Physics Letters B* 328.1 (1994), pp. 130–136.
- [131] M. Albanese, F. Costantini, G. Fiorentini, F. Flore, M. Lombardo, R. Tripicione, P. Bacilieri, L. Fonti, P. Giacomelli, E. Remiddi, M. Bernaschi, N. Cabibbo, E. Marinari, G. Parisi, G. Salina, S. Cabasino, F. Marzano, P. Paolucci, S. Petrarca, F. Rapuano, P. Marchesini, and R. Rusack. “Glueball masses and string tension in lattice QCD”. In: *Physics Letters B* 192.1 (1987), pp. 163–169.
- [132] C. Morningstar and M. J. Peardon. “Analytic smearing of SU(3) link variables in lattice QCD”. In: *Phys. Rev.* D69 (2004), p. 054501. arXiv: hep-lat/0311018 [hep-lat].
- [133] S. Gusken, U. Low, K. H. Mutter, R. Sommer, A. Patel, and K. Schilling. “Nonsinglet Axial Vector Couplings of the Baryon Octet in Lattice QCD”. In: *Phys. Lett.* B227 (1989), pp. 266–269.

- [134] C. R. Allton et al. “Gauge invariant smearing and matrix correlators using Wilson fermions at Beta = 6.2”. In: *Phys. Rev. D* 47 (1993), pp. 5128–5137. arXiv: hep-lat/9303009 [hep-lat].
- [135] M. H. Quenouille. “Problems in Plane Sampling”. In: *Ann. Math. Statist.* 20.3 (Sept. 1949), pp. 355–375.
- [136] M. H. QUENOUILLE. “NOTES ON BIAS IN ESTIMATION”. In: *Biometrika* 43.3-4 (1956), pp. 353–360. eprint: /oup/backfile/content_public/journal/biomet/43/3-4/10.1093/biomet/43.3-4.353/2/43-3-4-353.pdf.
- [137] “Abstracts of Papers”. In: *Ann. Math. Statist.* 29.2 (June 1958), pp. 614–623.
- [138] D. J. Toms. *The Schwinger Action Principle and Effective Action*. Cambridge University Press, 2012.
- [139] Y. Taniguchi. “One loop calculation of SUSY Ward-Takahashi identity on lattice with Wilson fermion”. In: *Phys. Rev. D* 63 (2000), p. 014502. arXiv: hep-lat/9906026 [hep-lat].
- [140] S. Luckmann. “Ward-Identitäten in der N=1 Super-Yang-Mills-Theorie”. Diplomarbeit. University of Münster, 1997.
- [141] T. Galla. “Supersymmetrische und Chirale Ward-Identitäten in einer diskretisierten N=1-SUSY-Yang-Mills-Theorie”. Diplomarbeit. University of Münster, 1999.
- [142] N. E. Bralić. “Exact Computation of Loop Averages in Two-Dimensional Yang-Mills Theory”. In: *Phys. Rev. D* 22 (1980), p. 3090.
- [143] A. A. Migdal. “Recursion Equations in Gauge Theories”. In: *Sov. Phys. JETP* 42 (1975). [*Zh. Eksp. Teor. Fiz.* 69,810(1975)], p. 413.
- [144] R. Sommer. “A New way to set the energy scale in lattice gauge theories and its applications to the static force and alpha-s in SU(2) Yang-Mills theory”. In: *Nucl. Phys. B* 411 (1994), pp. 839–854. arXiv: hep-lat/9310022 [hep-lat].
- [145] D. J. Gross, I. R. Klebanov, A. V. Matytsin, and A. V. Smilga. “Screening versus confinement in (1+1)-dimensions”. In: *Nucl. Phys. B* 461 (1996), pp. 109–130. arXiv: hep-th/9511104 [hep-th].
- [146] G. Munster. “The Size of Finite Size Effects in Lattice Gauge Theories”. In: *Nucl. Phys. B* 249 (1985), pp. 659–671.
- [147] M. Luscher. “Volume Dependence of the Energy Spectrum in Massive Quantum Field Theories. 1. Stable Particle States”. In: *Commun. Math. Phys.* 104 (1986), p. 177.
- [148] N. D. Mermin and H. Wagner. “Absence of Ferromagnetism or Antiferromagnetism in One- or Two-Dimensional Isotropic Heisenberg Models”. In: *Phys. Rev. Lett.* 17 (22 1966), pp. 1133–1136.

-
- [149] P. C. Hohenberg. “Existence of Long-Range Order in One and Two Dimensions”. In: *Phys. Rev.* 158 (2 1967), pp. 383–386.
- [150] S. Coleman. “There are no Goldstone bosons in two dimensions”. In: *Comm. Math. Phys.* 31.4 (1973), pp. 259–264.
- [151] Y. Imry. “Finite-size rounding of a first-order phase transition”. In: *Phys. Rev.* B21 (1980), pp. 2042–2043.
- [152] M. E. Fisher and A. N. Berker. “Scaling for first-order transitions in thermodynamic and finite systems”. In: *Phys. Rev.* B26 (1982), pp. 2507–2513.
- [153] A. Donini, M. Guagnelli, P. Hernandez, and A. Vladikas. “Quenched spectroscopy for the N=1 superYang-Mills theory”. In: *Nucl. Phys. Proc. Suppl.* 63 (1998), pp. 718–720. arXiv: hep-lat/9708006 [hep-lat].
- [154] R. Kirchner. “Ward Identities and Mass Spectrum of N=1 Super Yang-Mills Theory on the Lattice”. DESY-THESIS-2000-043. PhD thesis. Universität Hamburg, 2000.

Danksagung

An dieser Stelle möchte ich mich bei allen bedanken, die mich während meiner Promotion unterstützt haben.

An erster Stelle gilt mein Dank Prof. Andreas Wipf, der es mir ermöglichte, zu promovieren und der während der kompletten Promotionszeit immer als Ansprechpartner zur Verfügung stand.

Als Nächstes möchte ich mich bei all meinen Kollegen bedanken. Besonderer Dank gilt dabei Björn Wellegehausen, Daniel Körner, André Sternbeck, Georg Bergner, Daniel Schmidt und Marc Steinhauser, mit denen ich in Gesprächen über Physik und Gittersimulationen mein Wissen erweitert und neue Impulse für meine Arbeit gefunden habe. Insbesondere möchte ich mich bei Björn Wellegehausen und Marc Steinhauser für das Korrekturlesen dieser Arbeit bedanken.

Als Letztes möchte ich mich bei meinen Eltern und Großeltern für ihre kontinuierliche Unterstützung während meiner Promotion bedanken.

Diese Arbeit wurde durch die DFG im Rahmen des Graduiertenkolleg 1523 und des Projekts Wi777/11 finanziell unterstützt. Die Simulationen wurden auf den HPC-Clustern OMEGA und ARA der Universität Jena durchgeführt.

Ehrenwörtliche Erklärung

Ich erkläre hiermit ehrenwörtlich, dass ich die vorliegende Arbeit selbstständig, ohne unzulässige Hilfe Dritter und ohne Benutzung anderer als der angegebenen Hilfsmittel und Literatur angefertigt habe. Die aus anderen Quellen direkt oder indirekt übernommenen Daten und Konzepte sind unter Angabe der Quelle gekennzeichnet.

Bei der Auswahl und Auswertung folgenden Materials haben mir die nachstehenden aufgeführten Personen in der jeweils beschriebenen Weise unentgeltlich geholfen:

1. Prof. Andreas Wipf, Betreuung des Themas der Doktorarbeit und damit verbunden die Kooperation über das gesamte Projekt.
2. Björn Wellegehausen, Bereitstellung des, meines Codes zugrundeliegenden, C++ Frameworks und Kooperation während des gesamten Projekts.

Weitere Personen waren an der inhaltlich-materiellen Erstellung der vorliegenden Arbeit nicht beteiligt. Insbesondere habe ich hierfür nicht die entgeltliche Hilfe von Vermittlungs- bzw. Beratungsdiensten (Promotionsberater oder andere Personen) in Anspruch genommen. Niemand hat von mir unmittelbar oder mittelbar geldwerte Leistungen für Arbeiten erhalten, die im Zusammenhang mit dem Inhalt der vorgelegten Dissertation stehen.

Die Arbeit wurde bisher weder im In- noch im Ausland in gleicher oder ähnlicher Form einer anderen Prüfungsbehörde vorgelegt.

Die geltende Promotionsordnung der Physikalisch-Astronomischen Fakultät ist mir bekannt.

Ich versichere ehrenwörtlich, dass ich nach bestem Wissen die reine Wahrheit gesagt und nichts verschwiegen habe.

.....
Ort, Datum

.....
Daniel August